NASA/TM–2019-220423

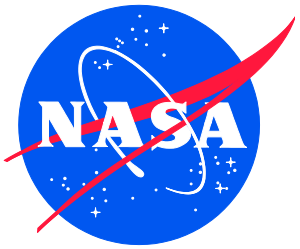

NESC Composite Overwrapped Pressure Vessel Hypervelocity Impact Study: Phase A–Acoustic Emission Review

Eric I. Madaras and Charles T. Nichols
Langley Research Center, Hampton, Virginia

November 2019

NASA STI Program . . . in Profile

Since its founding, NASA has been dedicated to the advancement of aeronautics and space science. The NASA scientific and technical information (STI) program plays a key part in helping NASA maintain this important role.

The NASA STI program operates under the auspices of the Agency Chief Information Officer. It collects, organizes, provides for archiving, and disseminates NASA's STI. The NASA STI program provides access to the NTRS Registered and its public interface, the NASA Technical Reports Server, thus providing one of the largest collections of aeronautical and space science STI in the world. Results are published in both non-NASA channels and by NASA in the NASA STI Report Series, which includes the following report types:

- TECHNICAL PUBLICATION. Reports of completed research or a major significant phase of research that present the results of NASA Programs and include extensive data or theoretical analysis. Includes compilations of significant scientific and technical data and information deemed to be of continuing reference value. NASA counter-part of peer-reviewed formal professional papers but has less stringent limitations on manuscript length and extent of graphic presentations.

- TECHNICAL MEMORANDUM. Scientific and technical findings that are preliminary or of specialized interest, e.g., quick release reports, working papers, and bibliographies that contain minimal annotation. Does not contain extensive analysis.

- CONTRACTOR REPORT. Scientific and technical findings by NASA-sponsored contractors and grantees.

- CONFERENCE PUBLICATION. Collected papers from scientific and technical conferences, symposia, seminars, or other meetings sponsored or co-sponsored by NASA.

- SPECIAL PUBLICATION. Scientific, technical, or historical information from NASA programs, projects, and missions, often concerned with subjects having substantial public interest.

- TECHNICAL TRANSLATION. English-language translations of foreign scientific and technical material pertinent to NASA's mission.

Specialized services also include organizing and publishing research results, distributing specialized research announcements and feeds, providing information desk and personal search support, and enabling data exchange services.

For more information about the NASA STI program, see the following:

- Access the NASA STI program home page at *http://www.sti.nasa.gov*

- E-mail your question to help@sti.nasa.gov

- Phone the NASA STI Information Desk at 757-864-9658

- Write to:
  NASA STI Information Desk
  Mail Stop 148
  NASA Langley Research Center
  Hampton, VA 23681-2199

NASA/TM–2019-220423

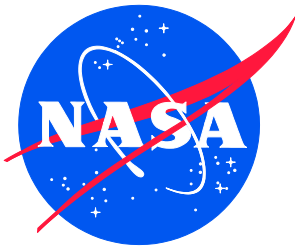

NESC Composite Overwrapped Pressure Vessel Hypervelocity Impact Study: Phase A–Acoustic Emission Review

Eric I. Madaras and Charles T. Nichols
Langley Research Center, Hampton, Virginia

National Aeronautics and
Space Administration

Langley Research Center
Hampton, Virginia 23681-2199

November 2019

Available from:

NASA Center for AeroSpace Information
7115 Standard Drive
Hanover, MD 21076-1320
443-757-5802

NESC Composite Overwrapped Pressure Vessel Hypervelocity Impact Study: Phase A–Acoustic Emission Review

Introduction

Acoustic emission (AE) measurements were performed as a component of a NASA Engineering and Safety Center (NESC) sponsored study to understand how Composite Overwrapped Pressure Vessels (COPV) respond to hypervelocity impacts (HVI) while pressurized. Of general interest to the NESC was whether there were any obvious indications in AE data that could foretell pending failure after an impact. It was of particular interest where an HVI event did not fully penetrate a pressurized COPV, to detect post-impact AE events that could indicate damage growth under continued pressure loading that might allow experts to anticipate future failure. Where an HVI event penetrated the COPV, it was of some interest to know if AE events supported an assessment of the initial degree of damage and correlated with whether the bottle vented or detonated.

Test Objectives

AE test objectives were to determine if AE could be used to predict the post-impact behavior of a pressurized COPV. Concerns raised by the test team focused on characterizing the damage to the composite overwrap by an HVI event and whether the damaged COPVs were stable under load or whether the damaged composite overwrap would further degrade under the pressure load and ultimately lead to COPV failure.

AE Test Setup

An acoustic emission system was employed to monitor a series of COPV HVI tests. The system was an eight channel laboratory system made by Digital Wave Corp. (DWC). This modular AE amplifier system was connected to a compatible digital acquisition computer system.

COPV test articles were manufactured by General Dynamics and had a nominal 0.5 m (20”) length by 0.16 m (6.5”) diameter. The cylindrical section of the COPV had an axial length of approximately 0.36 m (14”). Prior to the installation of the COPV into the hypervelocity test tank, the AE sensors were attached to the exterior of the COPV and their locations were measured and recorded. Fig. 1 shows the layout of the sensor installation pattern. Four factory calibrated AE sensors, DWC model B1025, were attached. Of the four transducers, one sensor was adhered onto the dome-shaped A-end of the tank as shown in Fig. 1 while the other three were located on the cylindrical section of the tank overwrap. The sensors were adhered to the COPV tank using Lord type 202/18 acrylic two-part adhesive. This adhesive was mixed in an off-specification ratio of about 25% extra of the Lord 202 part 1 to facilitate safe sensor removal from the tank after testing and thus allow for its subsequent reuse after the hypervelocity impact. Mixing at the manufactured specified ratios bonded the transducer so well that it led to the destruction of the sensors upon removal. At the off-nominal mixture ratio, the bond was slightly weaker, which generally allowed the sensors to be safely removed for reuse. This lower bond strength level came with a risk that a sensor might not stay bonded during a violent impact.

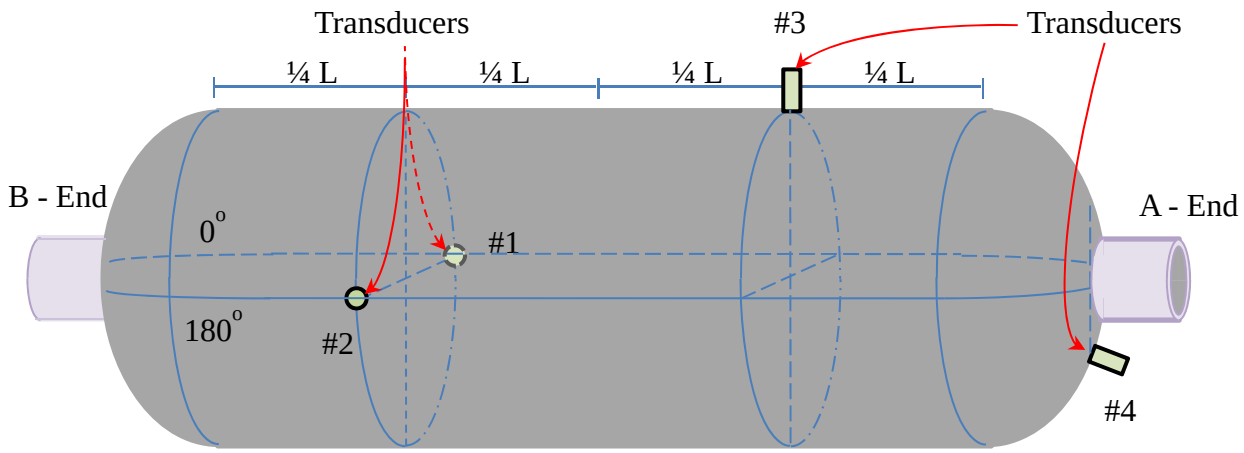

Figure 1. Illustration of a COPV tank type used for this effort showing the general AE transducer locations.

AE Equipment Configuration

Once the COPV was installed into the HVI target chamber and connected to the high-pressure feed line, the transducers were connected to the AE electronics. Each transducer was attached to either a six- or nine-foot-long, double-shielded sensor cable with a microdot connector on one end for connecting to the transducer and a BNC connector on the other end for connecting to an RF attenuator in line with a preamp/signal driver, DWC Model PA0. Initially, a 6 dB RF attenuator was used, though later that was swapped for a 20-dB RF attenuator, which helped to avoid signal clipping by the preamp. The six- or nine-foot sensor cable lengths allowed the preamp to be located a short distance away from the COPV. Besides preventing signal clipping in the first stage of gain, the RF attenuator provided some protection to the PA0 preamplifier from possible over voltages that an impact might generate within the sensor. The PA0 provided 0 dB of gain with the ability to drive the signals for 300 meters if needed. For HVI shots, the HVI target tank required evacuation during testing. Hence, the output from the PA0 line-drivers were connected by relatively short BNC cables to a pressure port feed-through in the HVI tank. On the outside of the HVI target tank, long 15 m BNC cables guided the signals into an underground bunker where they were connected to a DWC model FM1 signal conditioner/amplifier. The gain and filters of the FM1 signal conditioner/amplifier were set to provide the maximum non-saturating signal level for the HVI shot and for post impact AE event detection. The output of the signal conditioner was then connected to a computer that had an 8-channel, 10 MHz, 16-bit analog-to-digital converter installed. The computer had DWC software installed for recording the data. The amount of gain at the FM1 added into the DWC system was based on the experience gained from prior HVI impacts. All gains, filters, and trigger levels were recorded for post-test signal processing.

Once the AE system was connected, a pencil lead break on the COPV wall adjacent to the sensor's location using a 0.5 mm type H2 lead was performed to verify the sensor's operation. The test was performed in accordance with ASTM E976. For this test, the gains were adjusted and multiple lead breaks were performed. Subsequently, that data was reviewed to verify that the signal levels and

frequency content were as expected. If those signals were off-nominal, then efforts were made to check and replace any errant components, and the pencil lead break test procedure was repeated. This step was also repeated just prior to closing the impact chamber for an HVI shot to make sure that the system was working correctly from end to end at the last moment of access to the COPV. Common issues were sensors that became detached or poorly attached because of cable mishandling, pressure line installation interference, gun monitoring test hardware setup, exposure to severe temperature ranges, and inadvertent mishaps with other pretest operations. Sometimes inadvertent mishaps occurred after the final pencil lead break test during tank close out operations, which would affect a channel's recording of the HVI shot.

Test procedure

After the HVI tank was closed, it was evacuated and then pressurization of the COPV commenced. At that point, no further hands on testing of the enclosed AE hardware could be performed due to personnel safety rules. The AE system was then configured with gain and trigger settings estimated as appropriate for the HVI shot. The protocol was initially set up to have the AE system record the direct impact and if the COPV was not penetrated, then the protocol was to record all subsequent AE events for the next two hours. If the COPV was punctured, the COPV lost pressure quickly, ending the test.

After the first HVI shot on an unpressurized COPV tank, it was observed that many of the electronic activities related to operation of the gun controls along with the vacuum and pump controls of the gun barrel could cause errant triggers in the AE instrumentation. Protocols were modified to deal with these issues.

In addition, after the first few pressurized tests, the post impact AE events didn't happen frequently after the first ten minutes. Subsequently, the protocol for monitoring post impact AE events was shortened to fifteen minutes.

The initial gain settings for these hypervelocity shots were for a net gain of 42 dB. On the first shot, HITF16078, signal clipping was evident. For the second shot, HITF16079, the impactor was larger, so the net gain was reduced to 24 dB overall. There was still some clipping at this gain range. For the following shot, HITF16080, the gain was set at 12 dB on the signal amplifier. Again, some signal clipping occurred. For the fourth shot, the preamp and amplifier gain were set at 0 dB. This left only 6 dB RF attenuator in the signal line. Finally, values of 2 to 8 dB of total attenuation per channel were used for the remaining tests and provided good signal amplitude and linearity for an HVI.

Once a test was completed and the post-test documentation was accomplished, any sensors still attached after the test were removed by twisting the sensor from the surface of the COPV. If they were undamaged from the impact/removal process, then they could be cleaned up for subsequent reuse.

COPV AE Wave Velocity Measurements

For some types of AE calculations, such as event localizations, ultrasonic wave speeds are required. In a thin-walled COPV, ultrasonic waves travel as dispersive guided waves. They may be treated as guided flat plate waves for the wavelengths where the $\lambda <$ radius of the bottles. For longer wavelengths, one would need to consider general cylindrical guided wave modes. The wave speeds will be anisotropic because of the composite layup pattern. To measure these wave speeds, guided

waves were generated using pencil lead breaks and recorded with a pair of sensors. The pencil lead breaks were generated at the center of the cylindrical section of the COPV. An AE sensor was centered 0.0125 m (0.5")away from the pencil lead break point source and oriented along the COPV's axial direction from the point source. That sensor triggered the AE system and provided a known trigger time delay. With the pencil lead break's location used as the center of a 0.125 m (5") circle laid out on the surface of the COPV wall, a second sensor was moved along the 0.125 m (5") radial arc which provided the signal transit time. The distances were measured manually with a tape measure placed on the curved surface of the COPV. This has some small error associated with the distance measurement as the tape measure is affected by the roughness of the composite surface and the effects of manually measuring over a curved surface. Wave measurements were made in 10 degree increments along the circle to cover an angular range of 0 to 180 degrees. The measurements were then repeated in the reverse angular direction, travelling from 180 to 0 degrees, providing a duplicate measurement set. The two sets of angular measurements over the 180 arc were used to compute the resulting wave speed versus angle on the COPV surface.

Pencil lead breaks produce two readily distinguishable plate waves: a first-order symmetric mode wave, S_o, and a first-order flexural mode wave, A_o. The symmetric mode, which has a faster speed at low frequencies, arrives first and then the slower flexural wave arrives second. In these tests, the flexural waveform had about 90 percent of the wave energy while the symmetric mode was on the order of 10 percent of the wave energy. Despite the lower signal level of the symmetric mode, the relatively non-dispersive, low frequency components of the symmetric mode wave arrived first and were often easier to discern.

Fig. 2 shows a graph of the measured lowest order flexural wave speeds over the range of -90º to +90º and Fig. 3 shows a graph of the measured low order symmetric wave speeds over the same range. In both figures, because of the symmetry of the ply layups, the data was assumed to be symmetrical about the 0º angle, which is the hoop direction, so data from corresponding angles could be averaged together to improve the error bars of that data somewhat. Thus, the -90° to 0° wave speeds were treated as identical to the 0° to +90° data, as shown. The flexural wave speed ranged from about 1900 m/s up to 2500 m/s. The symmetric wave speed ranged from about 5500 m/s up to 7500 m/s. In both cases, the maximum speed is centered at the 0º direction where the hoop fibers affect the wave speed, and the minimum occurring at the ±90° direction, which is the axial direction. For AE data processing of an HVI impact, if an HVI impact produces both types of waves, then the faster symmetric wave should be the first to arrive at a sensor and will be the triggering wave. It should also be noted that the tensile loading of the pressure shell will have the effect of increasing the speed somewhat since the pressure-induced stresses will have the effect of stiffening the COPV shell. [1,2] In addition, during pressurization, the temperature of the bottles increased, which will affect wave speed. The pressurization protocol required that the bottle temperature be monitored and limited. The maximum temperature approached was controlled by the pressurization rate. The impact shots were supposed to be on bottles with a temperature below 50ºC.

A few comments about the wave speeds of additional relevant materials to consider to understand if there are other pathways for sound to travel, which could lead to premature triggers. Aluminum has a bulk compressional wave velocity of about 6400 m/s and is isotropic in character. Uniaxial composites often have bulk compressional wave velocities near 9000 m/s in uniaxial fibers and about ~2500 m/s across the fiber resin mixture demonstrating a large anisotropic character in between those directions. Also, it is appropriate to understand the ultrasonic velocity effects of N_2 gas under pressure. At one atmosphere, N_2 gas has a velocity of about 330 m/s, similar to air. Under very high pressures, the wave speeds increase. For example, for N_2 gas at room temperature and about 65,300 psi, the wave speed was reported to be near 1650 m/s. [3, 4] Even at that speed, the ultrasonic symmetric plate waves in the solid COPV shell should easily arrive at a transducer mounted on the

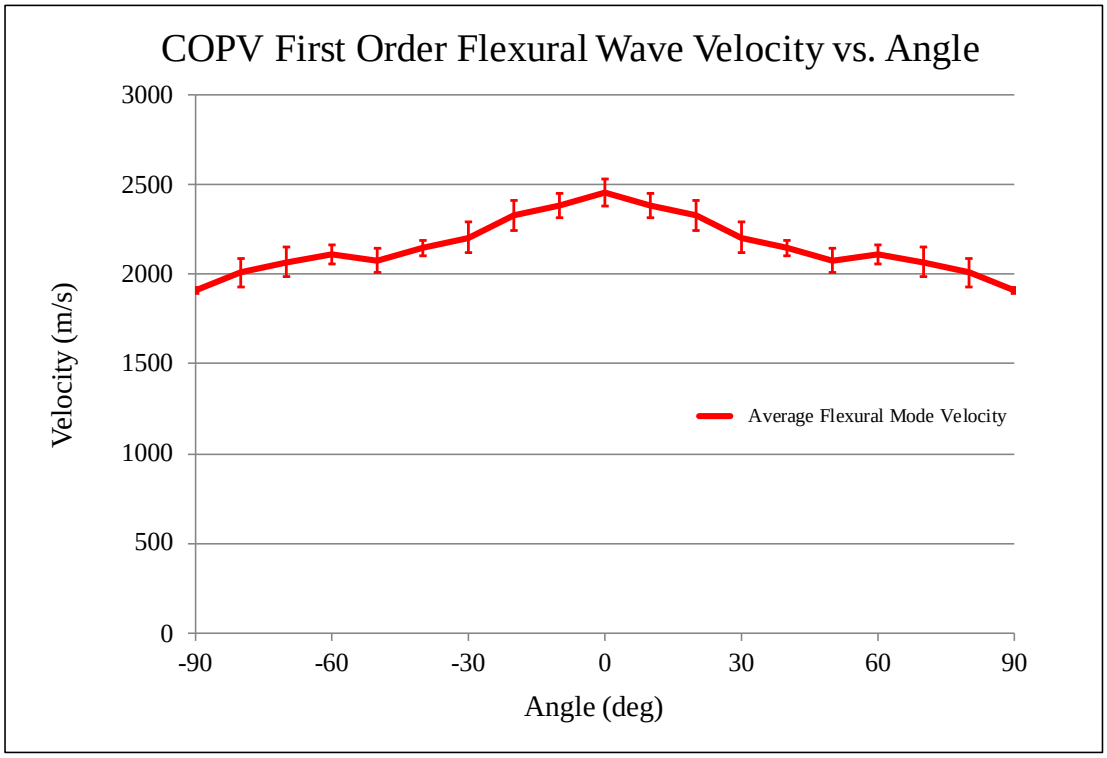

Figure 2. Flexural wave velocity in units of m/s vs. angle from -90 to 90 degrees. The vertical axis is velocity in m/s and ranges from 0 to 3500 m/s. The error bar estimates at each angle are shown.

COPV before any gas borne waves can arrive. At the COPV's Maximum Estimated Operating Pressure (MEOP) of 4200 psi, the gas wave speed will be significantly less than 1650 m/s that occur at 63,000 psi, so any gas borne waves can be ignored as a trigger source in these tests. Another possible trigger source could happen if the projectile struck the wall, and some material spalled off the interior wall and that debris might impact the back side of the COPV. Similarly, if a projectile fully punctured the COPV's pressure wall, and the projectile still maintained some of its mass, i.e. didn't vaporize or disintegrate, and it was still traveling at supersonic speeds, the projectile could impact the far wall of the inside of the COPV. In those cases, it is possible that the projectile's secondary impact might trigger a sensor before the initial impact generated symmetric wave triggers a sensor. Thus, which sensor is triggered first would depend on the geometry of the sensor locations relative to the sources for the two waves generated, either the primary impact wave vs. any secondary generated impact waves. For the geometries and sensor locations used in these tests, it is expected that all the first impact, plate wave signals on these tests should cause the triggering of the system. If a different wave source was to trigger the system, then the impact site location algorithm should indicate the discrepancy.

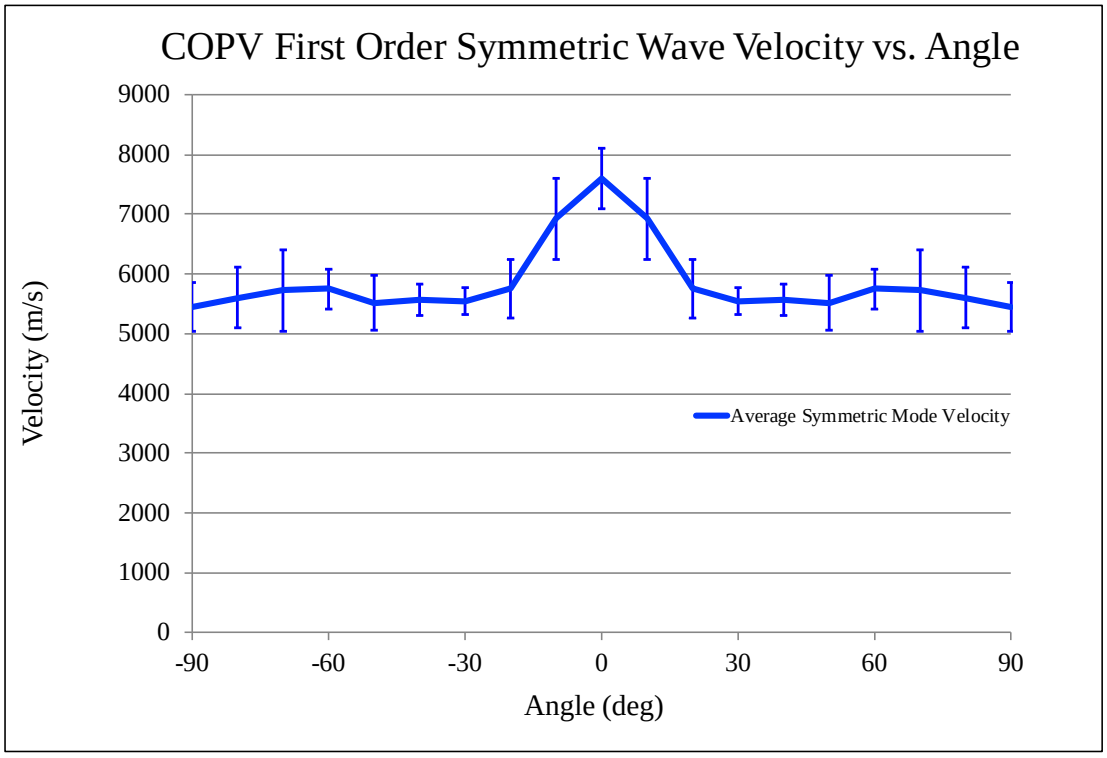

Figure 3. Symmetric wave velocity in units of m/s vs. angle from -90 to 90 degrees. The vertical axis is velocity in m/s and ranges from 0 to 9000 m/s. The error bar estimates at each angle are shown.

AE Event Location Methodology on COPV Impact Tests

The algorithm used for location of an impact is based on a minimization algorithm computing the minimized least square error between sensor impact times and the computed time of flight from the impact location to the sensor locations. In these equations, there are three unknown variables to solve for: the axial and circumferential locations of the impact and the time of flight of the impact signal to the first triggered sensor. While any three of the four sensor locations could be used to estimate the impact location algebraically, it was chosen to use a minimization algorithm based on the MatLab Curve Fitting Toolbox function called "lsqnonlin()". In principle, when using three or more sensor locations, this should give the best fit in the sense of least square error. For the case of three or more sensor locations, there might be multiple minima, so one needs to check for the lowest least square minimum point. With these bottles, when choosing an initial location near the target impact location, one always ended up with a solution typically within 0.032 m (~1.25") of the true impact location. That level of accuracy is most likely a reflection of the local velocity accuracies. While location accuracy results for simple aluminum plates are more like 0.00635 m (~0.25") or better, in those cases, velocities are accurately known. Here, the level of accuracy for COPV structures that is reported is close to what previous measurements have achieved with COPV structures, where the fiber wraps are a bit more structurally complex and variable than simple aluminum plates.

With the three sensors on the cylindrical part of the pressure wall, the geometry for the distance between two points is simple. Still, one needs to ensure that the correct circumferential distances are chosen for whether the shortest path from the impact location to the sensor is achieved by travelling clockwise or counterclockwise in the circumferential direction. For the case of the sensor on the dome region, sensor 4, the geodetic geometry becomes much more complicated for computing the geodesic distance and the solution is more convoluted. If the dome is truly a hemispherical shape, calculating the geodesic distance is in principle doable analytically. In reality, the dome is not exactly a hemisphere, but is somewhat flattened compared to a hemisphere. Further, the ply layups and densities, as well as the metal's thickness, varies in the dome region, which yields potentially very different speeds throughout that region. Thus, using the sensor on the dome in the lsqnonlin() function software was problematic as the algorithm requires a functional form for its fitting algorithm, which we don't have for the fourth sensor location. If we have larger cylinders and more sensors, this software framework can be adapted for cases where one might use more than three sensor locations placed on the cylindrical wall

One of the initial issues tested from this data was the validity of the velocity estimates measured from the pencil lead breaks both without pressurization and those velocity values affected by the pressure of the bottles. Using the symmetric mode velocity data, Fig. 3, with a spline interpolation produced more accurate answers than fitting a functional model to the velocity data, such as a Gaussian function.

By inverting the fitting algorithm to fit the velocity data using the known locations of the sensors and known impact locations for impacts on pressurized COPVs, one can develop an estimate of the velocity function over angles with both unpressurized and pressurized bottles. For that calculation, the shape of the velocity data curve in Fig. 3 was assumed, while the maximum and minimum range were treated as the unknowns. The pencil lead break derived symmetric velocities in the unpressurized COPVs uniformly appeared to be within 2% of the calculated values. In the case of the two unpressurized tests, the location calculations were within 0.025 m (~1") accuracy of the actual measured impact location for one test and 0.01 m (~0.4") for the second test. This level of accuracy reflects the variability between COPVs. Similar velocity computations were done for the flexural mode velocity, but the time of arrival signals was less accurate overall for the flexural mode.

As mentioned previously, the pressures inside the COPV should cause an increase in the wave velocities, and the wave velocities will also be affected by the elevated temperatures from the pressurization process. The aforementioned process for adjusting the velocity curves was again applied to COPV bottles that were pressurized, but did not rupture. In these bottles, the impact locations were known and thus the velocities could be estimated as in the unpressurized case. Subsequently, the Fig. 3 velocity profile's shape was fitted for the case where the COPVs were pressurized. That process suggested that the pressurized velocity data was between 10 to 20% higher when compared with the unpressurized test results. With the ruptured bottles, where there was no post impact information related to the exact impact location, velocity values that were adjusted upwards by 20% were used in the location fitting algorithm. With those levels of adjustments, the impact location accuracies in the pressurized bottles ranged from ~ 0.01 m to 0.036 m (~0.4" to ~1.4"), which were in a similar range to the unpressurized impact location accuracies.

AE Signal Energy

The signal energy (*SE*) from AE measurements are computed from the voltage vs. time recording of the AE data, according to the equation:

$$SE = \sum_i^n V(t_i)^2 \, \Delta t, \qquad \text{Eq. 1}$$

where $V(t_i)$ is the digitized voltage at time t_i and Δt is the sampling rate in time per data point and n represent the number of points used to compute the *SE*. In these tests, Δt was 0.5 μs/point. It is important to appreciate that in Eq. 1, the length of time that one takes data is important when comparing data.

In the first few pathfinder hypervelocity shots, 4096 μs of data were recorded after which it was realized that less than 25% of that data was actually of interest. Subsequently, in this early phase of this work, the time recorded was adjusted to 1024 μs per sensor. Later in the testing, after measuring the first few bottles that ruptured, it was deemed necessary to increase the time measured to 2048 μs to better document the results of those types of events, and that time length seemed to better represented all the data overall as the project progressed. The 2048 μs record length was used for the remainder of this study. The longer times of 2048 μs did not simply double the SE compared to the case of the 1024 μs measured data, since the majority of the signal's amplitude exists early in the recording, during the impact's response, and then died away. To make viable corrections to the signal energy calculation from the 1024 μs data to allow it to be compared to the 2048 μs data on an equal footing, one needs to understand the types of noise sources that were present and make adjustments accordingly.

We estimate that there are five types of noise sources that contribute to the signal energy overall. There is the initial impact signal that is a fast, large temporal initial signal with a following decaying signal which might last for many tens of microseconds as the signal radiates from the impact and spreads out and dissipates. There are also signals from the post impact damage growth in the composite and metal that are short burst signals that might occur during the following microseconds after the impact and could include some derivative impacts from debris striking areas of the inner liner after penetration. That signal can be erratic in its temporal and magnitude behavior as the type and degree of material damage effects are unpredictable. Third, there can be noise generated as high pressure air escapes through the leak orifice, if present. Fourth, with COPV detonation, there will be a fast rising signal at the time of detonation as the COPV rapidly comes apart and expands outward. Even when the sensors have disbonded because of the violence of the impact and appear to be "dead" for many microseconds, the detonation signal will be large at the transducers, as they will not have had any significant time to fall away and out of the path of the COPV debris. Hence, the sensors will be struck by the pieces of the COPV, which accelerate the sensors away from their resting positions. Finally, instrumentation noise can be a factor. In these tests, compared to the initial impact signals with the gain turned down to avoid signal saturation, the instrument noise is not a significantly contributing value to the signal energy in this part of the AE recordings.

For purposes of making adjustments to the signal energy as a result of different signal time lengths, in the case of the shorter signals, if one realizes that the noise from the initial impact will have dissipated by the end of the recorded AE signal, then the signal near the end of the record would mostly consist of latent post impact damage growth noise and leaking gas noise, if present. Thus, using a measurement of the signal energy at the end of the signal, one can obtain an approximate value for the leak noise and latent impact growth noise for the 1024μs recorded signals, Under the assumption that the noise components at the end of 1024μs of data will continue to make noise at that level for the next 1024μs one can use those values of signal energy to adjust the shorter time length signals to be equivalent to the longer time length signals. To estimate the leak noise and latent impact growth noise signal levels, both the last 10% and last 25% of the shorter data records were tested. They were isolated and scaled up respectively and used as an estimate of noise needed to correct the signal energy of the initial 1024μs time length to represent an estimate of signal energy for a longer

2048μs time length. Using this process, both the leak noise and latent impact growth noise ranges from the last 10% or 25%, were reasonably close to each in their size of the signal energy value corrections.

In the case of a simple impact that did not fully penetrate the wall, the main signal sources appear to be from the impact signal and any subsequent damage in the vicinity of the impact. If there are correlations between either the signal energy, the energy of the impactor, or some feature of the degree of damage, then the signal energy could be a predictor for the degree of damage. Some simple tests of this correlation concept were to: (1) plot the signal energy against the projectile energy; (2) plot the signal energy against the cross sectional area of damage; and (3) plot the signal energy against the circumference of the area of damage. Those three parameters were numbers that we could measure, compute, or estimate. First, the projectile's kinetic energy was measured by systems that were a part of the hypervelocity gun system and that impactor energy was deposited locally into the wall creating a small crater in the COPV wall. In this scenario, the proportionality with projectile energy would be disrupted once penetration occurred, as then, not all the impactor's kinetic energy is deposited into the COPV's wall, changing the nature of the damage process. Secondly, from the measurements of the damage crater, we generated rough dimensions of the area and circumference of the impact. Proportionality with volume couldn't be directly tested, since the crater depth information was not available, but the areal damage could be estimated as a simple ellipse. Interest in the circumference comparison arises as there may be contributions to the signal energy from the metal straining or failing at the outer edge of the impact, which is then an edge that is more free to move and create signal noise. The time course of the post impact damage growth, i.e. how long the damage growth might continue to occur within the pressurized bottle, was something that we could not predict in these tests.

In the case projectile penetration and therefore generation of leak noise, since that noise is related to the gas velocity as it escapes, which is proportional to the pressure drop, that effect should follow an exponential decay with time. But, over the first few milliseconds of time, the pressure won't have had much time to decay, hence for our purposes, we can estimate the leak noise signal energy as approximately constant over that short time frame. The amplitude of that noise also depends on the generation mechanism, which appears to be the turbulent gas flowing at the edges of the penetration. Other tests for the leak noise from an ISS metal skin showed an approximately direct correlation between the logarithm of the signal energy from the leak noise with the circumference of the hole. [5] It should be noted that the metal surface of the ISS skin is much less attenuative than the wall of a COPV and the reverberant noise effects will be different comparing the ISS structure to the COPV structure. Furthermore, the noise signal's generation is also affected by the roughness of the leak hole's edges, which in the case of an HVI test can vary significantly, sometimes being a rather simple hole and other times having a great deal of structure, such as rough metal edges. Hence, because of the complexity of the hole's dimension and complex shape from a hypervelocity impact, it is hard to predict the exact dependence of the signal energy vs. the hole's dimension and shape.

Hypervelocity COPV Tests

Table 1 shows the listing of the HVI testing of the Phase A work and is organized by the results of those shots. In this report, 19 HVI shots are reviewed regarding the acoustic emission measurements. Column one lists seven HVI shots that resulted in damage to the COPV that neither vented nor ruptured the COPV. Column 2 lists six HVI shots that resulted in penetration and venting, but not the rupture of the COPV. Column 3 lists another six HVI shots that resulted in the penetration and detonation of the COPV.

Table 1. List of HVI shots sorted by result

Non-Penetrating Shots	Penetrating/ Venting Shots	Penetrating/ Detonating Shots
HITF 16078	HITF 16160	HITF 16161
HITF 16079	HITF 16164	HITF 16162
HITF 16080	HITF 16165	HITF 16167
HITF 16081	HITF 16166	HITF 16168
HITF 16159	HITF 16169	HITF 16170
HITF 16163	HITF 16504B	HITF 16505
HITF 16171		

Non-Penetrating Shots

Table 2 provides a listing of the hypervelocity shot parameters for the cases where the projectile did not penetrate the COPV's wall. The table is broken into three sections: Pathfinder, Part 1, and Part 2. The first four shots were a part of a Pathfinder series of shots for defining the setup parameters. The first two shots of the Pathfinder series were not pressurized. For the remaining five shots, the tanks were pressurized. In the table, Part 1 refers to work focused on defining the region of the tank which is most vulnerable to a penetration. Part 2 refers to work to define the ballistic limit for the weakest region. Here, the ballistic limit is defined as the energy to penetrate the COPV wall fully. These non-puncturing shots were in the cylinder region except for shot HITF16163, which was referred to as a shoulder shot and was where the cylinder region transitioned into the dome region. The shots were generally in order of more severe projectile energies, not counting an impact to the COPV shoulder region.

Table 3 describes the resulting damage from the impacts for the non-penetrating shots. Table 3 is followed by graphs showing the AE signal vs. time or frequency for each of the non-penetrating shots that were recorded in these tests, and which correlate with the first column of HITF numbers in Table 1 and the listing of damage outlined in Table 3.

Figures 4 through 24 show the AE signal vs. time or frequency for each hypervelocity shot that did not fully penetrate the COPV target. The order of these figures directly correlates with the first column of HITF numbers in Table 2. The figures are ordered with the first view as an "early time close up", ~100 μs of data, view of each AE signal channel recording of an HVI shot. This is followed by a graph of the amplitude vs. the full-time sequence of the AE results for each channel. The third figure in each group shows the frequency data for each of the sensors for that shot. The frequency data is plotted on a frequency scale of 0 to 1000KHz. The figure formats have panels (a), (b), (c), and (d) as sensors 1, 2, 3, and 4, respectively.

Table 2. List of HVI shot parameters for shots that did not fully penetrate the COPV. The column labelled "Perpendicular Momentum" is the momentum component perpendicular to the surface at the impact point.

HITF Number/ Tank S/N / Impact Location	Actual Tank Pressure (psi)	Projec-tile Type	Projectile Diameter (mm)	Actual Projectile Mass (g)	Actual Velocity (km/s)	Impact Angle (deg)	Projectile Energy (J)	Momen-tum (Kg-m/s)	Perpen-dicular Momen-tum (Kg-m/s)
Pathfinder									
#A HITF16078 S/N 195 Cylinder	Ambient pressure	Al 2017-T4	0.3	0.00004	6.98	-45	0.9298	0.0002664	0.0001884
#B HITF16079 S/N 190 Cylinder	Ambient pressure	Al 2017-T4	0.5	0.00018	6.92	-45	4.2311	0.0012229	0.0008647
#1 HITF16080 S/N 201 Cylinder	4500	Al 2017-T4	0.3	0.00004	7.24	-45	0.9352	0.000267	0.0001889
#2 HITF16081 S/N 190 Cylinder	4500	Al 2017-T4	0.5	0.00018	6.82	-45	4.3295	0.001237	0.0008747
Part 1									
#3 HITF16159 S/N 190 Cylinder	4234	Al 2017-T4	1.0	0.00145	7.41	47	38.8122	0.0104756	0.0071444
#7 HITF16163 S/N 194 Shoulder	4212	Al 2017-T4	1.52	0.00514	7.04	45	123.0293	0.0349515	0.0247144
Part 2									
#15 HITF16171 S/N 202 Cylinder	4270	Al 2017-T4	2.01	0.01194	4.08	45	95.5522	0.0468393	0.0331204

Table 3 List of results of HVI shots shown in Table 2

Test Number / HITF Number/ Tank S/N / Impact Location	**Damage Assessments (dimensions are in mm)** Areal damage is denoted as a length x width. (Note, TBD values were not known at the time of the writing of this report. This table was copied from a preliminary report that was not complete at the writing of this report.)
Pathfinder	
#A HITF16078 S/N 195 Cylinder	**Overall impact damage** = severed fibers and ply delamination present within a 2.4 x 1.5 area surrounding the projectile entry crater. **Crater dimensions** = 0.8 x 0.5. **Maximum crater depth** = TBD. **Sub-surface damage** = TBD, **Liner damage** = TBD, Ten-minute monitoring time after impact.
#B HITF16079 S/N 190 Cylinder	**Overall impact damage** = severed fibers and ply delamination present within a 13.3 x 1.5 area surrounding the projectile entry crater. **Crater dimensions** = 1.4 x 1.1. **Maximum crater depth** = TBD. **Sub-surface damage** = TBD, **Liner damage** = TBD, Ten-minute monitoring time after impact.
#1 HITF16080 S/N 201 Cylinder	**No venting or rupture occurred. Overall impact damage** = severed fibers and ply delamination present within a 1.4 x 2.1 area surrounding the projectile entry crater. **Crater dimensions** = 0.9 x 0.8. **Maximum crater depth** = TBD. **Sub-surface damage** = TBD. **Liner damage** = TBD, Two-hour monitoring time after impact.
#2 HITF 16081 S/N 203 Cylinder	**No venting or rupture occurred. Overall impact damage** = severed fibers and ply delamination present within a 3.7 x 40.6 area surrounding the projectile entry crater. C**rater dimensions** = 1.6 x 1.4. **Maximum crater depth** = TBD. S**ub-surface damage** = TBD. **Liner damage** = TBD, Two-hour monitoring time after impact.
Part 1	
#3 HITF16159 S/N 190 Cylinder	**No venting or rupture occurred. Overall impact damage** = severed fibers and ply delamination present that has a 4.8 maximum height and extends around the tank ~270 degrees from the origin of impact. **Crater dimensions** = 3.5 x 3.2. **Maximum crater depth** = TBD **Sub-surface damage** = TBD **Liner damage** = visible bump to the liner inside of the tank
#7 HITF16163 S/N 194 Shoulder	**No venting or rupture occurred. Overall impact damage** = severed fibers and ply delamination present within 35.7 x 23.3 area from origin of impact, most damage contained within helical wrap area, minimal hoop wrap damage at wrap transition. Ball impacted 85.0 from tank boss **Crater dimensions** = 5.0 x 4.4 **Maximum crater depth** = 2.0 (estimated) **Sub-surface damage** = TBD **Liner damage** = crater present, visible bump present within liner
Part 2	
#15 HITF16171 S/N 202 Cylinder	**No venting or rupture occurred. Overall impact damage** = severed fibers and ply delamination present that has a maximum height of 9.2 that runs from 9 o'clock to 3 o'clock from the origin of impact that has a maximum length of 466.9 **Crater dimensions** = 4.1 x 4.5 **Maximum crater depth** = 4.5 (estimated) from overwrap surface plane. **Sub-surface damage** = TBD **Liner damage** = 4.1 x 4.5 exposed liner present, pronounced bump visibly present

Fig. 4 shows the signal amplitude vs. time for the four sensors mounted on the COPV for hypervelocity shot HITF16078. Inspection of Fig. 4 shows that the first arrival signal occurred on sensor 3, followed by sensor 1, sensor 2, and then sensor 4. The pre-trigger time was set to record 512 µs of data before the trigger for this shot. The high frequency, symmetric mode arrived first, followed by the lower frequency, flexural mode at about 30 µs later on the nearest sensors and about 50 µs later on sensor 2 which is further away. The wave types in Fig. 4d are more complex because the thickness is changing over the dome, which affects the plate wave's frequencies and velocities. It is clear in the graphs that a significant amount of saturation occurred on the sensors.

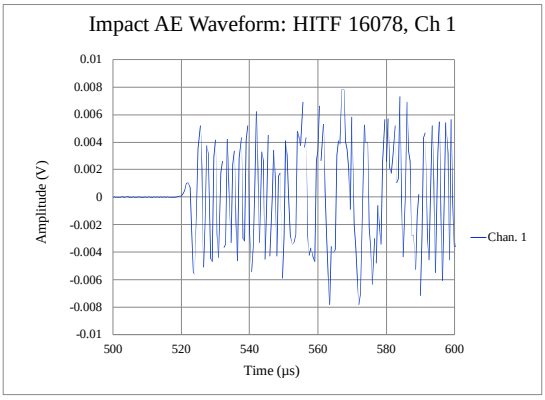

(a) Sensor Channel 1

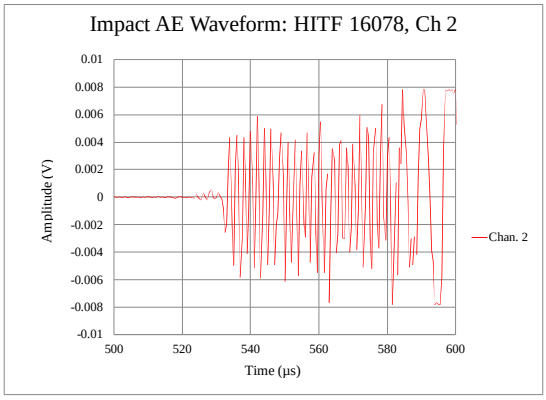

(b) Sensor Channel 2

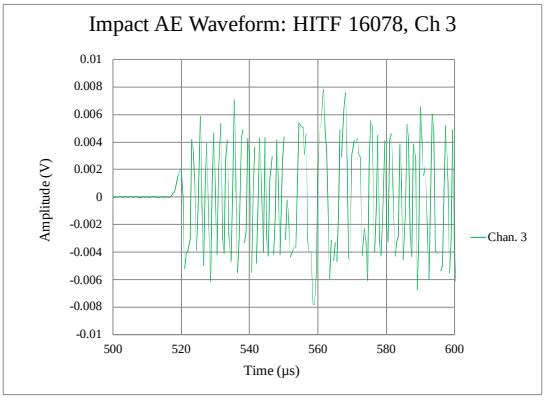

(c) Sensor Channel 3

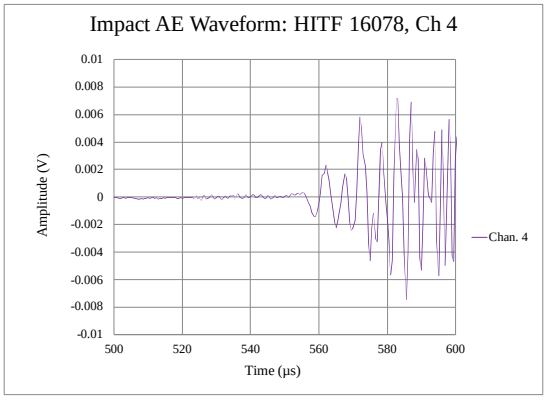

(d) Sensor Channel 4

Figure 4. Time of arrival/temporal results of HITF16078 in volts vs. time over the range of 500 to 600 µs.

Fig 5 shows the voltage vs. time for the first 4000 µs out of 4096 µs of the signal that was captured, and the full extent of the signal saturation is evident in this figure. The signal saturation lasted for about 400 µs on the furthest sensor from the impact site, chan. 4, and up to 600 µs on the closest sensor to the impact, chan. 3.

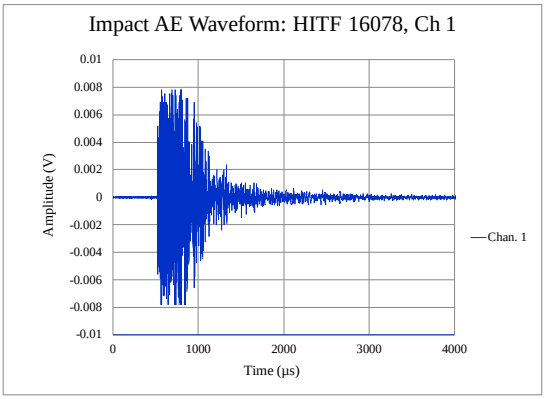

(a) Sensor Channel 1

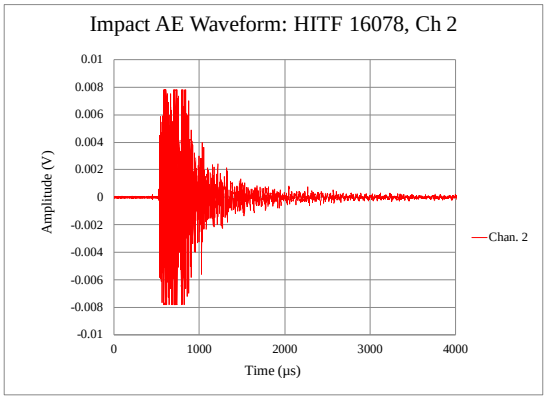

(b) Sensor Channel 2

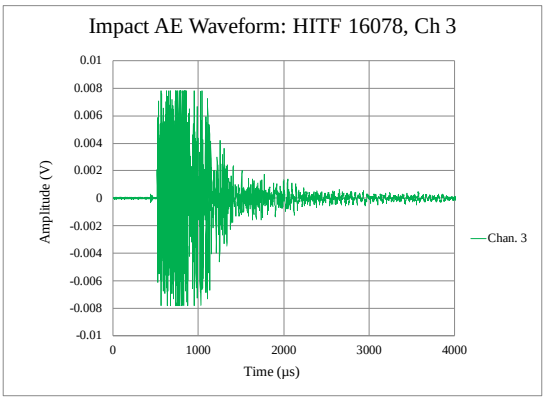

(c) Sensor Channel 3

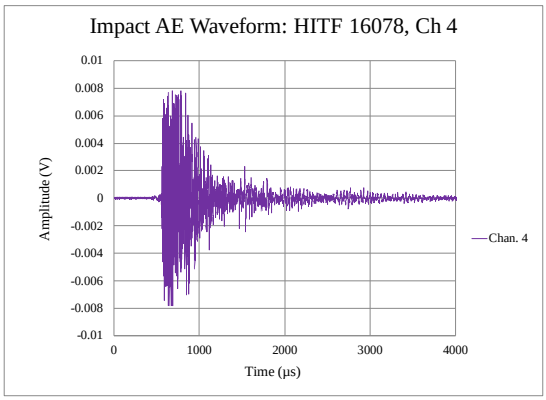

(d) Sensor Channel 4

Figure 5. Full temporal results of HITF16078 in volts vs. time over the range of 0 to 4000 µs.

Fig. 6 shows the amplitude vs frequency of the sensors' responses to the impact HITF16078. The main frequency peaks are broad and appear to be near 100 KHz and 500 KHz. The first peak amplitude is near -45 dB on all the channels. The sensor's response is specified as "flat" between 50 - 1,000 KHz. It is possible that the lower frequency peak is affected by the sensor's response cut-off below the 50 KHz frequency. Since the sensors were heavily saturated as seen in Fig. 5, the amplitudes will be strongly attenuated. Also, the saturation will introduce significant higher frequency distortion. For a thickness of composite overwrap of 2.54 mm thickness and a 2 mm thick liner, a simple calculation of the thickness resonant frequency would be slightly below 400 KHz. The 500 KHz peak, which is broad, probably represents the fundamental thickness vibration mode of the COPV wall in the cylinder section, which has relevance to the lowest symmetric wave mode. Sensor 4, which is on the dome region where the COPV wall becomes thicker, will experience shifts of the frequencies downwards and is probably why peaks are not as evident in sensor 4.

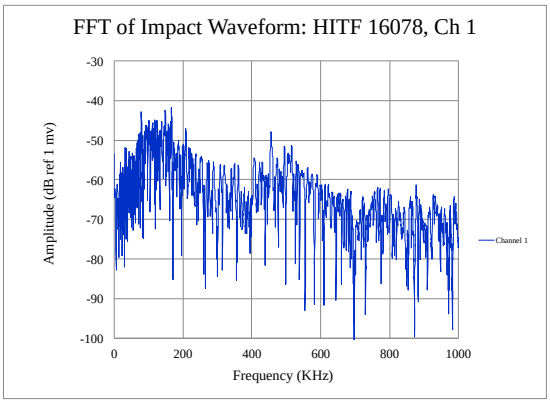

(a) Sensor Channel 1

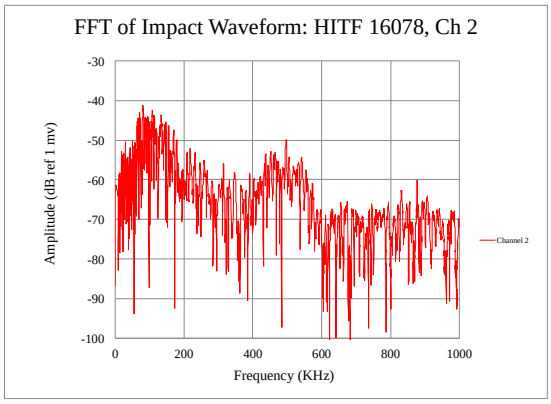

(b) Sensor Channel 2

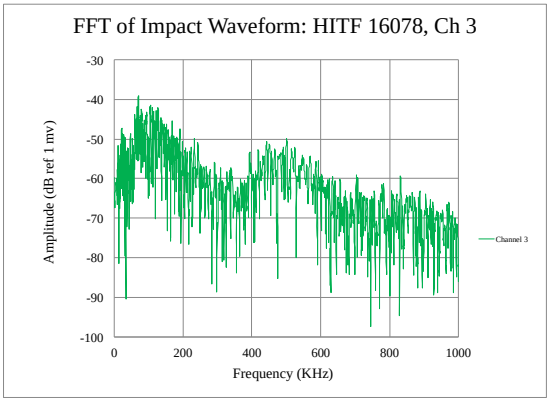

(c) Sensor Channel 3

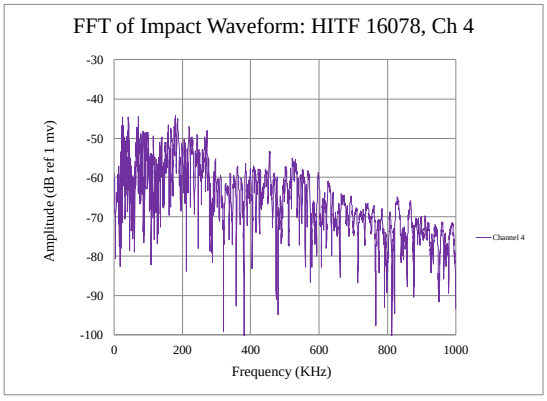

(d) Sensor Channel 4

Figure 6. Frequency results of HITF16078. The vertical data is amplitude on a dB scale, referenced to 1 mV. The amplitude ranges from -100 to -30 dB.

Fig. 7 shows the signal amplitude vs. time for the four sensors mounted on the COPV for the second hypervelocity shot, HITF16079. Inspection of Fig. 7 shows that the first arrival signal occurred on sensor 2, followed by arrival at sensor 3, sensor 1, and then sensor 4. The pre-trigger time was again set for 512 µs of data for this shot. The high frequency, symmetric mode arrived first, followed by the lower frequency, flexural mode at about 10 µs later on the nearest sensors, sensor 2, and about 20 µs later on sensor 3 which is slightly further away. Waves on channel 1 don't show any strong antisymmetric waves arriving within this time frame. As in Fig. 4, the wave types in Fig. 7d are more complex because the thicknesses are varying over the dome and the changes in thicknesses affect the plate wave's frequencies. It should be noted even after adjusting the gain for this shot to eliminate saturation, that a significant amount of saturation still occurred on the sensors, which is clear in these graphs and further evident in Fig. 8.

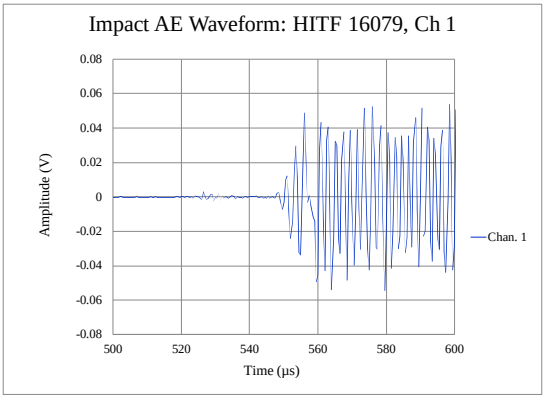

(a) Sensor Channel 1

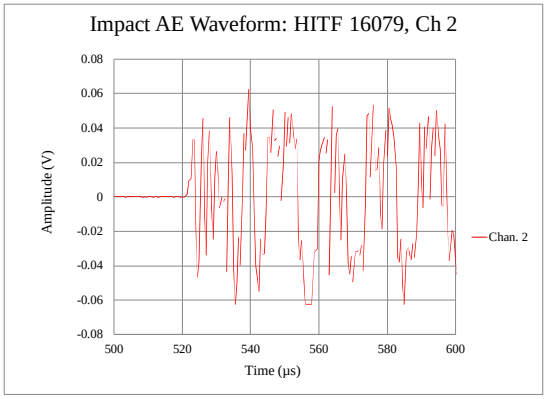

(b) Sensor Channel 2

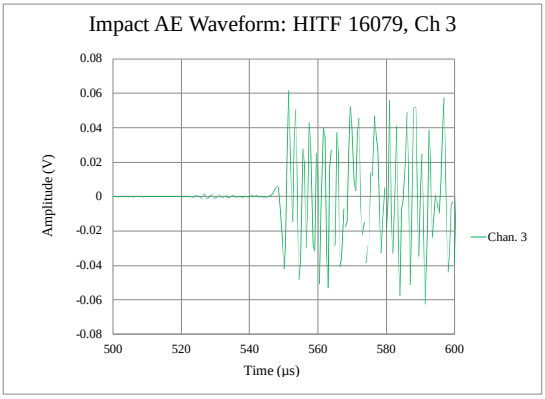

(c) Sensor Channel 3

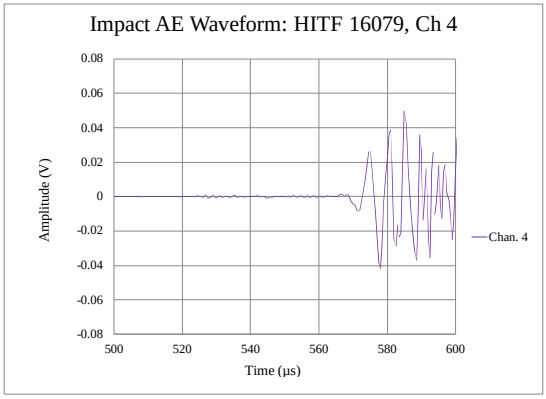

(d) Sensor Channel 4

Figure 7. Time of arrival/temporal results of HITF16079 in volts vs. time over the range of 500 to 600 µs. The amplitude of the graphs range from ±0.08 V.

Fig. 8 shows the voltage vs. time for the first 4000 µs of the 4096 µs of the signal that was captured. The extent of the signal saturation is clear in Fig. 8. Gains were adjusted lower for this shot to address the saturation in the previous shot, HITF16078. The projectile size was about 4.5 times more massive, so the impact was proportionally more energetic. Even with the reduced gain, there were significant saturations. The signal saturation times ranged from about 500 µs on sensor 3 down to ~100 µs on sensor 4. With the lower gain settings, the saturation was now clipping the signal at 0.06 V in contrast to the prior shot where the clipping was clear at 0.008 V.

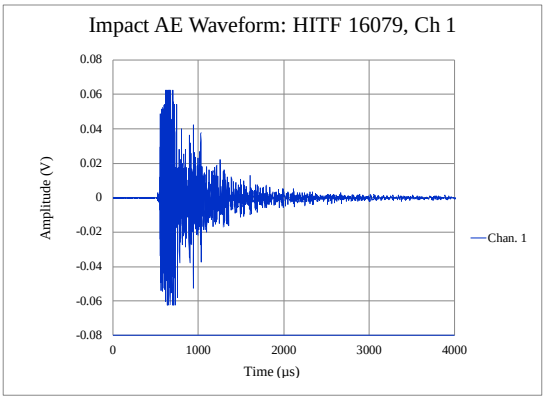

(a) Sensor 1

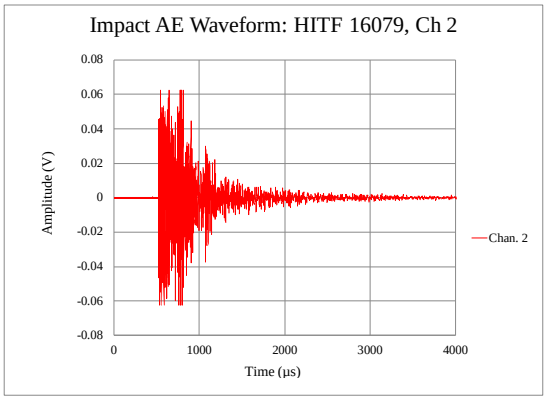

(b) Sensor Channel 2

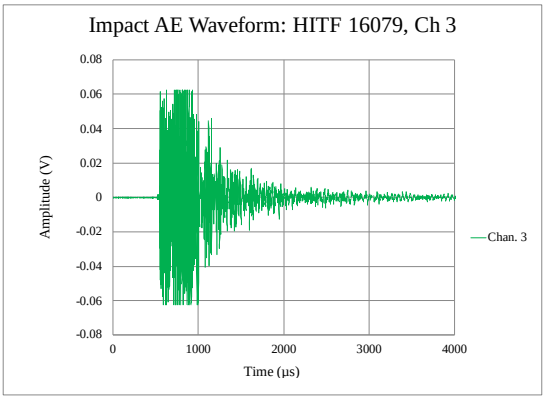

(c) Sensor Channel 3

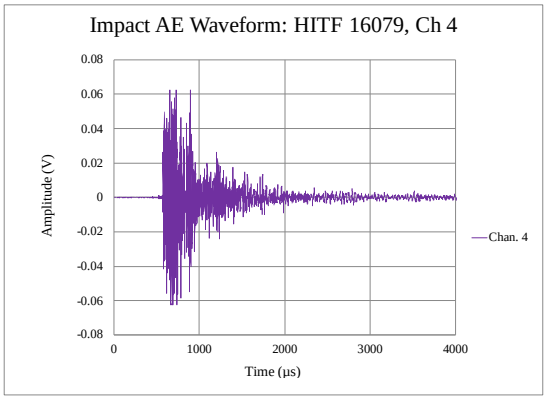

(d) Sensor Channel 4

Figure 8. Full temporal results of HITF16079 in volts vs. time over the range of 0 to 4000 µs.

Fig. 9 shows the amplitude vs. frequency of the sensors' response to the impact HITF16079. The data parallels the results from HTIF16078, except with the lower gain, less of the energy was lost and now the signal levels peaked near -25 dB around the first peak at 100 KHz. Again, since the sensors were heavily saturated, as seen in Fig. 8, the amplitudes will be strongly attenuated. Plus, the saturation will introduce significantly higher frequency distortion. As seen in HITF16078, the data has a similar peak just below 500 KHz. In this shot, Fig. 9(d), chan. 4 also shows a lower, broader amplitude peak in that frequency range.

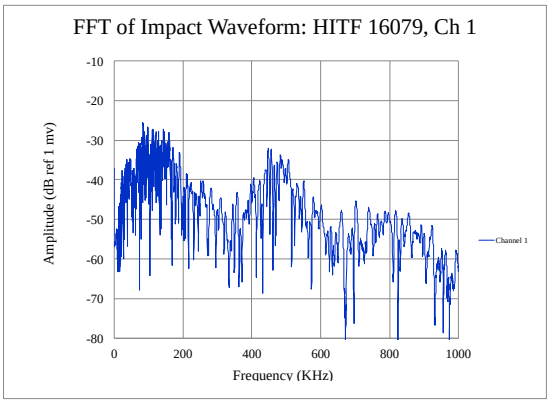

(a) Sensor Channel 1

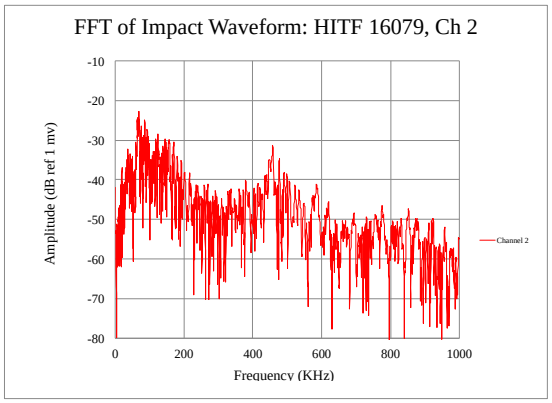

(b) Sensor Channel 2

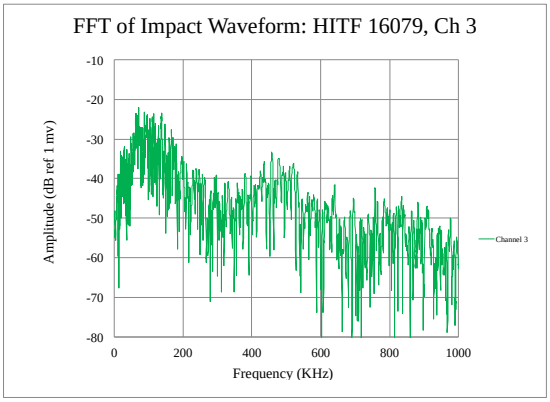

(c) Sensor Channel 3

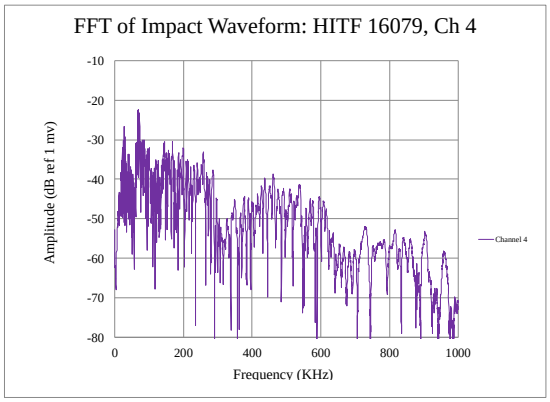

(d) Sensor Channel 4

Figure 9. Frequency results of HITF16079. The vertical data is amplitude on a dB scale referenced to 1 mV. The amplitude ranges from -80 to -10 dB.

Fig. 10 shows the signal amplitude vs. time for the four sensors mounted on the COPV for hypervelocity shot HITF16080. This was the first pressurized impact test. The projectile size and speed were comparable to the unpressurized hypervelocity shot HITF16078. The amplitude ranges between ±0.3 V and the time shown ranges from 120 to 240 µs. For all the remaining shots, the pre-trigger time was set for 128 µs of data and the plots show data from 120 to 240 µs. Inspection of Fig. 10 shows that the first arrival signal occurred on sensor 2, followed by arrival at sensor 3, then sensor 1, and finally sensor 4. The high frequency, symmetric mode arrived first, followed by the lower frequency, flexural mode at about 20 µs later on the nearest sensors, sensor 2, and about 20 µs later on sensor 3 which is slightly further away. Waves on channel 1 show the antisymmetric waves arriving possibly around 35 µs later. As shown in Fig. 7, the wave types in Fig. 10d are more complex because the thicknesses are changing over the dome. It should be noted that a significant amount of saturation occurred on the sensors, which is clear in these graphs and further evident in Fig. 11.

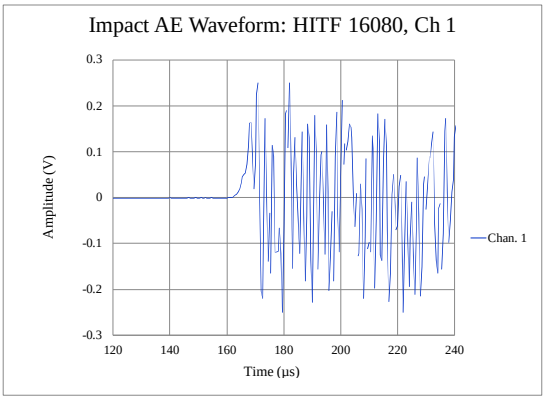

(a) Sensor Channel 1

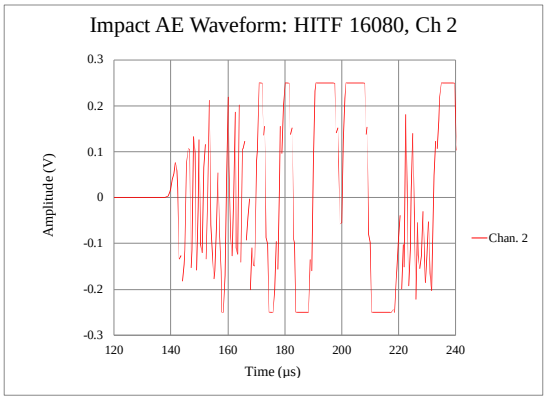

(b) Sensor Channel 2

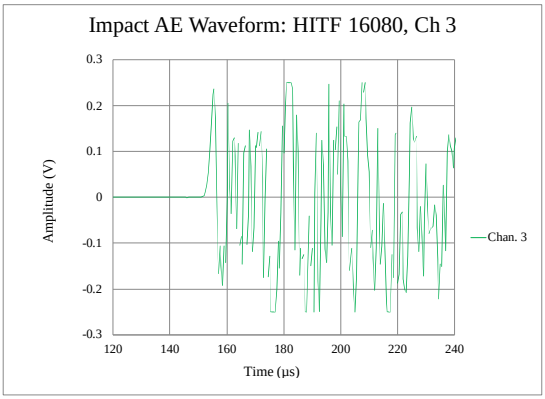

(c) Sensor Channel 3

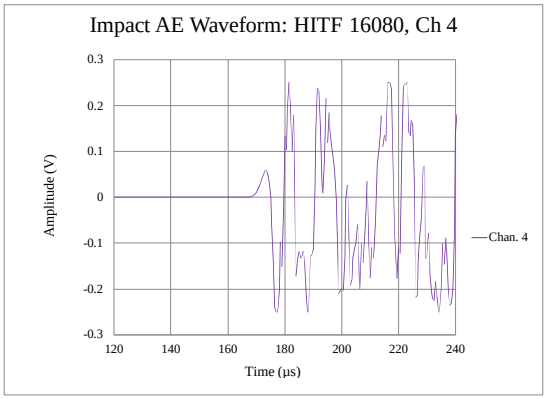

(d) Sensor Channel 4

Figure 10. Time of arrival/temporal results of HITF16080 in volts vs. time over the range of 120 to 240 µs. The vertical scale ranged from ± 0.3 V.

Fig 11 shows the voltage vs. time for the full signal of 1024 µs of data that was captured. For this shot, gains were adjusted to address the saturation in the previous shot, HITF16079 and to account for differences in the projectile's size, which was about 4.5 times less massive, than the previous shot. Even with the gain adjustments, significant saturation occurred as seen in Fig. 11. With these gain settings, the saturations were now clipping the signal at about 0.25 V in contrast to the prior shot where the clipping was evident at 0.06 V.

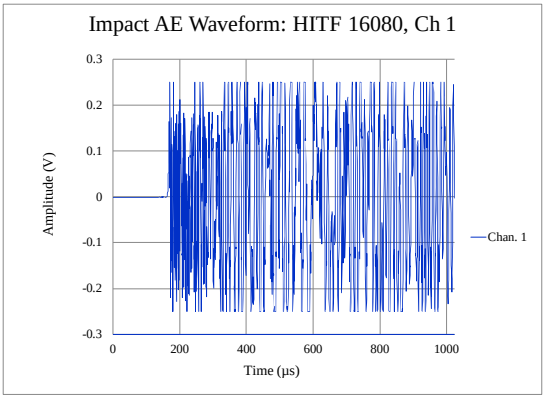

(a) Sensor Channel 1

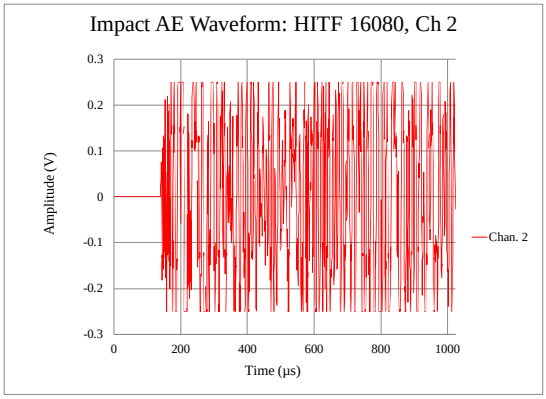

(b) Sensor Channel 2

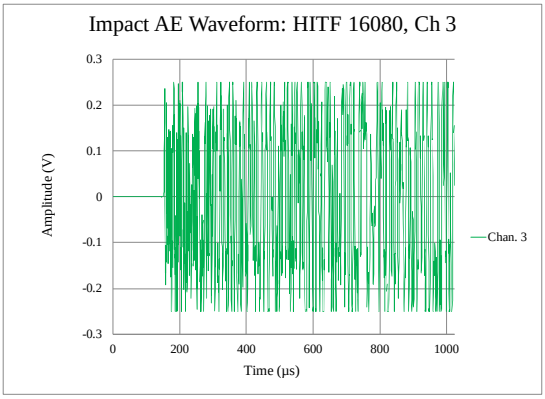

(c) Sensor Channel 3

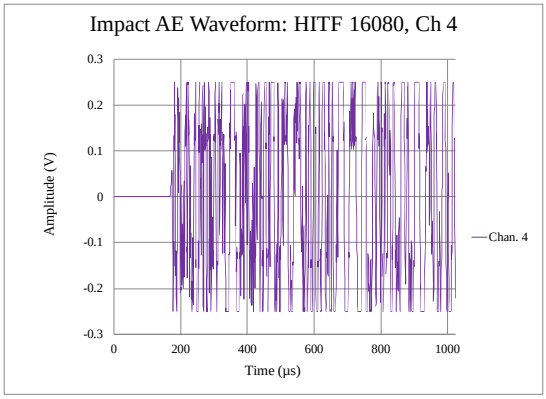

(d) Sensor Channel 4

Figure 11. Full temporal results of HITF16080 in volts vs. time over the range of 0 to 1000 µs. A significant amount of saturation occurred on the sensors.

Fig. 12 shows the amplitude vs frequency of the sensors' response to the impact of HITF16080. The signal levels peaked near 100 KHz near an amplitude of -5 dB. Again, since the sensors were heavily saturated the amplitudes are strongly attenuated. Plus, the saturation will introduce significantly higher frequency distortion. In this data, the peaks seen near 500 KHz are much weaker, which may result from the saturation effects. Finally, the added effect of the bottle's pressurization plays a large role in the differences between this shot and HTIF16078, which were similar in shot parameters.

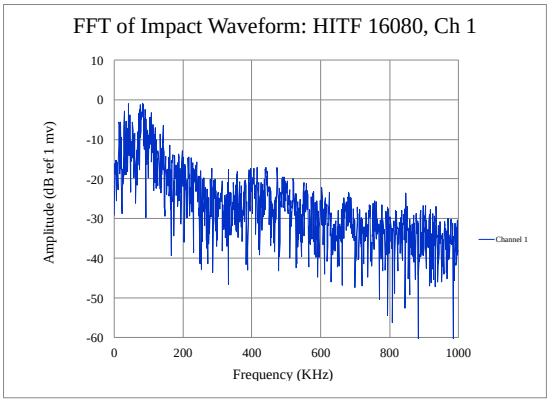

(a) Sensor Channel 1

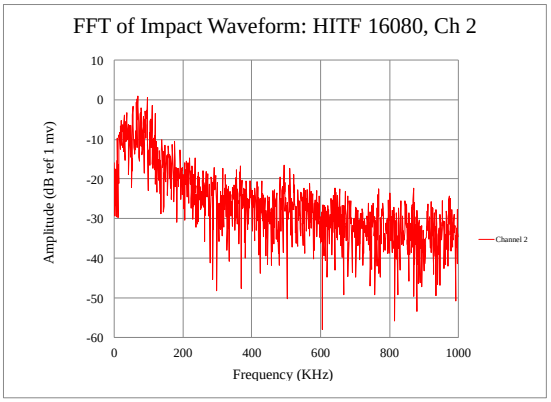

(b) Sensor Channel 2

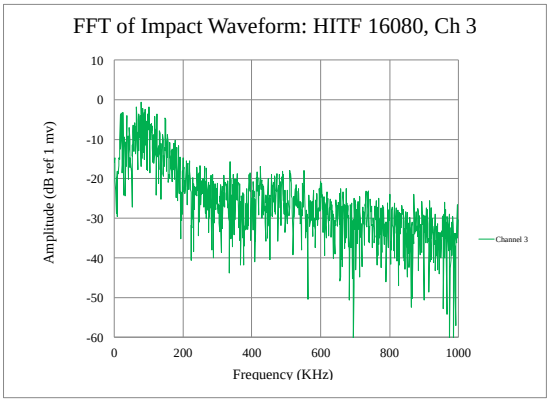

(c) Sensor Channel 3

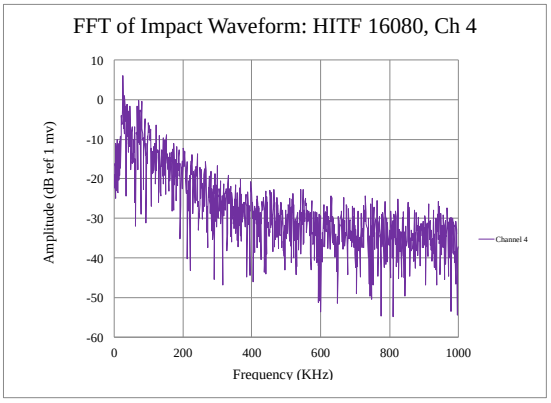

(d) Sensor Channel 4

Figure 12. Frequency results of HITF16080. The vertical data is amplitude on a dB scale referenced to 1 mV. The amplitude ranges from -60 to +10 dB.

Fig. 13 shows the signal amplitude vs. time for the four sensors mounted on the COPV for hypervelocity shot HITF16081. This was the second pressurized impact test. The projectile size and speed were comparable to the unpressurized hypervelocity shot HITF16079. Inspection of Fig. 13 shows that the first arrival signal occurred on sensor 2, followed quickly by arrival at sensor 3, then sensor 1, and then sensor 4. The high frequency, symmetric mode arrived first, followed by the lower frequency flexural mode at about 20 µs later on the nearest sensors, sensor 2, and about 40 µs later on sensor 3 which is slightly further away. Waves on channel 1 show the antisymmetric waves arriving possibly around 50 µs later. As in Fig. 10, the wave types in Fig. 13d are different in character because the COPV's wall thicknesses are varying over the dome causing the wave to show more low frequency character. With additional gain adjustments for this shot with a total gain = -6 dB, only a few saturations occurred on sensor 2.

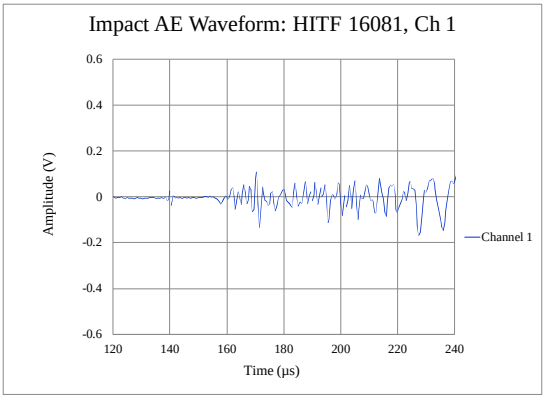

(a) Sensor Channel 1

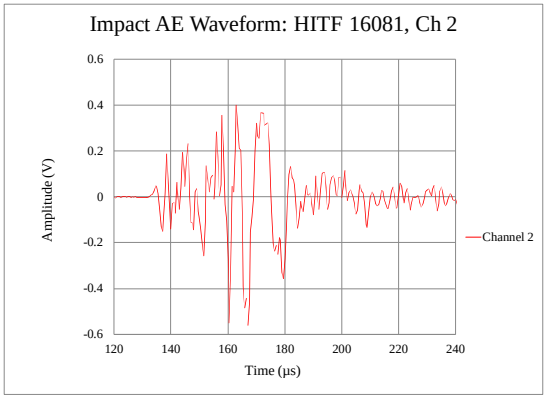

(b) Sensor Channel 2

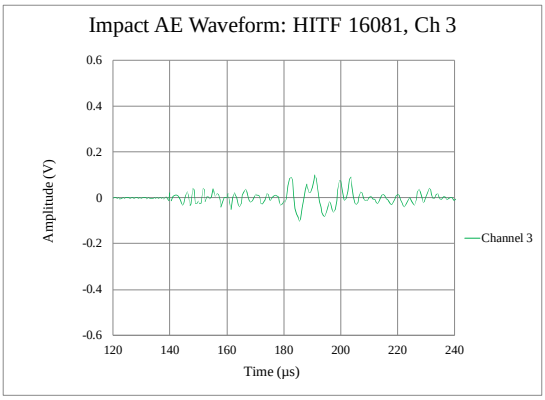

(c) Sensor Channel 3

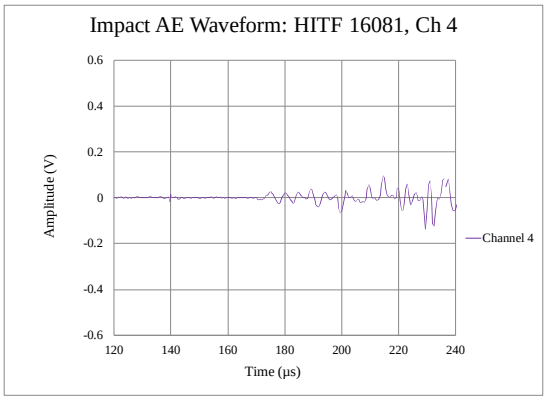

(d) Sensor Channel 4

Figure 13. Time of arrival/temporal results of HITF16081 in volts vs. time over the range of 120 to 240 µs. The vertical scale ranged from ± 0.6 V.

With those gain settings, secondary AE events are now visible above the bottle's impact signal's ring down. As seen in Fig. 14(a), there is a large signal that arrives on channel 1 at about 500 µs, which is about 350 µs after the impact trigger time. Comparison of that event and the timing of signal events from the other channels does not fit the same temporal pattern of signal arrivals from an AE event near the initial impact site. Hence, that event signal did not originate from near the impact site but from somewhere else. The large signal at sensor 1 is rather singular, with the other channels being much lower near the time of arrival time frames. The other sensors being rather low in signal amplitude near those times are compatible with the suggestion that the AE event is closer to or directly at sensor 1. Figs. 14(b), (c), and (d) also show a secondary event time near 550 µs. That time difference suggests that the events seen close in time at sensors 2, 3, and 4 are probably not related to the 500 µs signal detected at sensor 1. A closer look at the signal at 550 µs seen at sensors 2, 3, and 4, have arrival times roughly of 550 µs at sensor 2, 540 µs at sensor 3, and 560 µs at sensor 4, which is a pattern that mirrors the initial impact timing relationships, so those events are probably related to the impact site as the source. Another set of signals indicated an event was located near the axial-location of 0.027 m (1.06") and circumferential-location of 0.243 m (9.56"), which suggests that the signal source was possibly from the mounting bracket region of the bottle. It is possible there might have been some movement/recoil/ or friction at that point that generated some detectable signals.

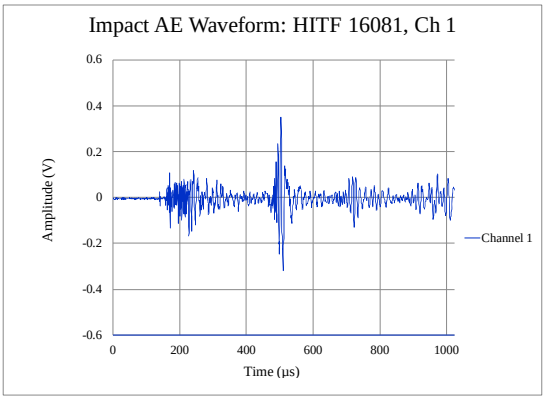

(a) Sensor Channel 1

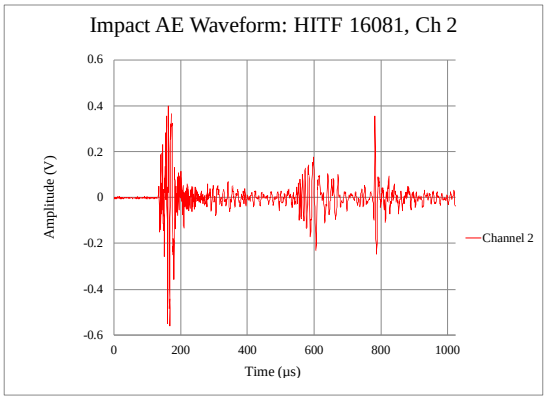

(b) Sensor Channel 2

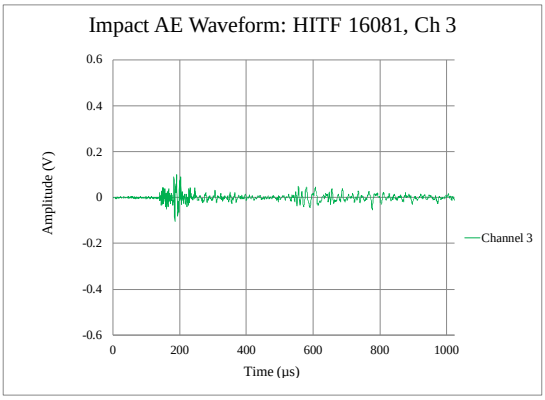

(c) Sensor Channel 3

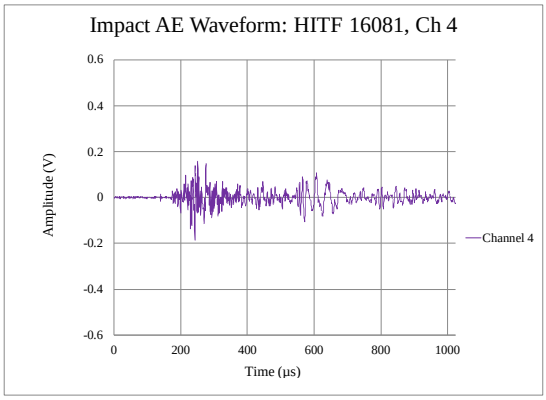

(d) Sensor Channel 4

Figure 14. Full temporal results of HITF16081 in volts vs. time over the range of 0 to 1024 µs. The vertical scale ranged from ±0.6 V.

Fig. 15 shows the amplitude vs frequency of the sensors' response to the impact of HITF16081. The signal levels peaked near 100 KHz near an amplitude of -10 to -20 dB. In this data, the peaks seen near 500 KHz are near -30 dB, similar to HTF16080. Finally, the effect of the added pressure plays a role in the differences between this shot and HTIF16079, which is shown in Fig. 9, which were similar in shot parameters. In all the remaining HVI shots, the frequency data is plotted with the vertical amplitude ranging from -70 to 0 dB and referenced to 1 mV. The frequency ranges from 0 to 1000 KHz.

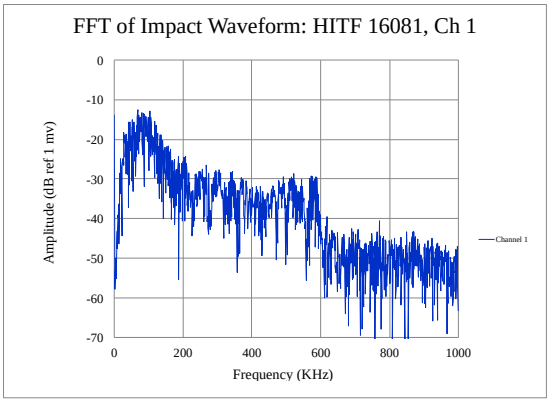

(a) Sensor Channel 1

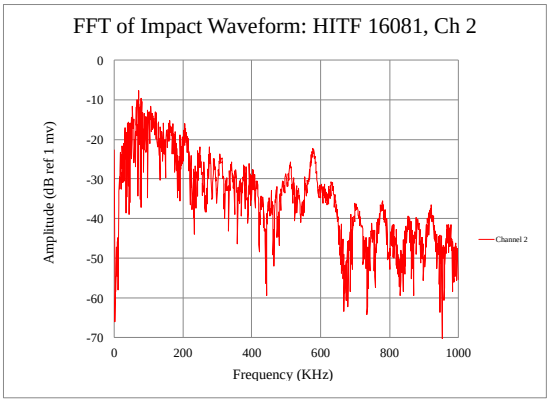

(b) Sensor Channel 2

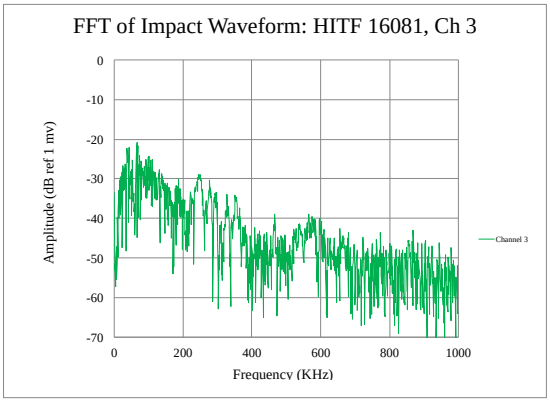

(c) Sensor Channel 3

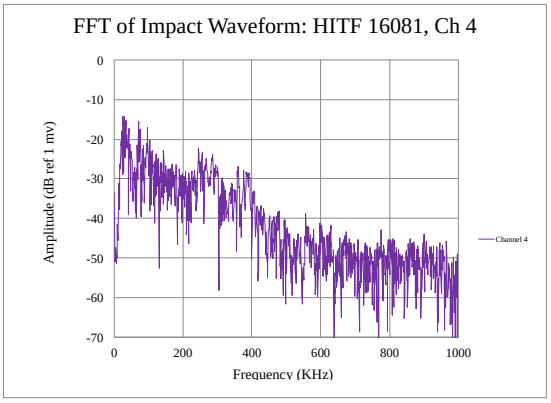

(d) Sensor Channel 4

Figure 15. Frequency results of HITF16081.

Fig. 16 shows the signal amplitude vs. time for the four sensors mounted on the COPV for hypervelocity shot HITF16159. This was the third pressurized impact test. The amplitude ranges between ±1.2 V and the time shown ranges from 120 to 240 µs. Inspection of Fig. 16 shows that the first arrival signal occurred on sensor 2, followed quickly by arrival at sensor 3, then sensor 1, and then sensor 4. The high frequency, symmetric mode arrived first, followed by the lower frequency, flexural mode at about 30 µs later on the nearest sensor, sensor 2. The antisymmetric signal on sensor 3 arrived about 35 µs after the symmetric mode arrived. Waves on channel 1 don't show the antisymmetric waves arriving very clearly. As in Fig. 13, the wave types in Fig. 16(d) are much lower in frequency because the COPV's wall thickness is different and the changes in thickness over the dome introduces complexity. With additional gain adjustments for this shot, the net attenuation was set at a 2 dB loss and now there are no measured saturation on the sensors in Fig. 16 and Fig. 17. The signal in Fig. 16 (a) has a unique character because the impact's location is very close to being directly on the opposite side from the sensor and therefore, the signal's arrival consists of waves travelling from the clockwise and counterclockwise directions. Hence, one can see two versions of the same signal very close to each other in the time signal.

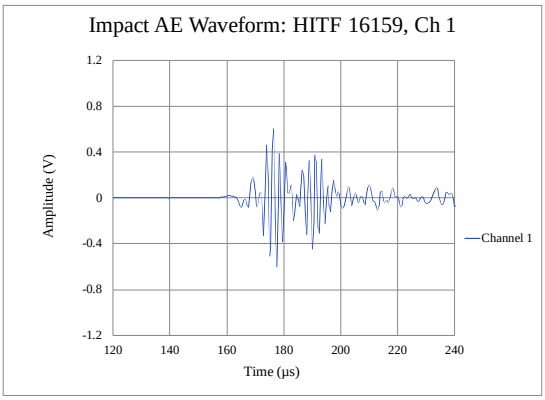

(a) Sensor Channel 1

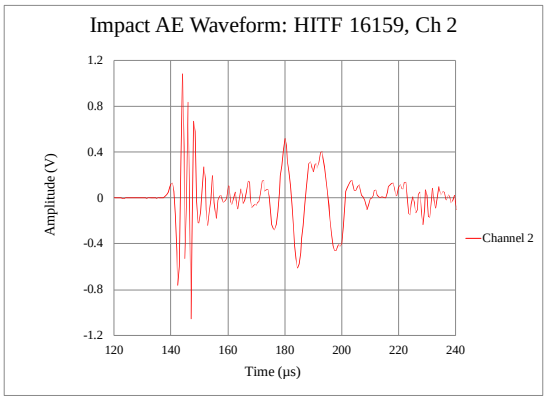

(b) Sensor Channel 2

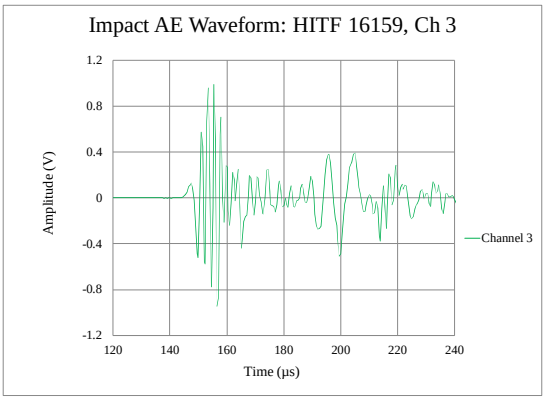

Sensor Channel 3

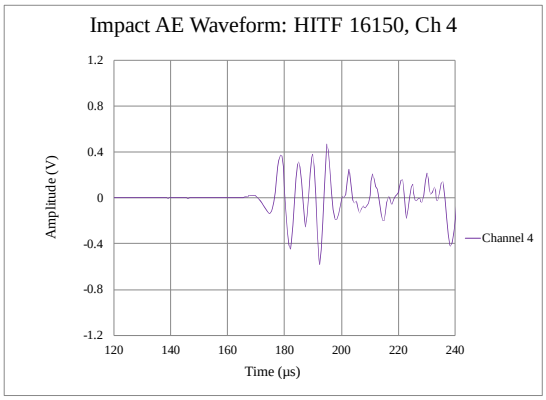

(c)

(d) Sensor Channel 4

Figure 16. Time of arrival/temporal results of HITF16159 in volts vs. time over the range of 120 to 240 µs.

Fig. 17 shows the full voltage vs. time signal. A signal on sensor 1 at roughly 500 µs doesn't appear to correlate with signals on the other signal channels. There are a few later indications on channels 2 and 3 at about 660 µs. The events on channels 2 and 3 and possibly near the 700 µs range on channel 4 might be a secondary event that aligns with a source roughly near the impact region, but the indication on channel 4 is pretty much at the noise levels after the signal's ring-down levels, as are the signals on channel 1.

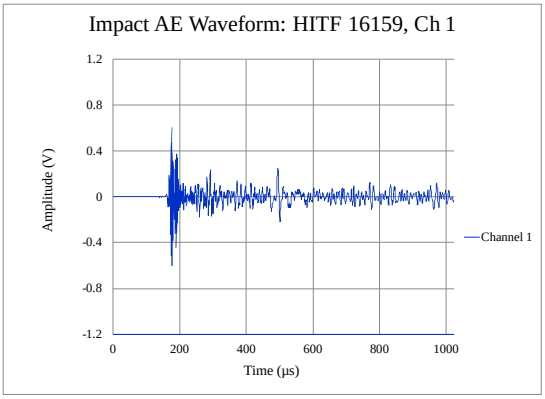

(a) Sensor Channel 1

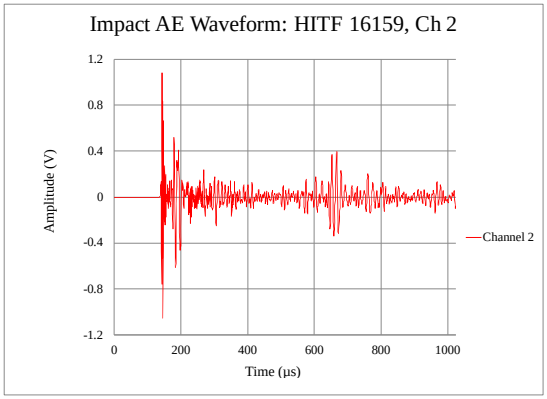

(b) Sensor Channel 2

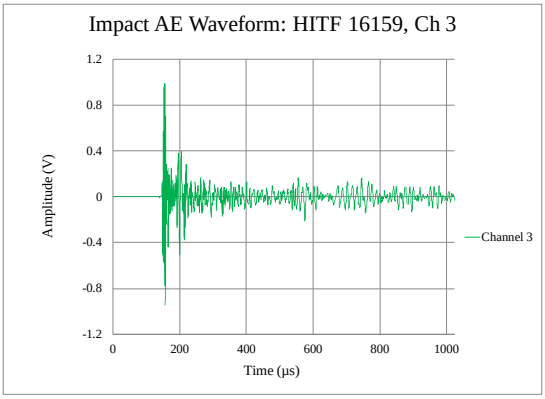

(c) Sensor Channel 3

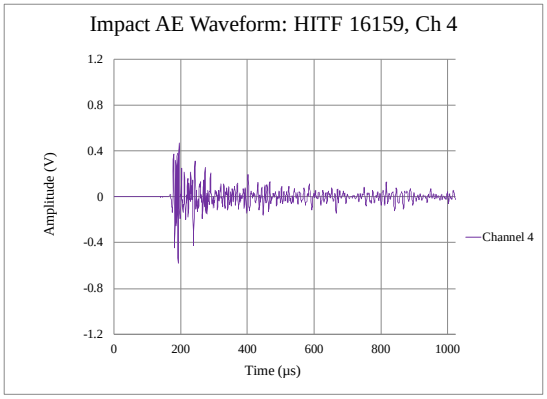

(d) Sensor Channel 4

Figure 17. Full temporal results of HITF16159 in volts vs. time over the range of 0 to 1024 µs.

Fig. 18 shows the amplitude vs frequency of the sensors' response to the impact of HITF16159. The signal levels peaked near 100 KHz near an amplitude of -5 to -15 dB. The signals near the 400-500 KHz frequency have an amplitude near -20 dB. In this data, the peaks seen near 400-500 KHz on channels 1 and 3 are almost as large as the peaks at 100 KHz. The 400-500 KHz peak on channel 2 is about 10 dB smaller than the peak at 100 KHz, and on channel 4 it is about 20 dB smaller.

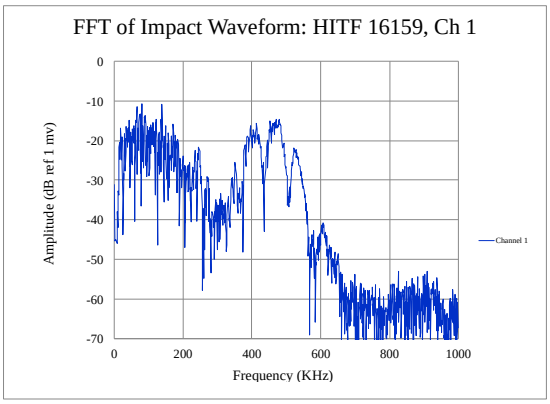

(a) Sensor Channel 1

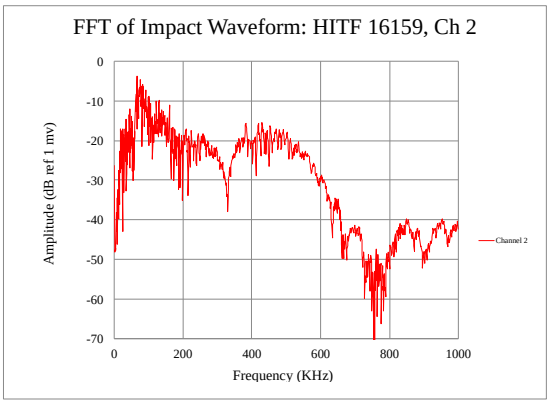

(b) Sensor Channel 2

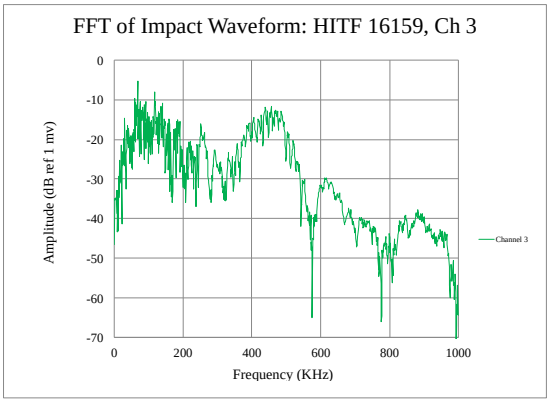

(c) Sensor Channel 3

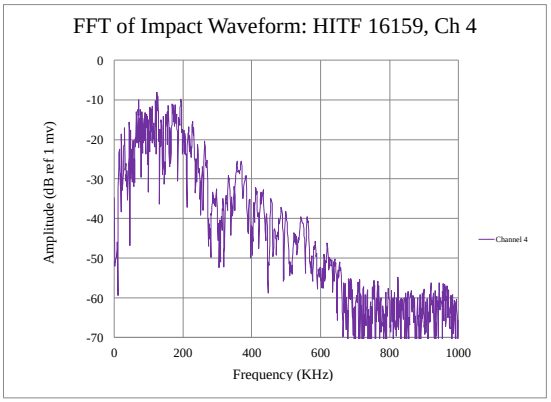

(d) Sensor Channel 4

Figure 18. Frequency results of HITF16159.

Fig. 19 shows the signal amplitude vs. time for the four sensors mounted on the COPV for hypervelocity shot HITF16163. This was the seventh pressurized hypervelocity impact in these test series. This shot was a shoulder site impact. For that sensor geometry, the first arrival signal occurred on channel 4, followed by channel 3, channel 2, and then channel 1. Sensor 4 had a few saturations in its signal. Channel 2 appeared to have suffered a partial sensor disbonding, as its signal was ~20 dB smaller than expected. As mentioned under earlier impacts, one would see low frequencies arrive first and then the higher frequencies arrive later, which is what is suggested by sensors 1, 2 and 3. Because of the COPV thickness variations at the shoulder, there might have been a wider number of frequencies generated than is seen in HVI shots in the barrel regions. For this figure and the remaining figures related to the signal-time presentations, the vertical amplitudes range from ±1.2 V unless otherwise noted in the figure caption.

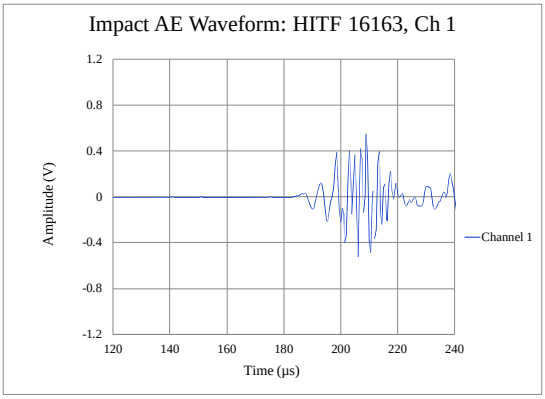

(a) Sensor Channel 1

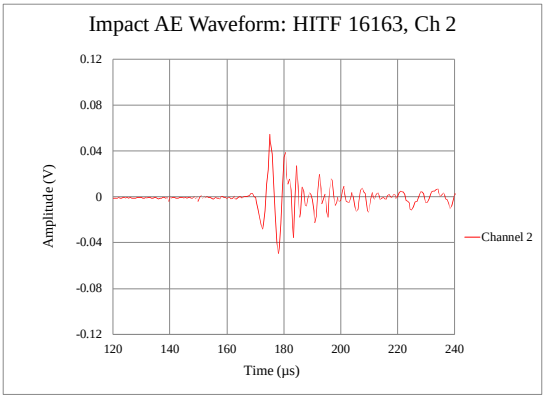

(b) Sensor Channel 2

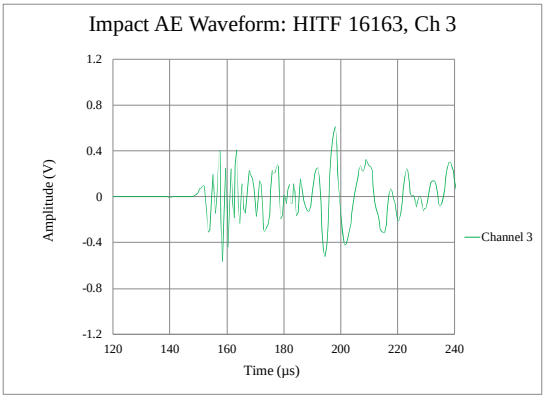

(c) Sensor Channel 3

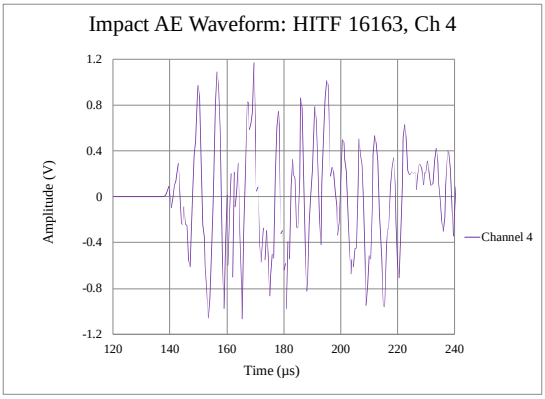

(d) Sensor Channel 4

Figure 19. Time of arrival/temporal results of HITF16163 in volts vs. time over the range of 120 to 240 µs. The vertical scale on channel 2 ranged from ± 0.12 V.

Fig. 20 shows the full time vs voltage plots of the data for HTIF16163. After the previous shot, HITF16162, which resulted in the bottle detonation just after 1ms, the time scale was expanded to 2048 µs to capture such failures on subsequent tests. A small amount of saturation appeared to occur on sensor 4, which was the closest sensor to the impact. Relatively large secondary events seemed to occur for sensor 3 at roughly 500 µs, on sensor 1 at roughly 600 µs, and followed by sensor 2 at roughly 650 µs. The timing of those secondary signal events times indicate signals that were not related to a single event source within the COPV. Other secondary signal events in this data did not arise above the background signal ring-down sufficiently to make any clear timing references for triangulations on this bottle.

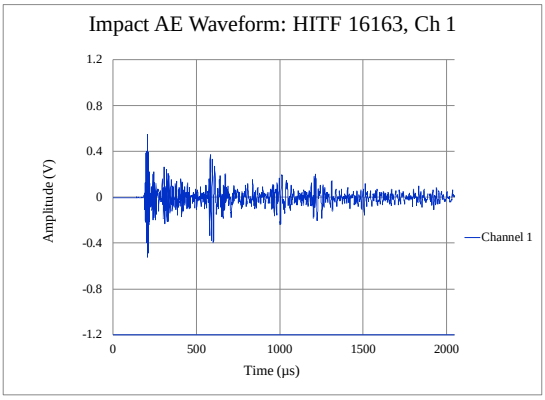

(a) Sensor Channel 1

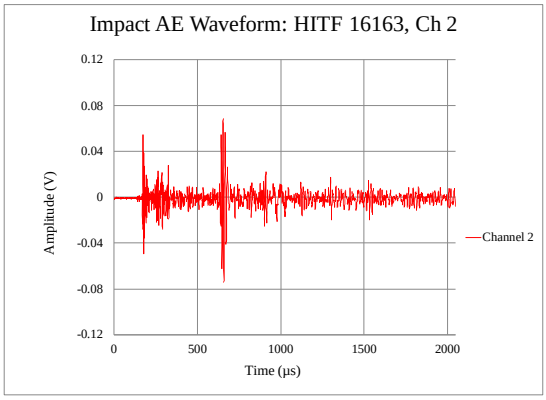

(b) Sensor Channel 2

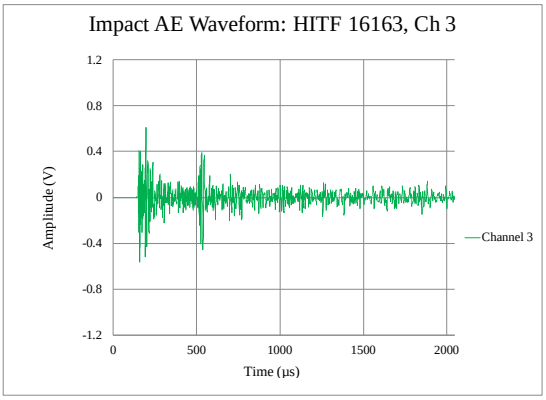

(c) Sensor Channel 3

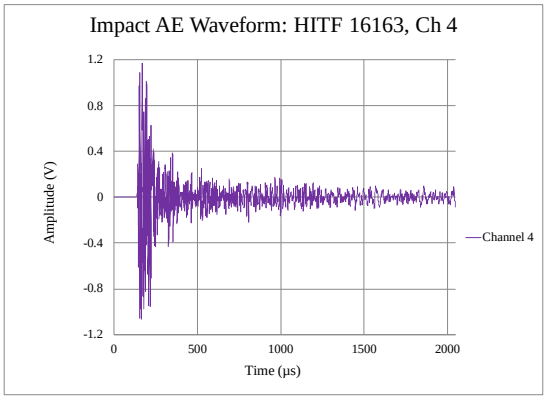

(d) Sensor Channel 4

Figure 20. Full temporal results of HITF16163 in volts vs. time over the range of 0 to 2048 µs. The vertical scale on channels 1, 3, and 4 ranged from ± 1.2 V. The vertical scale on channel 2 ranged from ± 0.12 V.

Fig. 21 shows the amplitude vs frequency of the sensors' response to the impact of HITF16163. The signal levels peaked near 100 KHz near an amplitude of -5 to -10 dB, except for channel 2 which appeared to have a 20 dB signal loss, hence that channel is -25 dB in amplitude. Channels 1 to 3 show a strong peak near the 500 KHz frequency. The peak at ~500 KHz probably is shifted to lower frequencies on channel 4, because channel 4 is on the "dome" region, which has varying thicknesses.

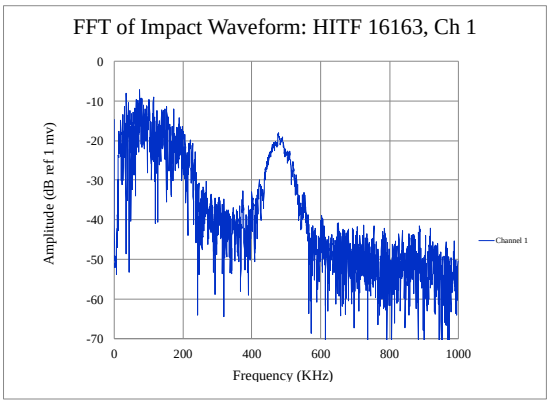

(a) Sensor Channel 1

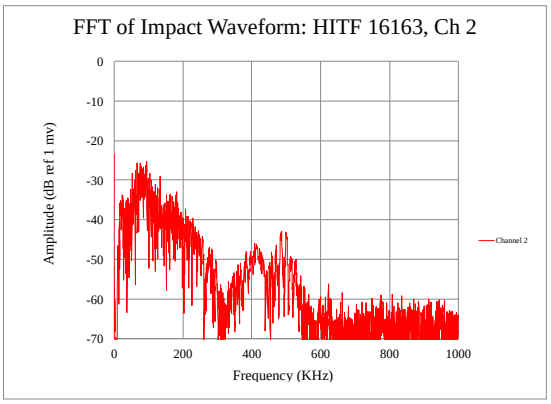

(b) Sensor Channel 2

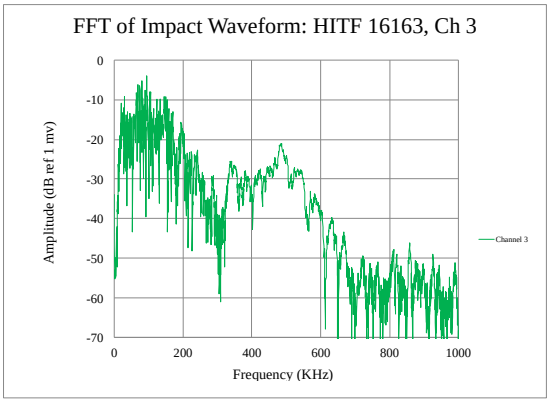

(c) Sensor Channel 3

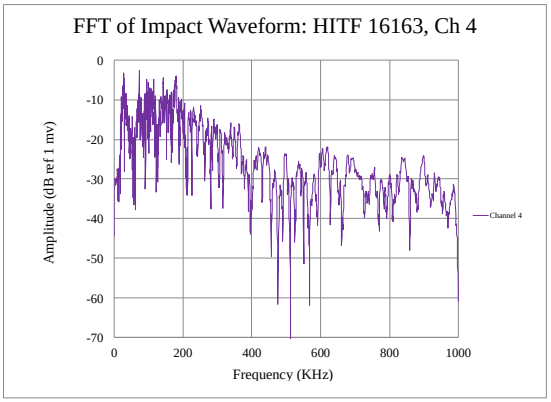

(d) Sensor Channel 4

Figure 21. Frequency results of HITF16163.

Fig. 22 shows the signal amplitude vs. time for the four sensors mounted on the COPV for hypervelocity shot HITF16171, the fifteenth pressurized shot. The figure shows the 120 µs of the early data. The first arrival signal occurred on channel 2, followed by channel 3, and channel 1. Channel 4 did not record any data.

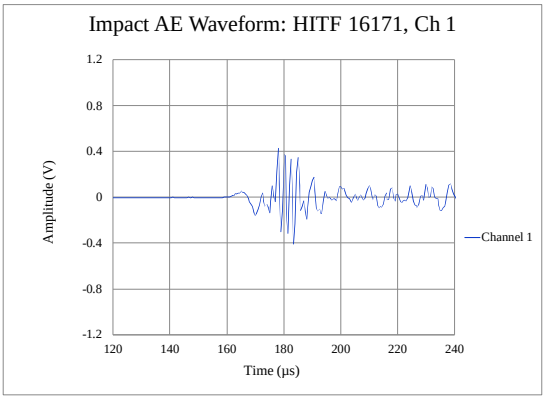

(a) Sensor 1

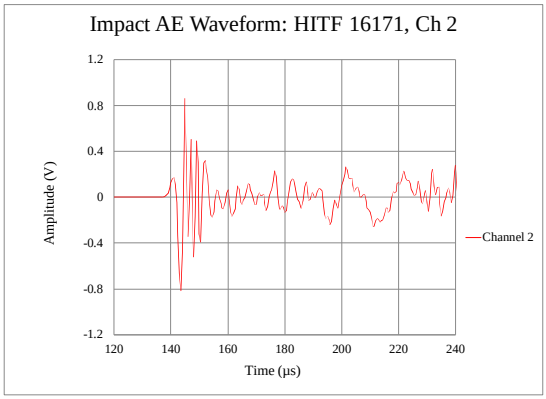

(b) Sensor Channel 2

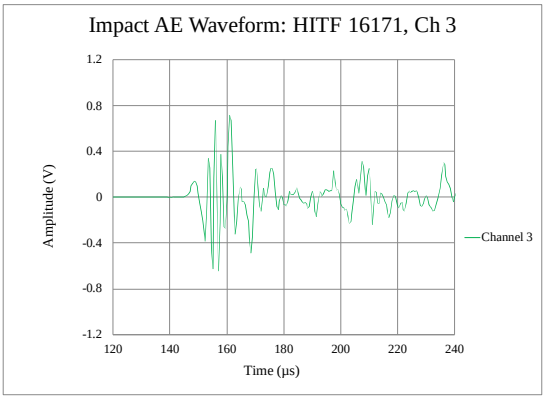

(c) Sensor Channel 3

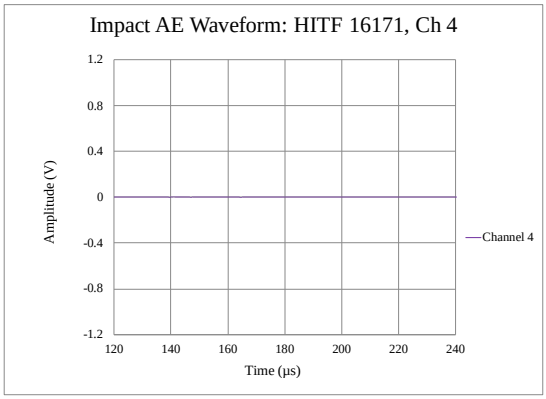

(d) Sensor Channel 4

Fig. 22. Time of arrival/temporal results of HITF16171 in volts vs. time over the range of 120 to 240 µs. Sensor 4 did not record any data.

Fig. 23 shows the full time vs voltage plots for HITF16171. Relatively large secondary events seemed to occur for sensors 1 to 3 at roughly 500 µs in the data. A review of some larger secondary signals showed that there were never three clear sensor events that correlated for the impact event location, which was like previously discussed results.

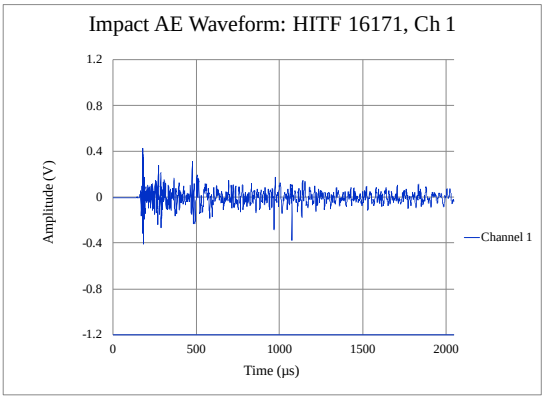

(a) Sensor Channel 1

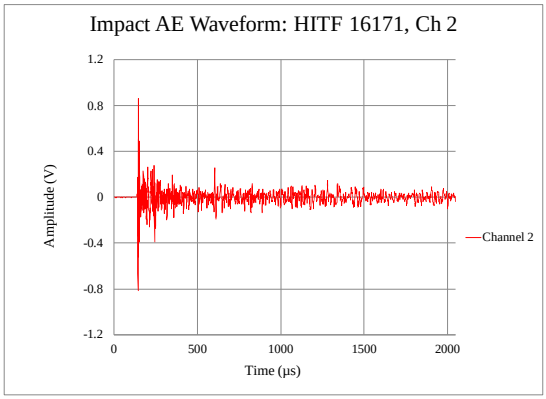

(b) Sensor Channel 2

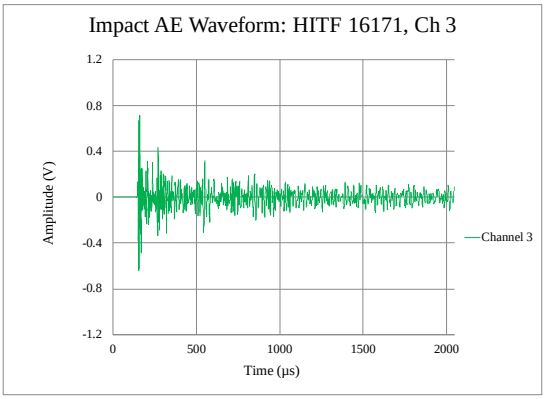

(c) Sensor Channel 3

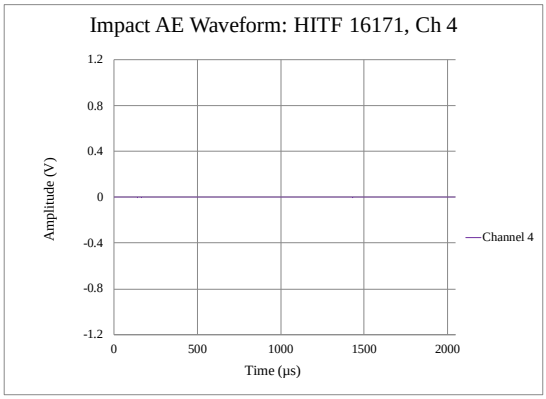

(d) Sensor Channel 4

Figure 23. Full temporal results of HITF16171 in volts vs. time over the range of 0 to 2048 µs. In this test, sensor 4 recorded no signal. The horizontal time scale ranges from 0 to 2048 µs.

Fig. 24 shows the amplitude vs frequency of the sensors' response to the impact of HITF16171. The signal levels peaked near 100 KHz near an amplitude of -10 dB, except for channel 4, which did not record a signal. Channels 1 to 3 show a strong peak near the 400-500 KHz frequency having an amplitude near -20 to -25 dB.

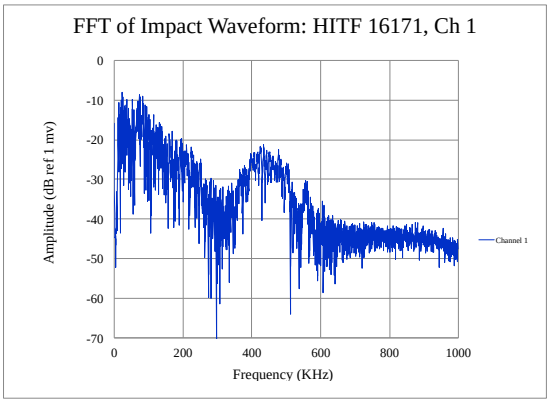

(a) Sensor Channel 1

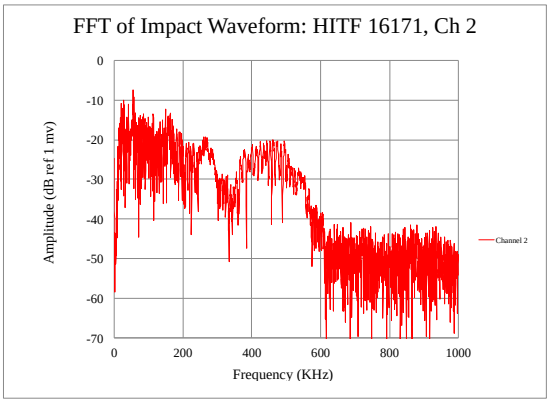

(b) Sensor Channel 2

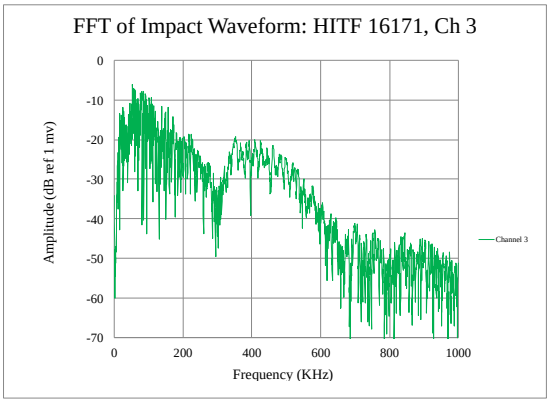

(c) Sensor Channel 3

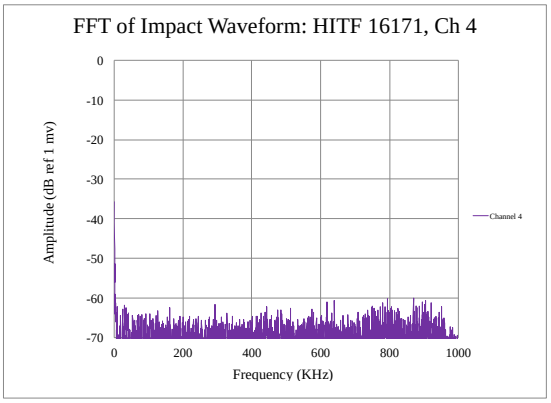

(d) Sensor Channel 4

Figure 24. Frequency results of HITF16171.

Table 4 shows the targeting parameters and the relative times of arrival from the trigger signal that were measured for the impact signal on each sensor for the list of shots shown in Table 2. These temporal reference times were subsequently used in the fitting algorithm to identify the estimated impact location. Most of the hypervelocity shots in these tests were done at approximately the same axial locations on the cylindrical section of the bottles, except HITF16163, which was a shoulder shot.

Table 4. List of target locations and the corresponding temporal results of HVI shots shown in Table 2

Test Number / HITF Number/ Tank S/N / Impact Region	Target position axial (m)	Target position circum. (deg)	Target angle (deg)	Delta time sensor 1 (μs)	Delta time sensor 2 (μs)	Delta time sensor 3 (μs)	Delta time sensor 4 (μs)
Pathfinder							
#A HITF16078 S/N 195 Cylinder	0.254	0	-45	7.5	13.5	0	38.5
#B HITF16079 S/N 190 Cylinder	0.254	90	-45	27	0	25.5	48
#1 HITF16080 S/N 201 Cylinder	0.254	180	-45	24.4	0	13.8	29.3
#2 HITF 16081 S/N 203 Cylinder	0.254	180	-45	22.5	0	7.5	40
Part 1							
#3 HITF16159 S/N 190 Cylinder	0.254	180	-45	25.5	0	7	30.5
#7 HITF16163 S/N 194 Shoulder	0.0805	180	-45	35.5	21.7	0	-10.4
Part 2							
#15 HITF16171 S/N 202 Cylinder	0.254	180	-45	23	0	7	--

Table 5 lists the measured impact locations in the COPVs that were not penetrated and the resultant estimates of the impact locations computed from the data in Table 4 and the sensor locations. The table also computes the accuracy of the computed position estimate relative to the actual measurements. As explained in the section "COPV AE Wave Velocity Measurements" from the first two unpressurized bottles listed in the table, a 10-20% increase in the symmetric wave speed was required to get accurate impact locations on the subsequent pressurized bottles in this section because of pressurization and temperature effects on the velocity of ultrasound in the bottle's walls. For the rest of the testing, where the bottles were penetrated, a velocity adjustment of 20% was made to the velocities of Fig. 3 for computing the impact locations in those bottles.

Table 5. Impact location table for non-penetrating impact showing the AE triangulation results. Increases in the velocity values of 10 to 20% were required because of pressurization effects on the bottles compared to the unpressurized bottle velocities. Accuracies in the location estimation and are noted in the 7th column of the table. Finally, the shoulder shot was computed as if it was located on the barrel area even though it was just above that region. Note, Bottle #190 was used for two impact tests.

Shot No.	Bottle #	Axial Location of Impact (in)	Circum. Location of Impact (m)	Estimated Axial Location of Impact (m)	Estimated Circum. Location of Impact (m)	Velocity Adjustment for Pressure*	Location Error (m)
HITF16078	195	0.264	-0.0318	0.276	-0.0099		0.0251
HITF16079	190	0.300	0.130	0.310	0.130		0.0102
HITF16080	201	0.248	0.248	0.266	0.275	additional 10%	0.00968
HITF16081	203	0.264	0.257	0.276	0.256	additional 20%	0.0126
HITF16159	190	0.257	0.229	0.237	0.252	additional 20%	0.0313
HITF16163	194	0.086	0.270	0.0686	0.277	additional 10%	0.0185
HITF16171	202	0.232	-0.227	0.259	-0.247	additional 10%	0.0337

*Note, velocity shifts were required due to the pressurization effects as noted in text.

Post impact AE event data.

After the initial impact signals on bottles that did not penetrate, the equipment was monitored for additional events. These events could indicate that the pressurized bottles were continuing to suffer matrix and fiber damage due to the stresses in the pressure wall. In all those bottles, the gain had to be adjusted upward post impact. This required that the measurements be halted while the gain settings were being adjusted on the equipment. During that period, the HVI gun operator was also venting gases from the gun barrel, which would trigger the AE equipment if it was actively monitored at that moment. For the first two pressurized bottles tested, HITF16080 and HITF16081, the AE equipment

was monitored for one-hour post impact. During the first pressurized test, there were four post impact triggers that had signals commensurate with fiber matrix damage generating AE like signals. These signals all occurred within the first 10 minutes after the impact. Table 6 lists the event times, event location estimates in minutes after impact, and the signal energies of the AE events. During the second test, there was one post impact trigger that had signals commensurate with a fiber matrix event causing AE like signals. That event occurred within a few minutes after the impact. Since the post

Table 6. Event location table, resulting from non-penetrating impacts. Includes the AE triangulation calculation for AE events for the initial impact plus subsequent events that were recorded post impact. The table also shows the signal energy levels of each event.

Shot No.	Bottle #	Axial Location of Impact (m)	Circum. Location of Impact (m)	Estimated Axial Location of Impact (m)	Estimated Circum. Location of Impact (m)	Time from HVI shot (in min)	Distance from impact Location Estimate (m)	Average Total Signal Energy (in V^2-µs)
HITF16080	201	0.248	0.248	0.266	0.275	0	0.0968	1.63E+02†* (~5.04E-01)**
1st event post shot				0.266	0.271	0.38	0.0297	3.44E-01*
2nd event post shot				0.293	0.303	3.95	0.0714	4.18E-02*
3rd event post shot				0.216	0.120	4.08	0.132	3.91E-02*
4th event post shot				0.300	0.348	6.51	0.113	9.29E-02*
HITF16081	203	0.264	0.257	0.276	0.256	0	0.0126	2.16E+00**
1st event post shot				0.256	0.288	1.22	0.0126	6.06E-01*
HITF16159	190	0.257	0.229	0.237	0.252	0	0.0313	7.12E+00**
HITF16163	194	0.086	0.270	0.069	0.277	0	0.0185	1.34E+01˜
HITF16171	202	0.232	-0.227	0.259	-0.247	0	0.0337	5.40E+00˜
1st event post shot				0.259	-0.257	10.46	0.0406	5.57E-01˜

† Significant saturation present, which resulted in lost information. Estimated energy is relative to HITF16081 projectile energy ratio to HITF16080.
* Signal length is 1024 µs.
** Signal length is 1024 µs. Signal Energy was adjusted to represent 2048 µs. **(**see "Signal Energy and AE Results" section)
˜ Signal length is 2048 µs

impact AE signals all occurred within the first ~10 minutes after impact, subsequent bottles that did not result in penetration were only monitored for about 10 minutes.

HITF16171 had a post impact event that occurred just after the 10-minute mark and was recorded. Two of the pressurized bottles with non-penetrating impacts did not record any post impact AE events. In bottle 201, HITF16080, the four post impact events had axial dimensions not too far from the axial location of the impact point, but the circumferential location dimensions were greater and seemed to correlate roughly with more distance from impact. The 1st, 2nd, and 4th post impact events seemed to have positions diagonal to the impact locations and circumferentially counterclockwise from the impact location. The 3rd post impact event was clockwise diagonal from the impact location. This suggests that the helical fiber directions are more affected by the impact than the hoop directions at these damage orientations.

Also of interest was the signal energy of these events. Comparing the signal energies from the impacts with subsequent AE event noises in Table 6 show that the impact signal energies from the impacts are much greater than the signal energies for AE events that followed the impact. The estimate for the signal energy from HITF16080 had a signal energy nearly 1 to 2 orders of magnitude larger than the following AE events in that bottle. The first AE event after the impact, which occurred about 30 seconds after the impact was about one order of magnitude smaller, and the subsequent later events at two orders smaller. Similarly, HITF16081 had a following AE event with a signal energy about two orders of magnitude smaller. HITF16171 had a secondary AE event that was about three orders of magnitude smaller than the signal energy from the impact. It appears that because there weren't very many succeeding AE events to these impacts that the damage growth quickly stabilized in the damaged, but unpenetrated COPVs.

The signal energy for impact shot 16080 was highly saturated which makes the energy calculation in that case inaccurate. If we assume that the signal energy of the impact is proportional to the energy of the projectile, then by comparing HITF16080 with HITF16081, we would estimate that the signal energy of the impact would be about 1.6×10^{1} V^2 μs. Comparing the signal energies of the pressurized impact bottles from Table 6 with the projectile energies in table 2 one can see that there is a rough correlation between the two energies: as the projectile energies increase, so do the average signal energies for these impacts on the COPVs, which support the assumption about the correlation between the signal energies and the projectile energy between HITF16080 and HITF16081.

Fig. 25 shows a graph of the relationship between projectile energies and the resulting average signal energies recorded by the four sensors attached to the COPV. As noted in the earliest impact test, HITF16080, had significantly saturated signals and hence are not reported in this graph because of the distortion that saturation introduces into a signal energy calculation. Two of the impact tests in this graph had a signal length of only 1024 μs, while the other two had signal lengths of 2048 μs. With the shorter data lengths, their signal energy was adjusted to represent 2048 μs as explained in the section on "Signal Energy and AE Results". In Fig. 25, the projectile energies ranged from 4 to 127 J for impact numbers HITF16081, HITF16159, HITF16163 and HITF16171. The signal energies represent several noise sources, such as the impact noise and noise from subsequent damage growth in the COPV. Since the projectile did not penetrate the pressure wall, almost all the projectile energy will be deposited into the COPV wall with resulting damage in the form of a small crater, plus there will be damage growth resulting from the shock wave in the COPV wall generated by the impact and the high resulting stresses from the pressure and the damage near the impact point and any residual stresses within the COPV. These damage growth mechanisms will generate AE noises that contribute to the signal levels besides the impact noise.

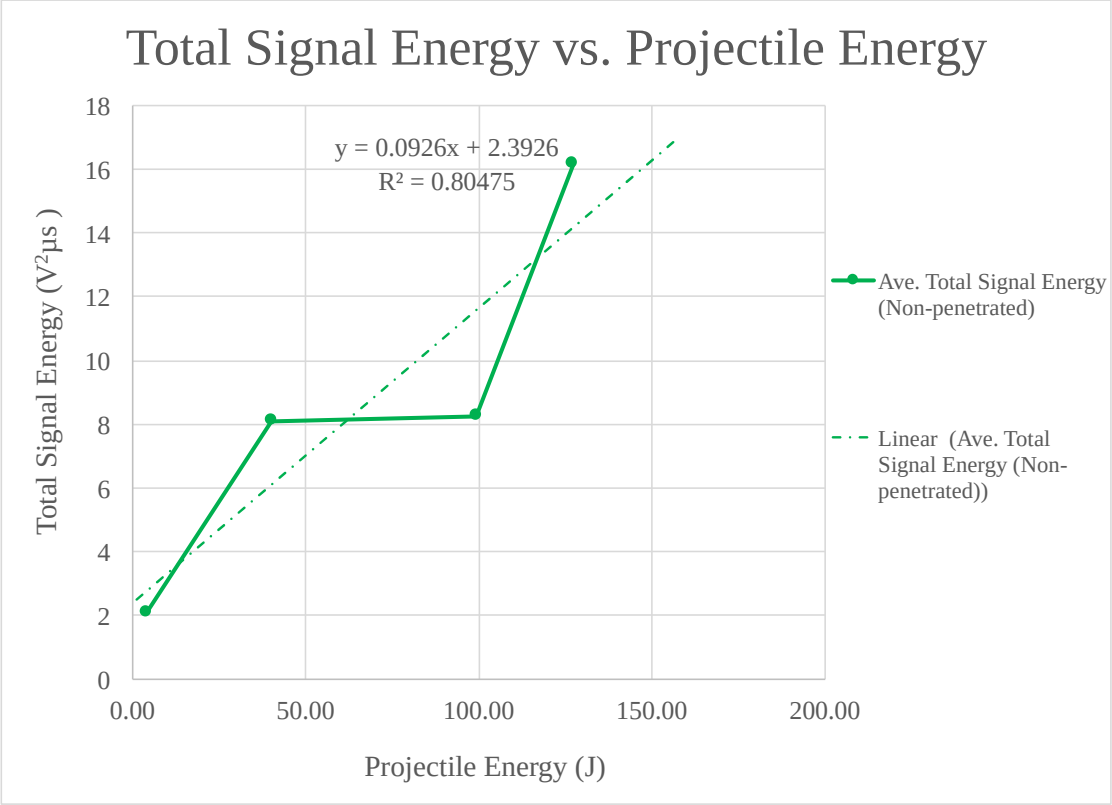

Figure 25. Shows the relationship between projectile energies for projectiles that did not penetrate the pressurized COPV wall of HITF16081, HITF16159, HITF16163 and HITF16171 and the resulting average signal energies recorded by the four sensors mounted on the COPV. The vertical scale is the signal energy and scales from 0 to 18 V^2 µs. The horizontal scale is the projectile energy and ranges from 0 to 200 J. The general trend is roughly an increasing linear relationship.

Fig. 26 shows the relationship between the impact signal energies vs. damage circumference and Fig. 27 shows the relationship between the impact signal energies vs. damage area. The circumference and area of damage is estimated from equations for ellipses with the major and minor axis known, which is taken from the measurements reported in Table 3. These AE signals, which were the same data shown in Fig. 25, are not saturated signals and hence not biased by saturation in the data. Both graphs show the total signal energy of each sensor and their average values. Both graphs also show moderate correlation coefficients for a linear line of the average data, with the correlation to the damage area being slightly better than the correlation with the damage circumference. Presumably, the correlation with damage volume might be even better, since the three-dimensional crater might correlate better with the projectile's energy. Unfortunately, the impact's crater depth was not available so that volumetric comparison with projectile energy wasn't graphed.

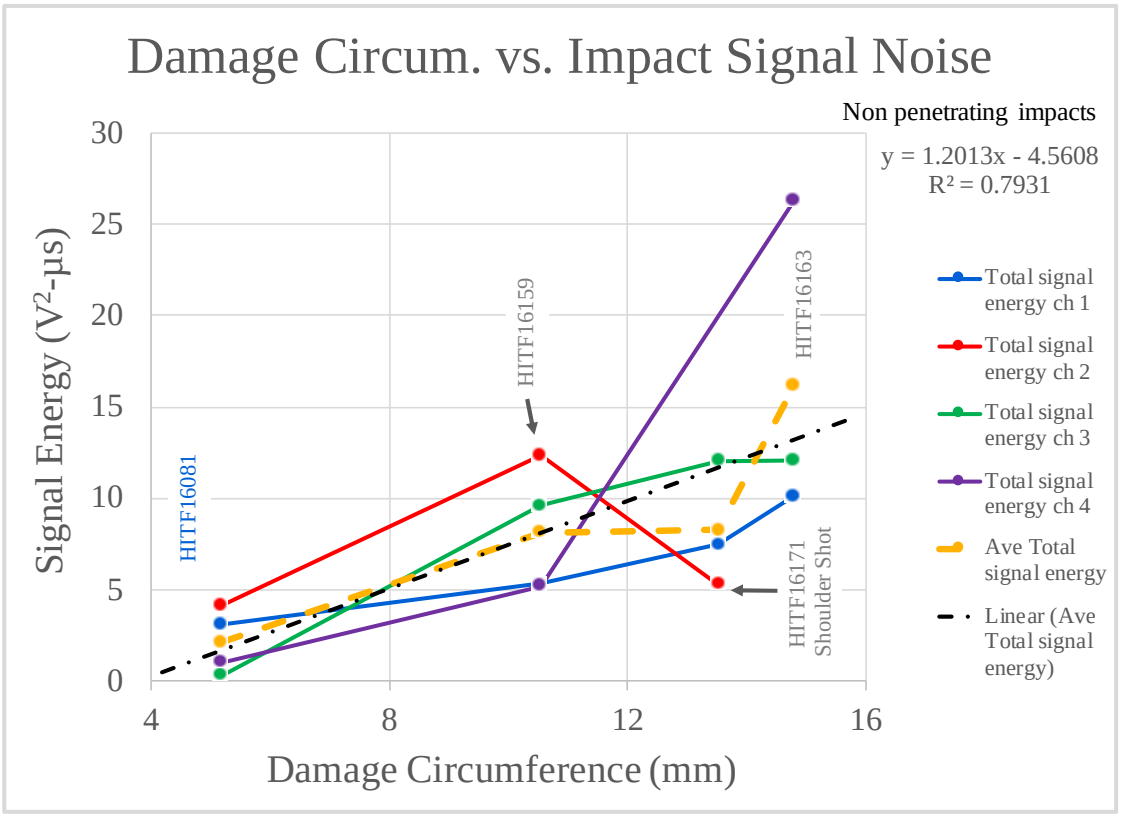

Figure 26. Shows the relationship between the impact's damage circumference and average signal energy for projectiles that did not penetrate the pressurized COPV wall. The horizontal axis is the estimate of the damage circumference at the outer wall surface, which was based on the assumption of an elliptical-shaped damage region. The general trend of the average total signal energy is roughly an increasing linear relationship.

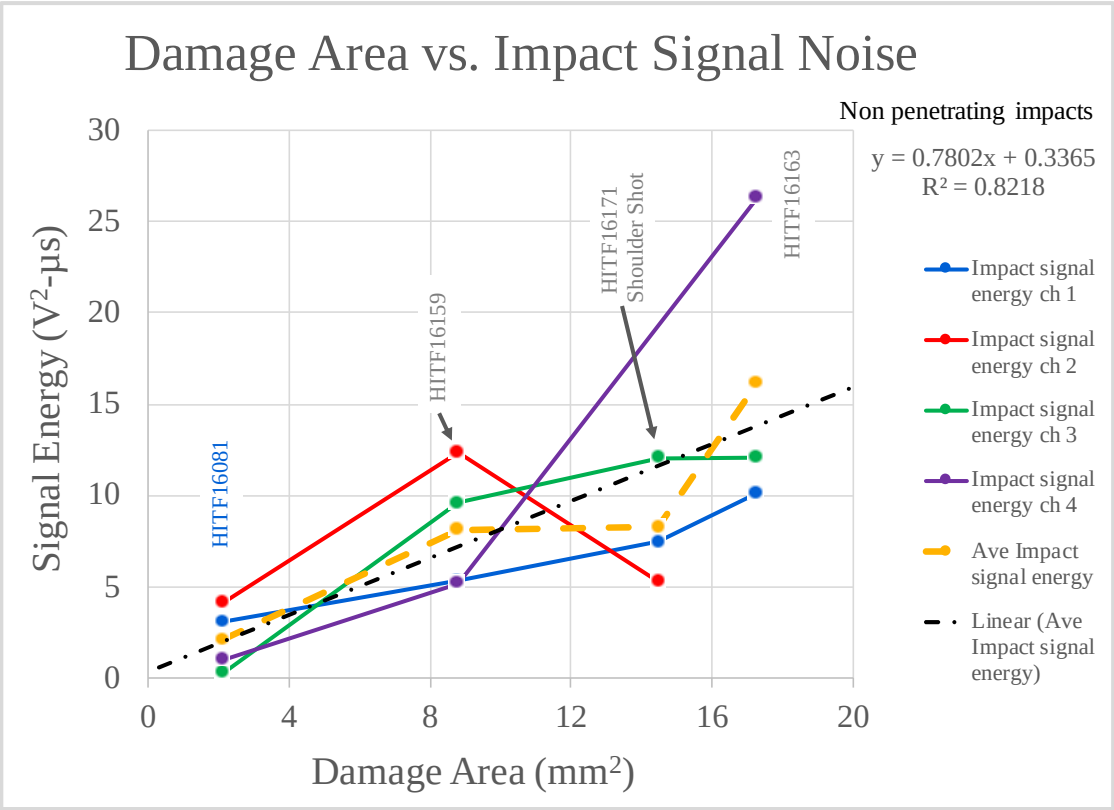

Figure 27. Shows the relationship between impact's damage area and average signal energy for projectiles that did not penetrate the pressurized COPV wall. The horizontal axis is the estimate of the damage area at the outer wall surface, which was based on the assumption of an elliptical-shaped damage region. The general trend is roughly an increasing linear relationship.

Penetrated and Vented Shots

Table 7 is a listing of the hypervelocity shot parameters for the six cases where the projectile penetrated the COPV's wall, resulting in the gas venting but did not cause these bottles to detonate. These puncturing shots were in the cylinder region except for the one shoulder shot, HITF16164. These HVI shots were made with aluminum projectiles, except for HITF16504B, which was a small but denser stainless steel projectile. The projectile energies ranged from 127 to 308 J. The projectile momenta ranged from 0.036 to 0.0856 Kg-m/s. The column labelled "Perpendicular Momentum" is the momentum component perpendicular to the surface at the impact point. Table 8 describes the resulting damage for each of the shots in Table 7.

Table 7. provides a listing of the hypervelocity shot parameters for the six cases where the projectile penetrated the COPV's wall and resulted in the gas venting, but did not rupture the COPV.

Test Number / HITF Number/ Tank S/N / Impact Location	**Actual tank Pressure (psi)**	**Projectile Type**	**Projectile Diameter (m)**	**Actual Projectile Mass (Kg)**	**Actual velocity (m/s)**	**Impact Angle (deg)**	**Projectile Energy (J)**	**Momen-tum (Kg-m/s)**	**Perpen-dicular Momen-tum (Kg-m/s)**
Part 1									
#4 HITF16160 S/N 193 Cylinder	4186	Al 2017-T4	0.00152	0.00000510	7060	48	127.10	0.0360	0.0241
#8 HITF16164 S/N 223 Shoulder	4214	Al 2017-T4	0.00201	0.0000119	7190	45	307.59	0.0856	0.0605
Part 2									
#9 HITF16165 S/N 205 Cylinder	4226	Al 2017-T4	0.00172	0.00000741	7230	45	193.67	0.0536	0.0379
#10 HITF16166 S/N 192 Cylinder	4075	Al 2017-T4	0.00151	0.00000505	7240	0	132.35	0.0366	0.0366
#13 HITF16169 S/N 198 Cylinder	4220	Al 2017-T4	0.00201	0.0000119	7080	60	298.50	0.0843	0.0422
#16 HITF16504 B S/N 201 Cylinder	4175	SS	0.00110	0.00000534	7130	45	135.73	0.0381	0.0269

Table 8 List of Results of HVI shots that penetrated and vented the COPV and are shown in Table 7

Test Number / HITF Number/ Tank S/N / Impact Location	**Damage Assessments (mm)**
Part 1	
#4 HITF16160 S/N 193 Cylinder	**Venting occurred/no rupture. Overall impact damage** = severed fibers and ply delamination present that has a 14.9 maximum height and extends completely around tank from origin of impact. **Crater dimensions** = perforation. **Maximum crater depth** = perforation. **Sub-surface damage** = TBD. **Liner damage** = 2.0 x 2.3 irregular shaped perforation, no cratering or pitting found on far side liner.
#8 HITF16164 S/N 223 Shoulder	**Venting occurred/no rupture. Overall impact damage** = severed fibers and ply delamination present that has a maximum height of 39.4 that runs from 9 o'clock to 3 o'clock from the origin of impact that has a maximum length of 124.3. Projectile impacted 90.0 from tank boss. **Crater dimensions** = N/A. **Maximum crater depth** = N/A. **Sub-surface damage** = TBD. **Liner damage** = 6.1 x 5.3 perforation, four fragments found within the COPV tank post-test (likely liner material), with the largest being 6.0 x 5.6 (irregular shaped).
Part 2	
#9 HITF16165 S/N 205 Cylinder	**Venting occurred/no rupture. Overall impact damage** = severed fibers and ply delamination present that has a 17.3 maximum height and extends around tank from origin of impact. **Crater dimensions** = perforation. **Maximum crater depth** = N/A. **Sub-surface damage** = TBD. **Liner damage** = 3.3 x 3.3 perforation, a single 3.8 x 3.7 (irregular shaped) fragment found within the COPV tank post-test (likely liner material).
#10 HITF16166 S/N 192 Cylinder	**Venting occurred/no rupture. Overall impact damage** = severed fibers and ply delamination present that has a 16.3 maximum height and extends around tank from origin of impact. **Crater dimensions** = N/A. **Maximum crater depth** = N/A. **Sub-surface damage** = TBD. **Liner damage** = 4.4 diameter perforation, a single 3.7 x 3.0 (irregular shaped) fragment found within the COPV tank post-test (likely liner material).
#13 HITF16169 S/N 198 Cylinder	**Venting occurred/no rupture. Overall impact damage** = severed fibers and ply delamination present that has a 31.3 maximum height and extends around tank from origin of impact. **Crater dimensions** = TBD. **Maximum crater depth** = N/A. **Sub-surface damage** = TBD. **Liner damage** = 7.5 x 7.9 exposed liner visibly present, liner has a 2.4 x 2.1 perforation, a single 3.6 x 2.3 fragment found within the COPV tank post-test (likely liner material), no visible pitting or cratering present on far side liner.
#16 HITF16504B S/N 201 Cylinder	**Venting occurred/no rupture. Overall impact damage** = severed fibers and ply delamination present that has a 31.3 maximum height and extends around tank from origin of impact. **Crater dimensions** = TBD. **Maximum crater depth** = N/A. **Sub-surface damage** = TBD. **Liner damage** = 6.6 x 6.4 exposed liner visibly present, liner has a 4.4 x 3.5 perforation, multiple fragments found within the COPV tank post-test with the largest being 4.1 x 3.8, no visible pitting or cratering present on far side liner.

Figs. 28 through 44 show the AE signal vs. time or frequency for each of the COPV hypervelocity shots that were recorded in these tests with projectile penetration and gas venting only. The order of these figures directly correlates with the first column of HITF numbers in Table 7. The figures are ordered with the first view as an "early time close up" view of each AE signal channel recording of an HVI shot's AE result over the time range of 120 μs to 240 μs, followed by a graph of the full amplitude vs. time sequence of the AE results for that shot, and then followed by the frequency data for each of the sensors for that shot, with the frequency over the range of 0 to 1000 KHz. In each figure, panels (a), (b), (c), and (d) are for sensors 1, 2, 3, and 4, respectively. Generally, all of these impacts recorded 2048 μs of data with 128 μs of pre-trigger data, except for the first shot of this series which recorded only 1024 μs of data. The system's gain was at -2 dB per channel. The vertical scale for the figures was set to ±1.2V for the voltage vs. time graphs unless noted otherwise. For the voltage vs. frequency graphs, the vertical scale was -70 dB to 0 dB referenced to 1 mv.

A few general notes on this group of impacts. Because of the projectile's penetration of these COPV bottles, not all the projectile's energy is being deposited into the wall as for the previous cases where the shots did not breach the wall fully. Thus, less signal energy may be generated in the COPV wall in these shots in relation to the impactor's total energy. This is especially true for the component of the signal energy derived by flexural waves. Also, for these impacts which only vented, the ringing down of the initial signals, plus the venting noises are sufficiently loud enough to make any clear timing references for triangulating of post impact events on these bottles problematic.

Figure 28 shows the signal amplitude vs. time for the four sensors mounted on the COPV for hypervelocity shot HITF16160, the fourth pressurized shot. The first arrival signal occurred on channel 2, followed by channel 3, then channel 1 and then channel 4. The first triggered channel had the largest signal, while channels 3 and then 1 were decreasing in amplitude as the distance from the impact site increased. Channel 4, which was the furthest from the impact site, had a large amplitude. It is believed that the mounting hardware, which includes the gas feed line and was closest to sensor 4, could contribute to the increase in noise at that location.

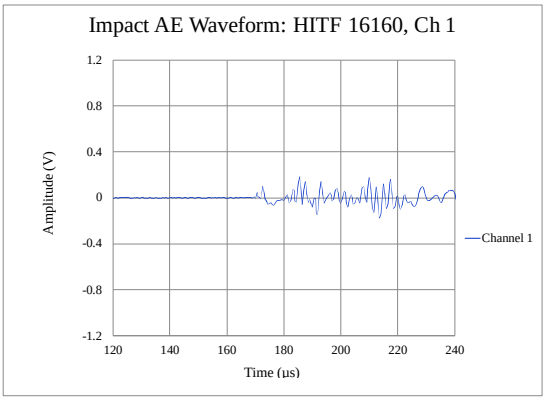

(a) Sensor Channel 1

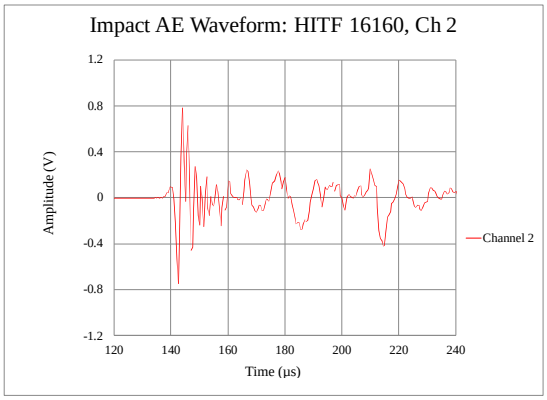

(b) Sensor Channel 2

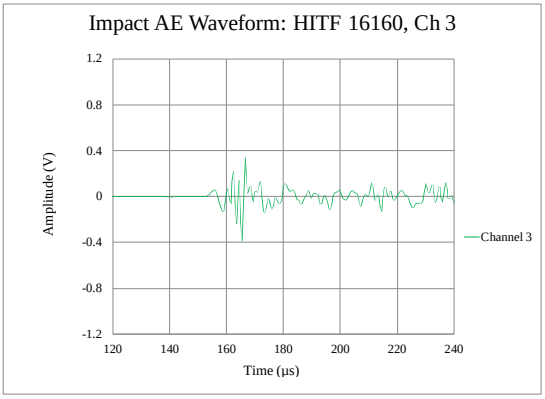

(c) Sensor Channel 3

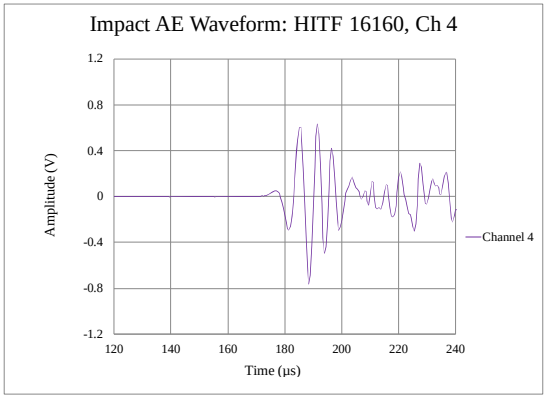

(d) Sensor Channel 4

Figure 28. Shows the signal amplitude vs. the time for the four sensors mounted on the COPV for hypervelocity shot HITF16160.

Figure 29 shows the signal amplitude vs. the full recorded time for the four sensors mounted on the COPV for hypervelocity shot HITF16160. In this view, the signal amplitudes from the leaking gas signals are reverberating throughout the bottle. The recorded data for sensors 1, 2, and 3 show a parallel pattern to the impact amplitudes with the closest sensor being loudest, while further away sensors have correspondingly smaller amplitudes. Sensor 4 shows a higher signal level during the leaking sound, which we attribute to the effects of that sensor being near the mounting structure, which includes the gas feed line. This was the only impact in this group of COPVs that the time recorded covered 0 to 1024 µs.

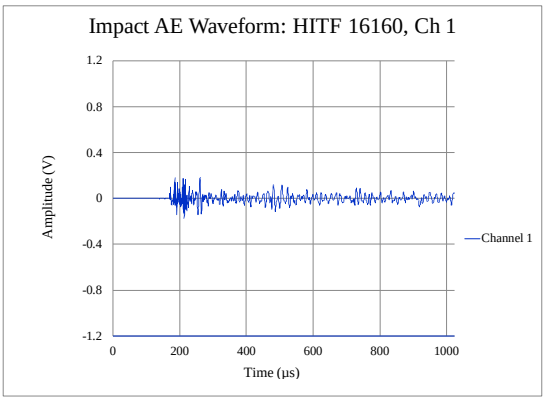

(a) Sensor Channel 1

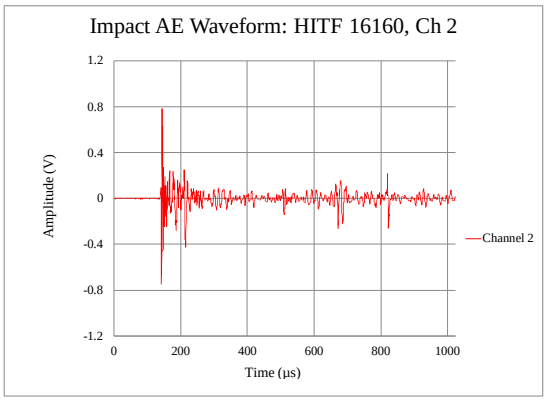

(b) Sensor Channel 2

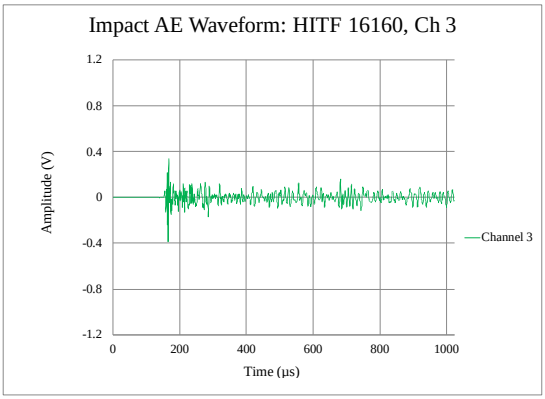

(c) Sensor Channel 3

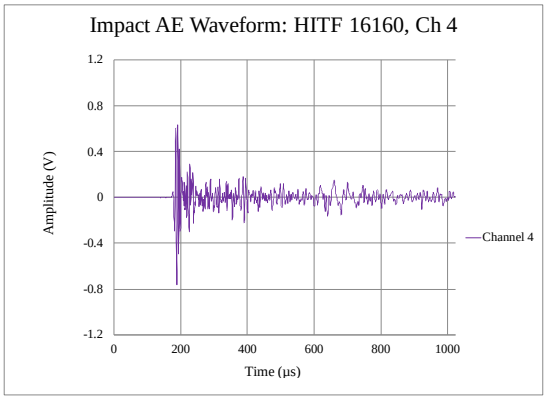

(d) Sensor Channel 4

Figure 29. Shows the signal amplitude vs. the full recorded time for the four sensors mounted on the COPV for hypervelocity shot HITF16160.

Figure 30 shows the amplitude vs frequency of the sensors' response to the impact of HITF16160. The signal levels peaked near 100 KHz near an amplitude of -10 dB. Channels 1 to 3 show a strong broad peak near the 400-500 KHz frequency having an amplitude near -25 dB.

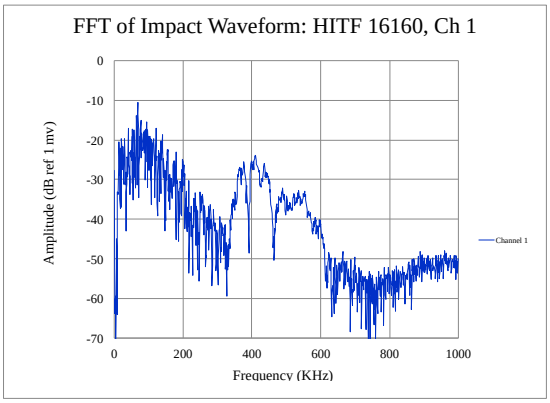

(a) Sensor Channel 1

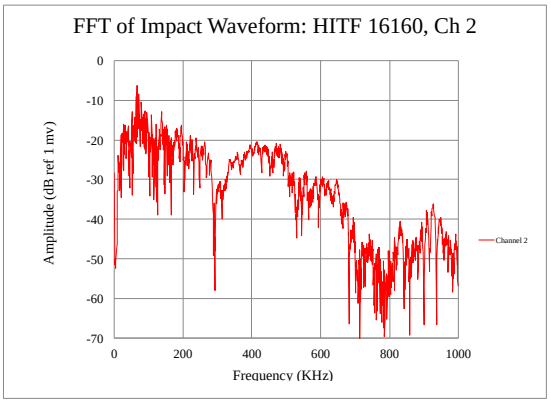

(b) Sensor Channel 2

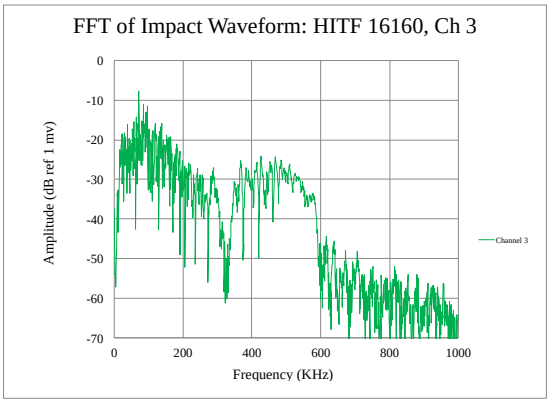

(c) Sensor Channel 3

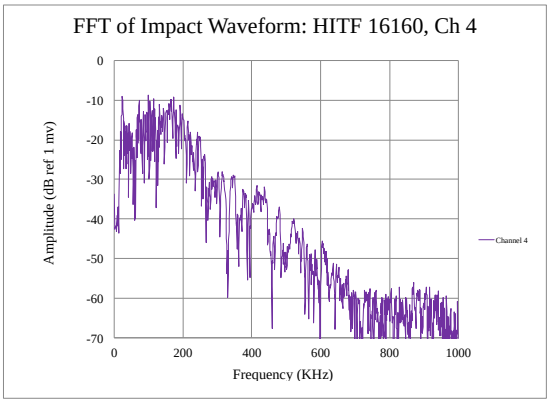

(d) Sensor Channel 4

Figure 30. Frequency results of HITF16160.

Figure 31 shows the signal amplitude vs. time for the four sensors mounted on the COPV for hypervelocity shot HITF16164, the eighth pressurized shot. HITF16164 impacted the COPV in the shoulder region of the COPV. The first arrival signal occurred on channel 4 followed by channel 3, then channel 2 and then channel 1. Channels 2 and 3 both appeared to suffer partial sensor disbonding with sensor recording a much smaller signal than recorded by channels 1 and 4. To compensate for that effect, Fig 31(b) and (c) have the vertical ranges of the graphs adjusted to ± 0.24 V to make the data more visible.

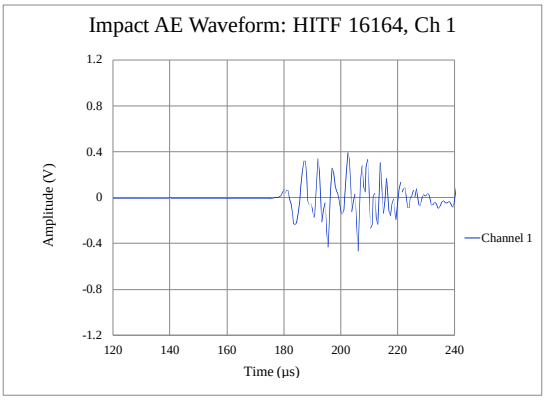

(a) Sensor Channel 1

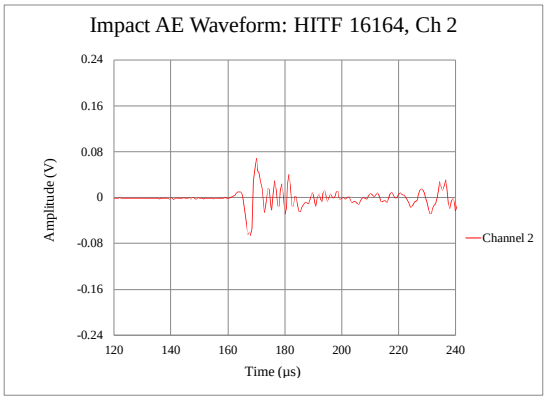

(b) Sensor Channel 2

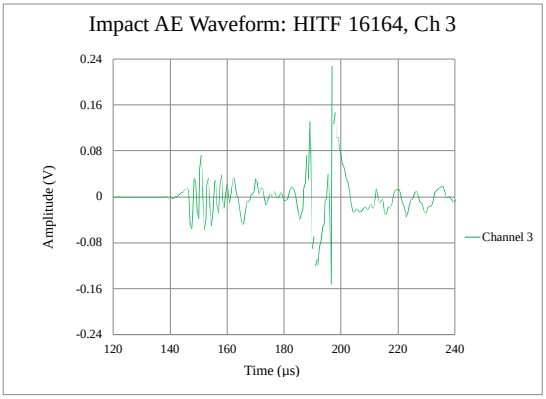

(c) Sensor Channel 3

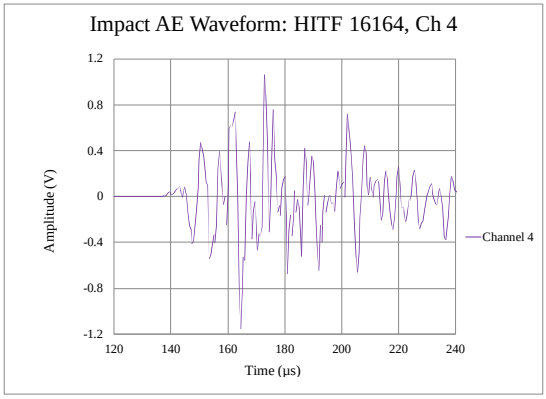

(d) Sensor Channel 4

Figure 31. Shows the signal amplitude vs. the time for hypervelocity shot HITF16164. The vertical scale ranged from ±1.2 V on channels 1 and 4 and ± 0.24 V for channels 2 and 3. Channels 2 and 3 appeared to have suffered partial disbonding

Figure 32 shows the full-time vs voltage plots for HITF16164.

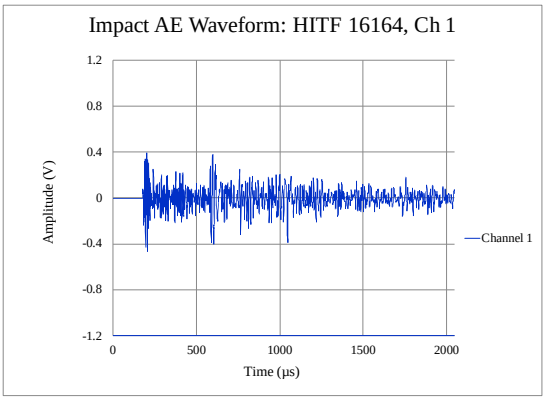

(a) Sensor Channel 1

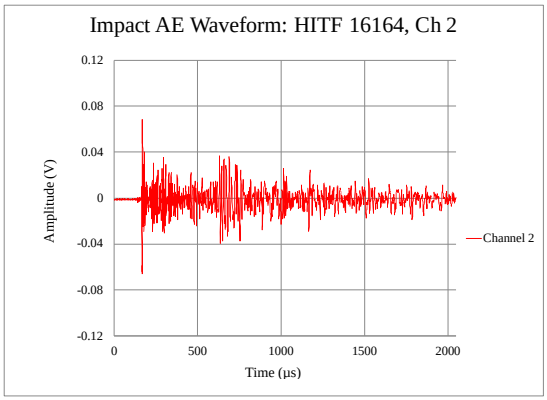

(b) Sensor Channel 2

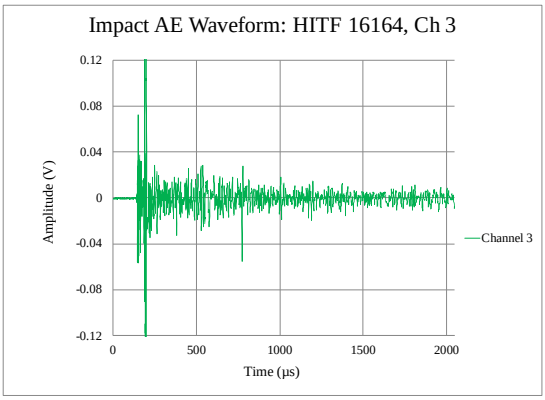

(c) Sensor Channel 3

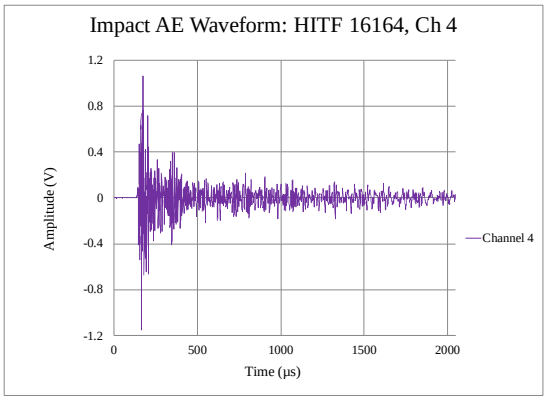

(d) Sensor Channel 4

Figure 32. Full temporal results of HITF16164 in volts vs. time. The vertical scale ranged from ±1.2 V on channels 1 and 4 and ±0.24 V for channels 2 and 3. Channels 2 and 3 may have suffered a partial disbonding of the transducer.

Figure 33 shows the amplitude vs frequency of the sensors' response to the impact of HITF16164. The signal levels peaked near 100 KHz near an amplitude of -5 dB on channels 1 and 4. The 100 KHz peak in channels 2 and 3 are near the range of -25 dB. Channels 1, 2, and 3 show a broad peak near the 400-500 KHz frequency having an amplitude near -25 dB on channel 1 and ~ -40 dB on channels 2 and 3.

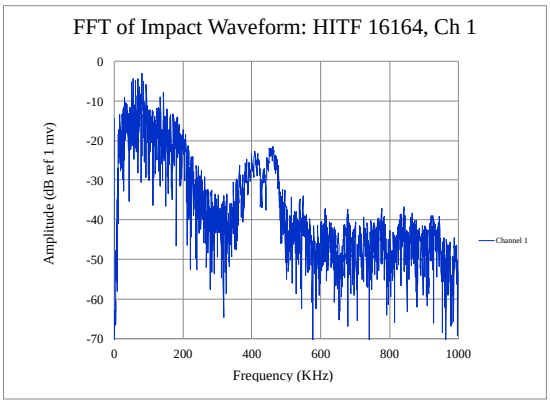

(a) Sensor Channel 1

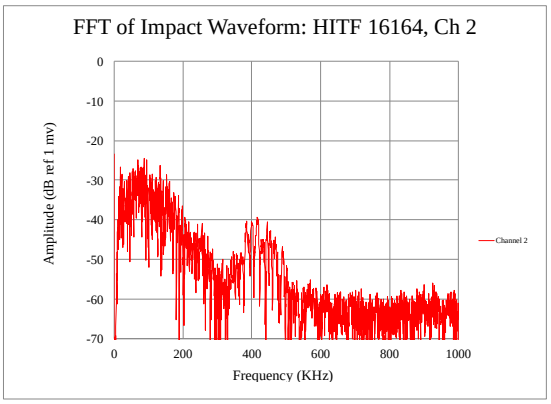

(b) Sensor Channel 2

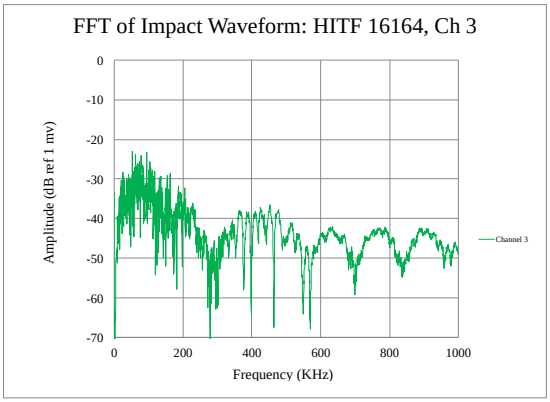

(c) Sensor Channel 3

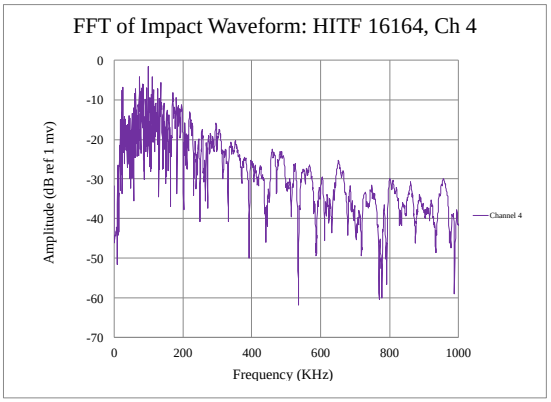

(d) Sensor Channel 4

Figure 33. Frequency results of HITF16164.

Fig. 34 shows the signal amplitude vs. time for the four sensors mounted on the COPV for hypervelocity shot HITF16165, the ninth pressurized shot, which was in the cylinder region of the COPV. The first arrival signal occurred on channel 2, followed by channel 3, then channel 1, and then channel 4. The signal from sensor for channel 1 appears to be much weaker after 185 µs, which indicates the sensor becoming detached from the COPV after the impact. After the test, inspection showed that this transducer was no longer attached and was on the bottom of the target tank.

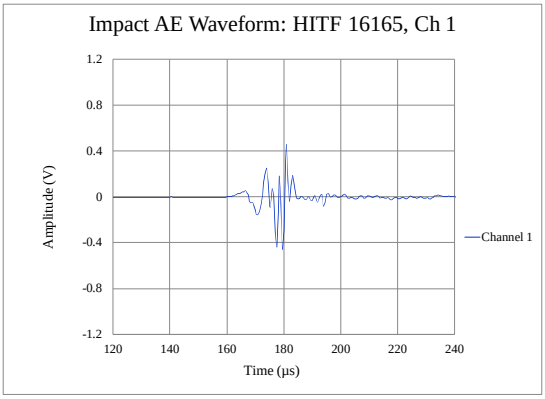

(a) Sensor Channel 1

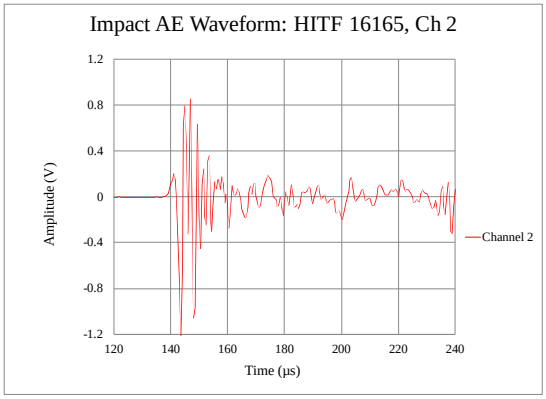

(b) Sensor Channel 2

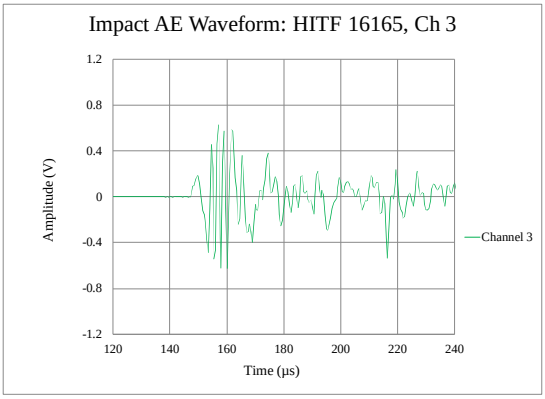

(c) Sensor Channel 3

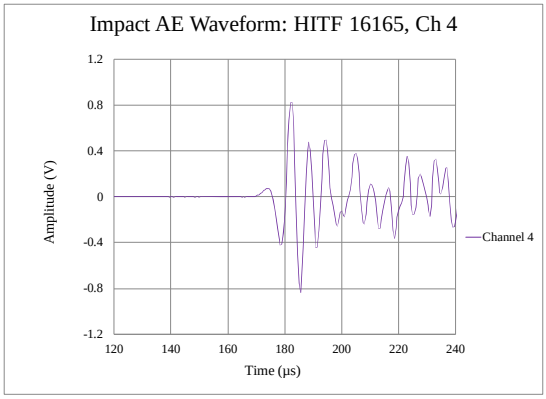

(d) Sensor Channel 4

Figure 34. Shows the signal amplitude vs. the time for the four sensors mounted on the COPV for hypervelocity shot HITF16165.

Figure 35 shows the full-time vs voltage plots for HITF16165. The signal on channel 1 looks very abnormal at about 180 µs and 500 µs in the data. That type of signal is seen with sensor failures, such as disbonding where the sensor is nearly broken away and then additional separation follows with ultimate disbonding. This correlates with the signal characteristics seen in Fig. 34(a) which also appears to have an odd amplitude drop at 185 µs. Even though this sensor appears to be suffering disbonding, within this short time frame of 2ms, the sensor will not have had time to fully move away from the surface of the COPV and hence it may still detect some surface wave motions before it fully drops away.

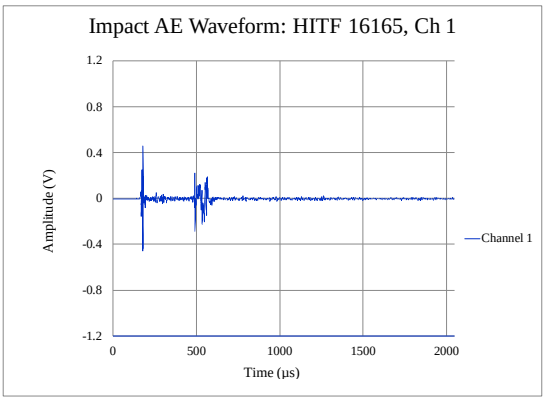

(a) Sensor Channel 1

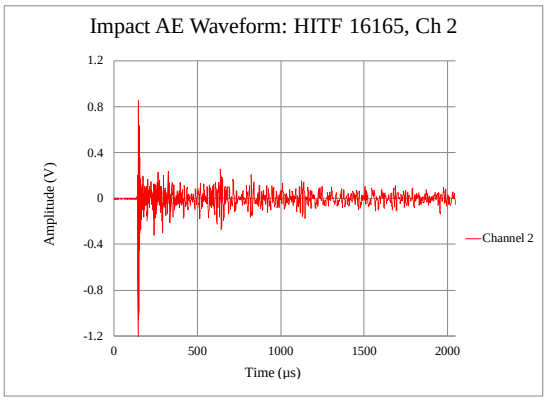

(b) Sensor Channel 2

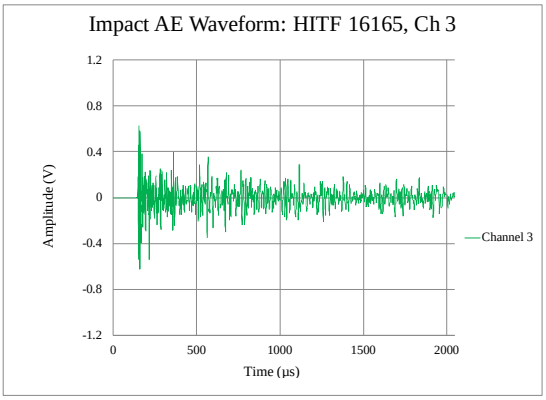

(c) Sensor Channel 3

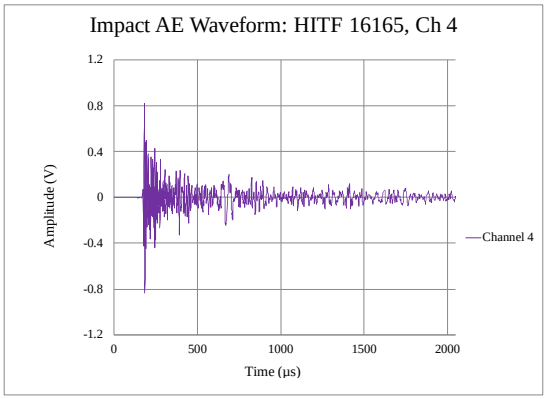

(d) Sensor Channel 4

Figure 35. Full temporal results of HITF16165 in volts vs. time. Besides the odd amplitude drop at 185 µs noted in Fig. 34(a), there was another abnormal signal at 500 µs on channel 1, after which the lack of a signal shows that transducer was no longer attached.

Fig. 36 shows the amplitude vs frequency of the sensors' response to the impact of HITF16165. The signal levels peaked near 100 KHz near an amplitude of -10 dB on channels 2 and 4. The 100 KHz peak in channel 1 was near the range of -25 dB. The apparent loss of good sensor contact to the COPV after 185 µs on channel 1 resulted in the lower signal amplitude recorded. Channels 1 to 3 show a broad peak near the 400-500 KHz frequency range, having an amplitude near -20 dB on channels 2 and 3 and ~ -30 dB on channel 1.

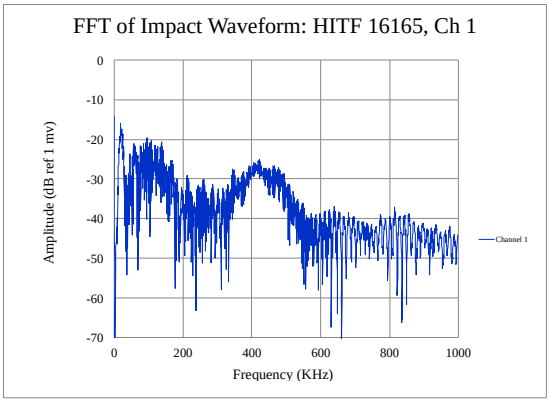

(a) Sensor Channel 1

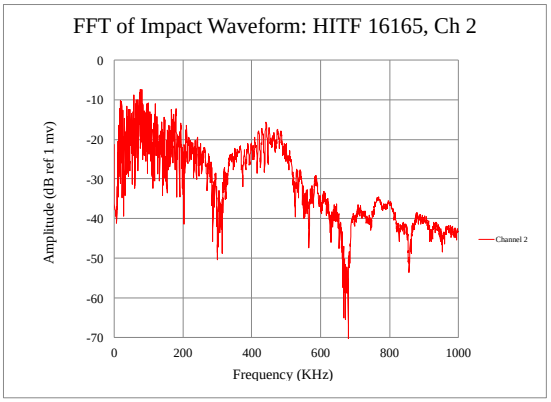

(b) Sensor Channel 2

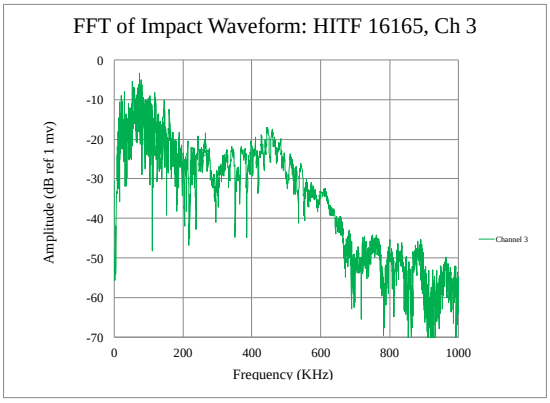

(c) Sensor Channel 3

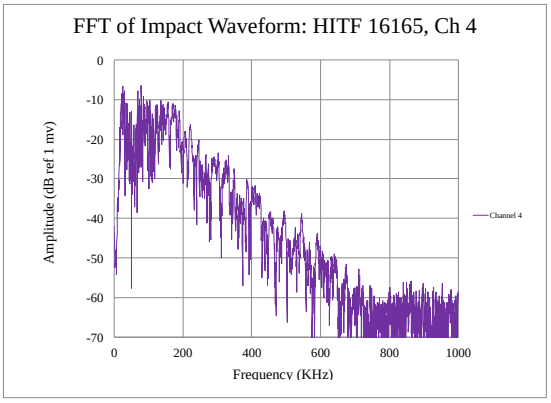

(d) Sensor Channel 4

Figure 36. Frequency results of HITF16165.

Figure 37 shows the signal amplitude vs. time for the four sensors mounted on the COPV for hypervelocity shot HITF16166, the tenth pressurized shot, which was in the cylinder region of the COPV. The first arrival signal occurred on channel 2, followed by channel 3, then channel 1, and then channel 4.

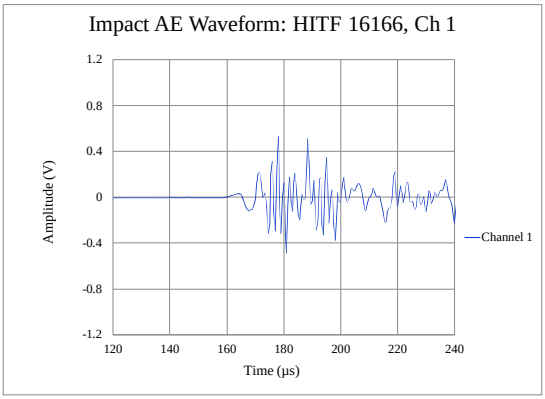

(a) Sensor Channel 1

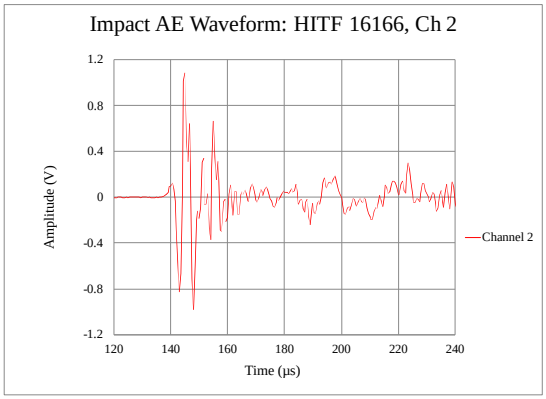

(b) Sensor Channel 2

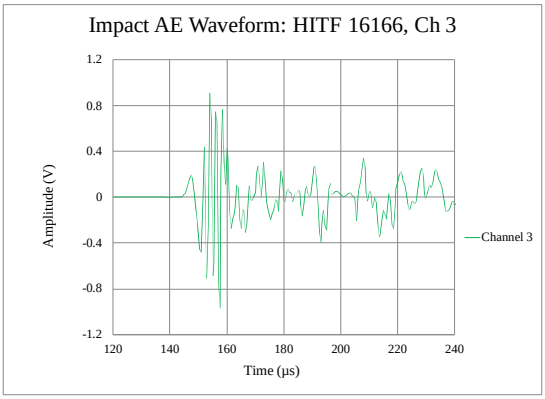

(c) Sensor Channel 3

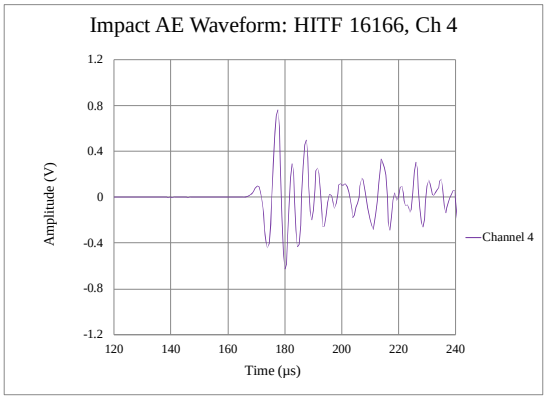

(d) Sensor Channel 4

Figure 37. Shows the signal amplitude vs. the time for the four sensors mounted on the COPV for hypervelocity shot HITF16166.

Figure 38 shows the full-time vs voltage plots for HITF16166.

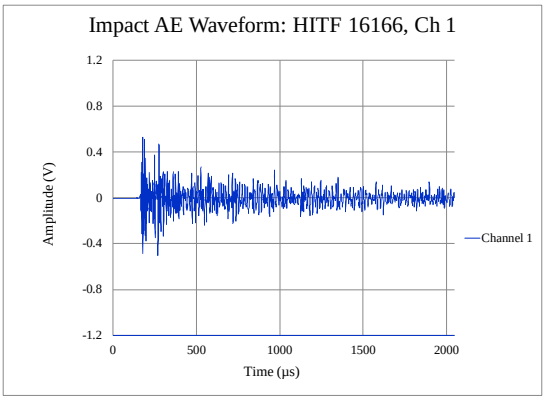

(a) Sensor Channel 1

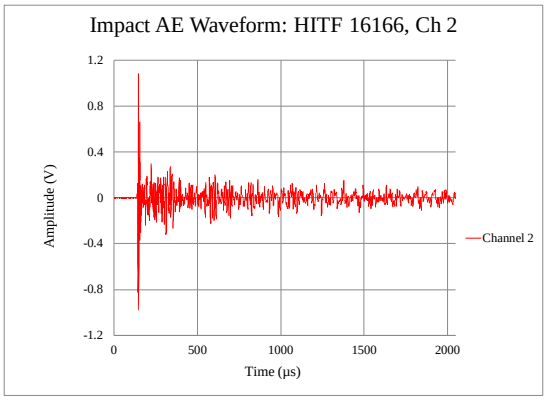

(b) Sensor Channel 2

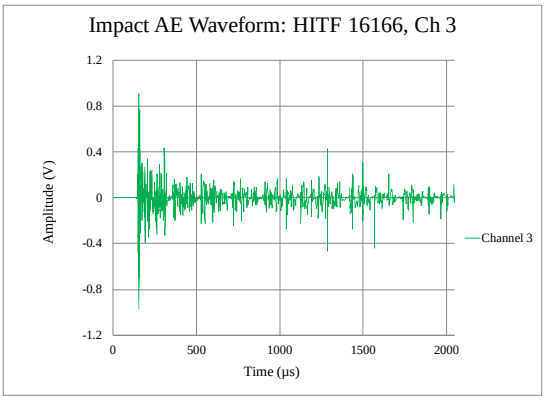

(c) Sensor Channel 3

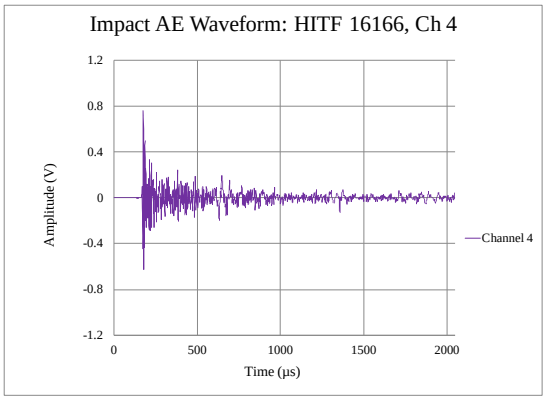

(d) Sensor Channel 4

Figure 38. Full temporal results of HITF16166 in volts vs. time.

Figure 39 shows the amplitude vs frequency of the sensors' response to the impact of HITF16166. The signal levels peaked near 100 KHz at an amplitude of -5 to -10 dB on channels 1 through 4. Channels 1 to 3 show a broad peak near the 400-500 KHz frequency range, having an amplitude near -20 to -25 dB

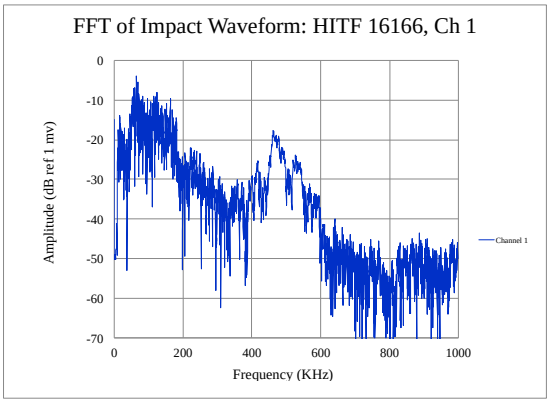

(a) Sensor Channel 1

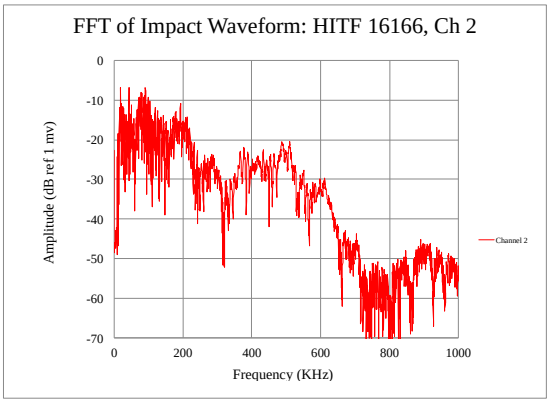

(b) Sensor Channel 2

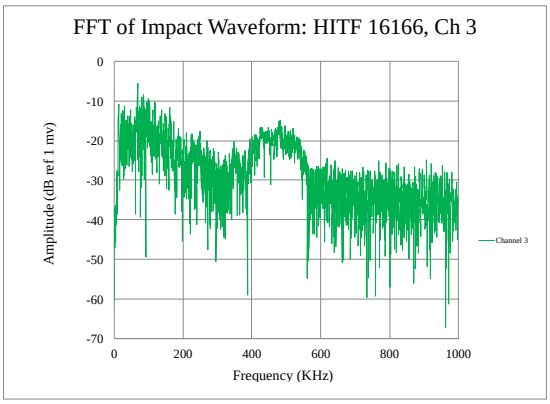

(c) Sensor Channel 3

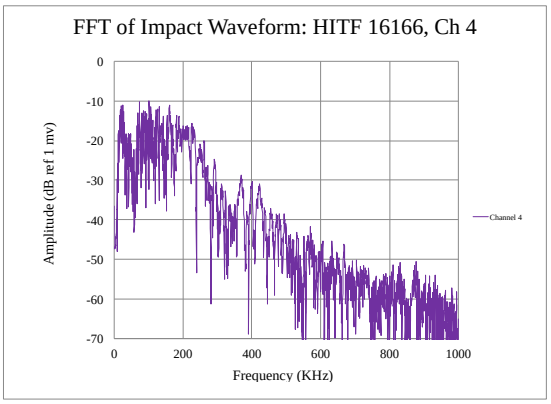

(d) Sensor Channel 4

Figure 39. Frequency results of HITF16166.

Figure 40 shows the signal amplitude vs. time for the four sensors mounted on the COPV for hypervelocity shot HITF16169, the thirteenth pressurized shot, which was in the cylinder region of the COPV. The first arrival signal occurred on channel 2, followed by channel 3, then channel 1 and then channel 4.

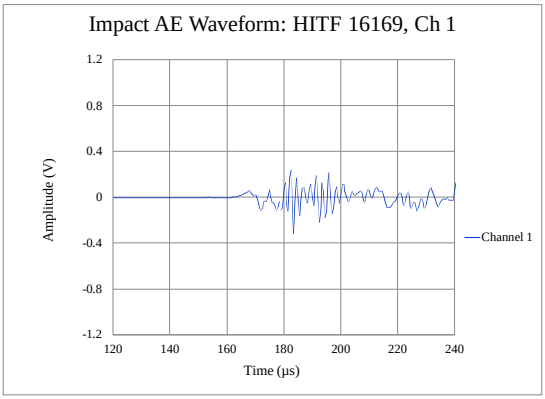

(a) Sensor Channel 1

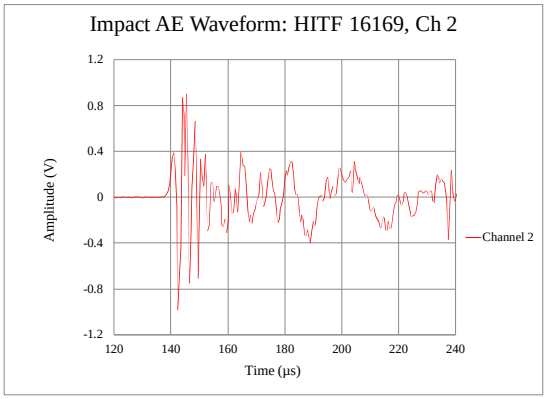

(b) Sensor Channel 2

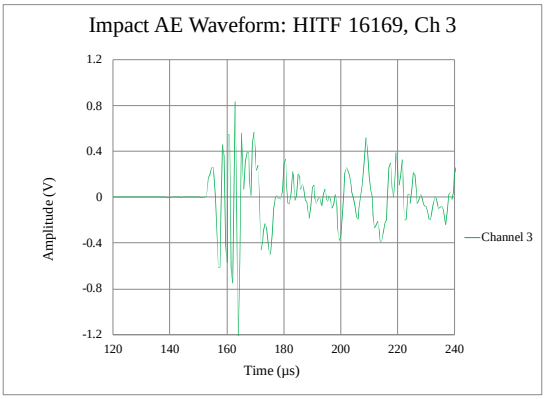

(c) Sensor Channel 3

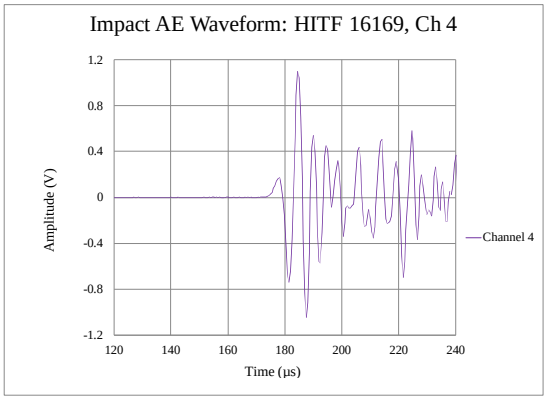

(d) Sensor Channel 4

Figure 40. Shows the signal amplitude vs. the time for the four sensors mounted on the COPV for hypervelocity shot HITF16169.

Figure 41 shows the full-time vs voltage plots for HITF16169. Around 400 µs, channel 3 was failing, followed by channel 1 failing at ~600 µs. After the test, the two suspect transducers were verified as no longer attached.

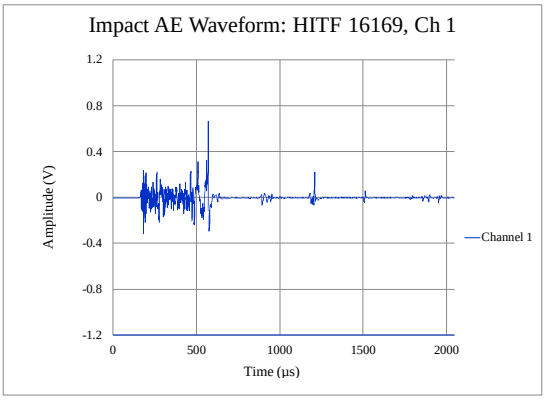

(a) Sensor Channel 1

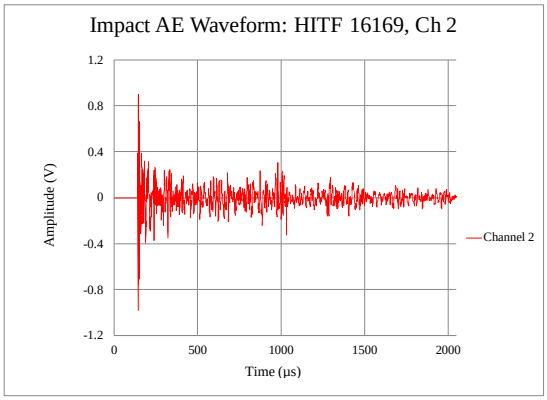

(b) Sensor Channel 2

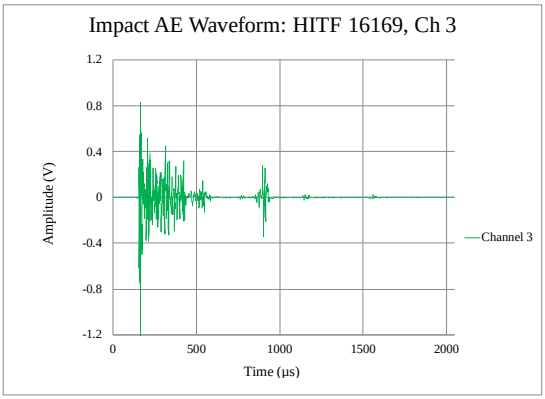

(c) Sensor Channel 3

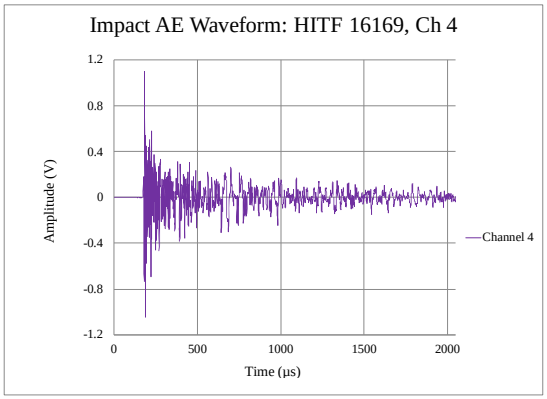

(d) Sensor Channel 4

Figure 41. Full temporal results of HITF16169 in volts vs. time.

Figure 42 shows the amplitude vs frequency of the sensors' response to the impact of HITF16169. The signal levels peaked below 100 KHz near an amplitude of -10 dB on channels 1 through 4. Channels 1and 3 show a broad peak near the 400-500 KHz frequency range, having an amplitude near -20 to -25 dB. The small peaks near the 400-500 KHz frequency range for channels 2 and 4 also have an amplitude near -20 to -25 dB, although their amplitudes aren't as prominent

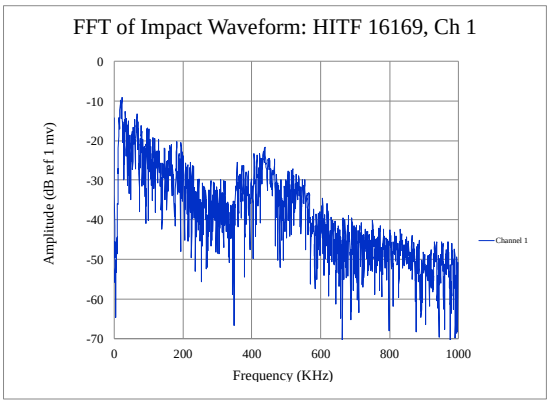

(a) Sensor Channel 1

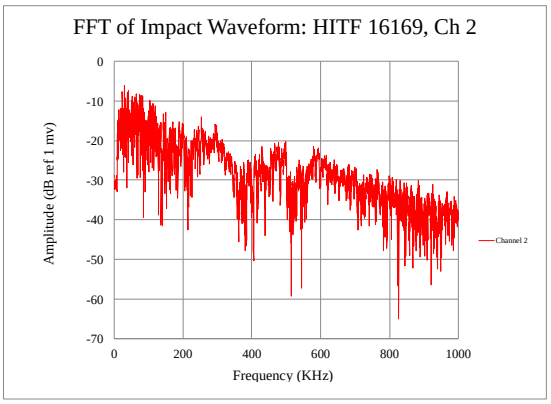

(b) Sensor Channel 2

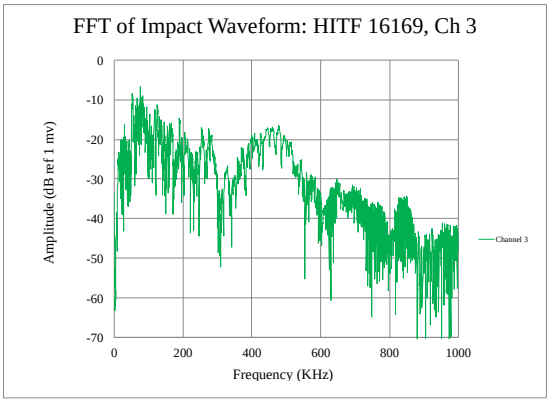

(c) Sensor Channel 3

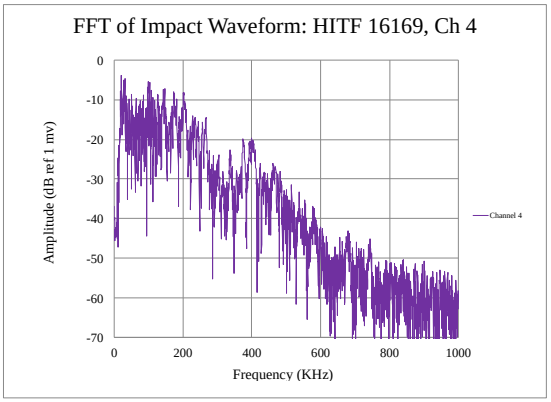

(d) Sensor Channel 4

Figure 42. Frequency results of HITF16169.

Fig. 43 shows the signal amplitude vs. time for the four sensors mounted on the COPV for hypervelocity shot HITF16504-B, the sixteenth pressurized shot, which was in the barrel region of the COPV. This shot used a stainless steel impactor instead of the aluminum balls used for other shots. This bottle had been used for a previous pressurized test with a tiny impactor, HITF16080. The area targeted was in a different location from the previous barrel shots to avoid effects from the previous impact, hence the first arrival timing is noticeably different from the other barrel shots. The first arrival signal occurred on channel 2, followed by channel 1, then channel 3 and finally on channel 4.

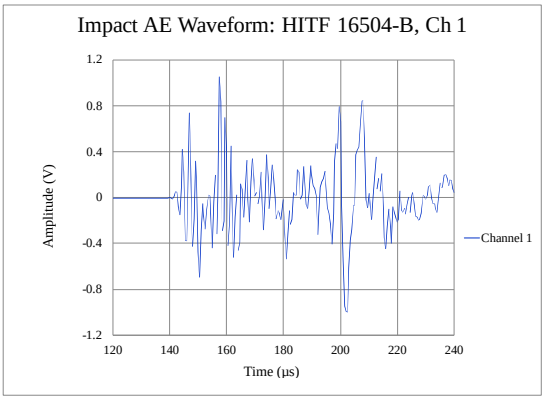

(a) Sensor Channel 1

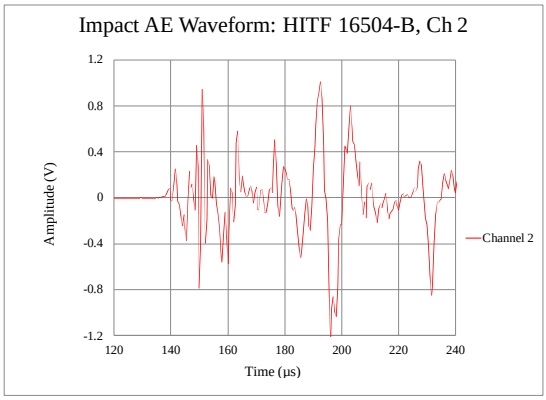

(b) Sensor Channel 2

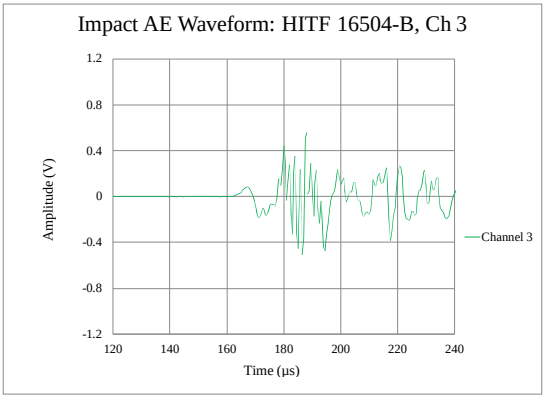

(c) Sensor Channel 3

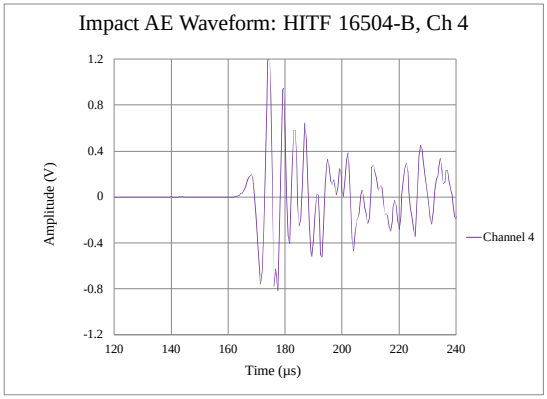

(d) Sensor Channel 4

Figure 43. Shows the signal amplitude vs. the time for the four sensors mounted on the COPV HITF16504-B,

Figure 44 shows the full-time vs voltage plots for HITF16504-B. At around 300 µs, the sensor on channel 2 was starting to disbond. After the test, the suspect transducer was verified as no longer attached.

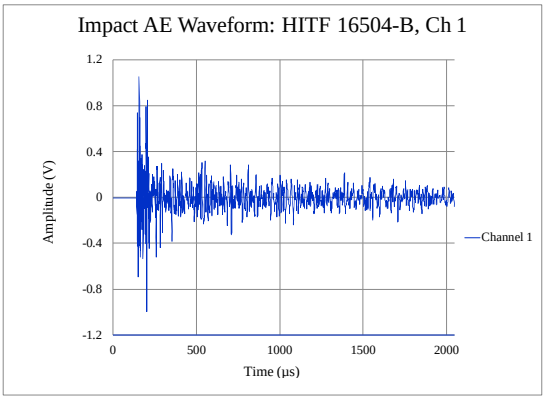

(a) Sensor Channel 1

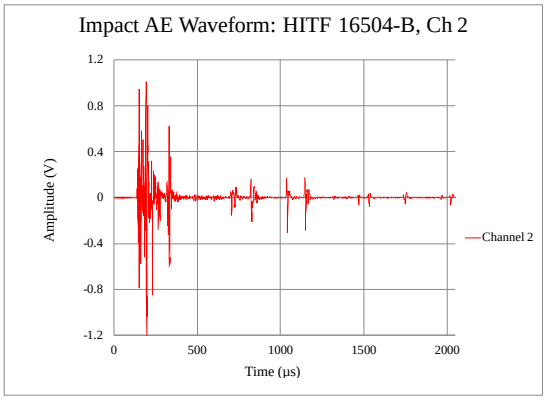

(b) Sensor Channel 2

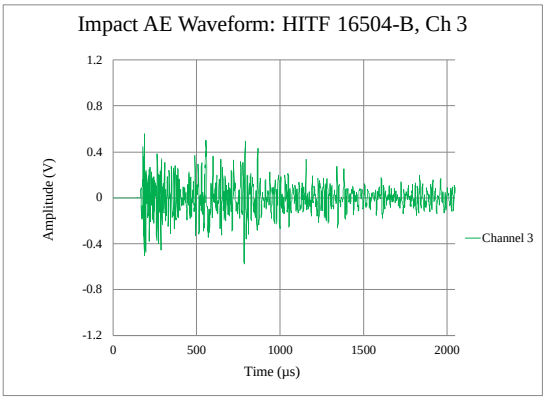

(c) Sensor Channel 3

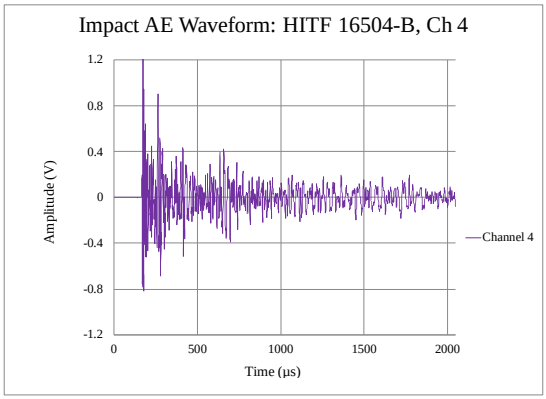

(d) Sensor Channel 4

Figure 44. Full temporal results of HITF16504-B. At around 400 µs that channel 2 had disbonded.

Fig. 45 shows the amplitude vs frequency of the sensors' response to the impact of HITF16504-B. The signal levels peaked near 100 KHz near an amplitude of -5 to -10 dB on channels 1 through 4. Channels 1 to 3 show a broad peak near the 400-500 KHz frequency range, having an amplitude near -20 dB.

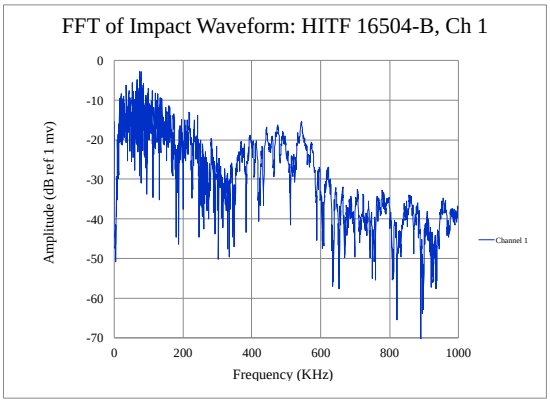

(a) Sensor Channel 1

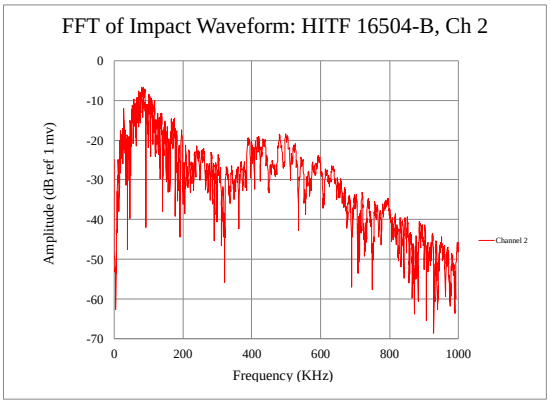

(b) Sensor Channel 2

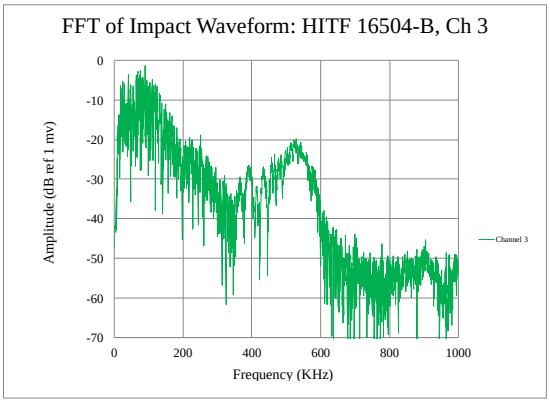

(c) Sensor Channel 3

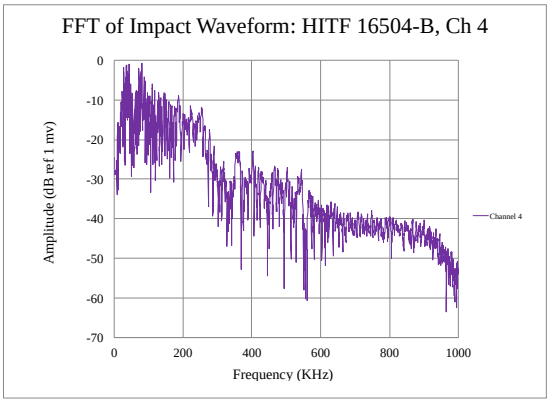

(d) Sensor Channel 4

Figure 45. Frequency results of HITF16504-B.

Table 9, entitled “List of Location and Temporal Results of HVI shots that penetrated and vented the COPV” shows timing and location parameters in these HVI tests. The temporal reference times were subsequently used in the fitting algorithm to identify the estimated impact location. Most of the hypervelocity shots in these tests were done on the cylindrical section of the bottles, except for HITF16164, which was a shoulder shot. Of the cylindrical shot locations, HITF16504-B was unique because the impactor was stainless steel plus the COPV had previously been used for HTIF16080. While the COPV was pressurized for HITF16080, the impactor used for that shot was the smallest impactor used in these tests at 0.0003 m. Note, it was of interest to re-use a test article if possible, since there were a limited number of test samples. The impact from HTIF16080 produced only a small region of local damage in this bottle, and it was determined via x-ray CT that another impact in another region would allow a viable test.

Table 9: List of Location and Temporal Results of HVI shots that penetrated and vented the COPV

Test Number / HITF Number/ Tank S/N / Impact Location	Target position axial (m)	Target position circum. (deg)	Target angle (deg)	Delta time sensor 1 (in μs)	Delta time sensor 2 (in μs)	Delta time sensor 3 (in μs)	Delta time sensor 4 (in μs)
Part 2							
#4 HITF16160 S/N 193 Cylinder	0.254	180	-45	29	0	16	37
#8 HITF16164 S/N 223 Shoulder	0.0805	180	-45	36.4	19.1	0	-3.5
#9 HITF16165 S/N 205 Cylinder	0.254	180	-45	23.5	0	8.5	32
#10 HITF16166 S/N 192 Cylinder	0.254	180	0	23.5	0	7	29
#13 HITF16169 S/N 198 Cylinder	0.254	180	-60	26	0	15	34.5
#16 HITF16504-B S/N 201 Cylinder	0.311	90	-45	3.7	0	26.0	27.2

Table 10 lists the measured impact locations in the COPVs that were penetrated and vented. The resultant estimates of the impact locations were computed from the data in Table 9 and the sensor locations. The table also computes the accuracy of the computed position estimate relative to the actual measurements. Adjustments in the velocity in this group of shots was set at 20% above the velocities shown in Fig. 3 to account for the effects of the high temperature and pressure of the bottles on the velocity of ultrasound in the bottle's walls. In the short time of these recorded events, ~2ms, the bottles did not have sufficient time to reduce the pressure appreciably. Shot HITF16164 was a shoulder shot. For computational simplicity, that shot was computed as if the impact was located on the barrel area by treating the barrel as being a slightly longer cylinder. This allowed the shoulder shot location to be treated as if it were on the barrel region. The error in these impact location estimates are of the same order of magnitude as for the case of the location estimates for impacts that did not penetrate as seen in Table 5.

Table 10. "Impact location table for penetrating and venting impacts, showing the results of the AE triangulation calculation."

Shot No.	Bottle #	Axial Location of Impact (m)	Circum. Location of Impact (m)	Estimated Axial Location of Impact (m)	Estimated Circum. Location of Impact (m)	Velocity Adjustment for Pressure*	Error Estimate (m)
Part 2							
HITF16160	193	0.254	0.257	0.279	0.254	additional 20%	0.0251
HITF16164	223	0.0889	0.275	0.0665	0.254	additional 20%	0.0304
HITF16165	205	0.251	0.229	0.251	0.254	additional 20%	0.0254
HITF16166	192	0.263	0.241	0.238	0.242	additional 20%	0.0246
HITF16169	198	0.260	0.249	0.264	0.254	additional 20%	0.00584
HITF16504 -B	201	0.318	0.130	0.307	0.133	additional 20%	0.0106

* See ref. [1, 2]

The signal energies of the pressurized impact bottles that vented are shown in Table 11, along with estimates of the damaged regions' circumference and area. The damage dimensions are based on equations for the circumference and area of a simple ellipse shape. The true area and edge of the impact can differ somewhat from that shape estimate because of the roughness of the edge, including petals of metal at the impact hole's edge. The signal energy levels are for 1) the total signal energy of a data record, 2) an estimate of the background noise energy, and 3) the resultant signal energy found by subtracting the background noise level from the total signal energy. In addition, as described in the section: "Signal Energy and AE results", estimates were made to adjust for differences in record lengths as the signal energy is directly related to the amount of data included in the calculation. Shot HITF16160 had 1024 μs of data as compared to the other impact tests in this grouping, which had 2048 μs of data.

Table 11. Signal Energy calculations for shots that penetrated and vented, along with estimates of the circumferences and areas of the damage regions. The signal energy calculations are for the average background noise levels, the average total signal energies, and the average impact signal energies.

Shot no.	Dim. 1 (m)	Dim. 2 (m)	Circum-ference (m)	Area m^2	Ave Total Signal Energy V^2-μs**	Ave Background Signal Energy V^2-μs**	Ave Impact Signal Energy V^2-μs**
HITF16160†	0.002	0.0023	0.00677	0.000036	4.494	1.045	3.449
HITF16165	0.0033	0.0033	0.01037	0.000086	13.210	3.384	7.754
HITF16166	0.0044	0.0044	0.0138	0.000152	10.917	2.249	8.668
HITF16164	0.0061	0.0053	0.0180	0.000254	17.018	3.505	6.849
HITF16504B*	0.0066	0.0064	0.0204	0.000332	28.441	5.196	21.272
HITF16169	0.0075	0.0079	0.0242	0.000465	12.765	1.153	11.611

† The time record for this shot was 1024 μs. The Signal Energy levels were adjusted to represent an equivalent 2048 μs time record.

* This shot was made with a stainless-steel projectile.

** These Ave. Signal Energy values did not include channels that disbonded.

Fig. 46 is an extension of Fig. 25. It shows the total signal energy vs. the impactor energy for the COPV's that involve impacts that did not penetrate, shown as green markers, and impacts that penetrated and vented, shown as red markers. While the non-penetrating impacts show a general linear trend, once the impactor penetrates the COPV, the linear trend no longer is supported as shown by the red data in Fig. 46. In the case of full penetration by the projectile, less of the projectile's energy is converted into acoustic energy. Thus, the linear trend of the signal energy following the projectile energy changes and the signal drops in magnitude. In addition, as seen in Fig. 46, the correlation between the impact energy and the signal energy appears to lose its linear trend with the projectile energy as implied by the low correlation coefficient value listed. The relationship is quite complex with noises coming from the impact, the post impact damage growth, and the venting noises for these impacts.

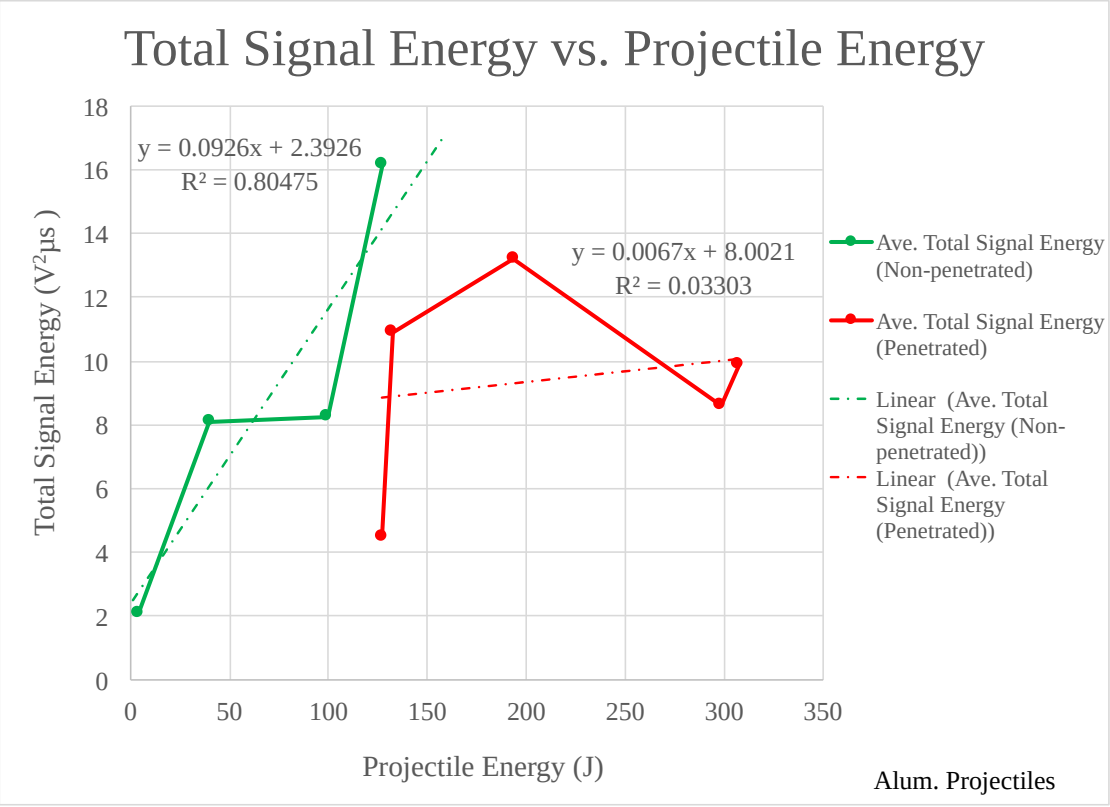

Figure 46. This figure shows the total signal energy vs. the impactor energy for the COPV's that involve impacts that did not penetrate, shown as green color data, and impacts that penetrated and vented, shown as red-colored data. The vertical scale is the signal energy and scales from 0 to 18 V^2 µs. The horizontal is the projectile energy and ranges from 0 to 350 J. The data were fitted with a linear relationship separately and shown as a dashed green line for the impacts that did not penetrate and a dashed red line for the impacts that penetrated and vented. The fitted equations along with their correlation coefficients are shown.

To understand what physical features some of these signal sources might depend on, Figs. 47 through 51 attempt to segregate noise components regarding the impact damage geometry as was investigated in Figures 26 and 27. The graph shows the data for the four transducers and their averages for the data from impacts that did not penetrate and those that penetrated and vented. In those graphs, the blue labelled data came from the pathfinder test. The grey labels represent data from Phase A testing where the impacts did not penetrate the COPV. The black labels represent data from the Phase A testing where the impactor penetrated and vented the COPV.

Fig. 47 shows how the total signal energy for the non-penetrating shots and penetrating shots with venting relates to the circumference of the damaged impact site, while Fig. 48 shows how the total signal energy relates to the area of the damaged impact site. Fig. 47 shows that the data has a weak linear trend with a correlation coefficient of $R^2 = 0.53$. The presence of the stainless-steel impactor appears to bias the relationship a good bit. Similarly, Fig. 48 also illustrates a weak linear trend with an even lower correlation coefficient of $R^2 = 0.428$. Considering how variable the actual damaged circumference and area are regarding the simple method of calculation used and how complex the noise elements contributions are, these poor correlations should be expected.

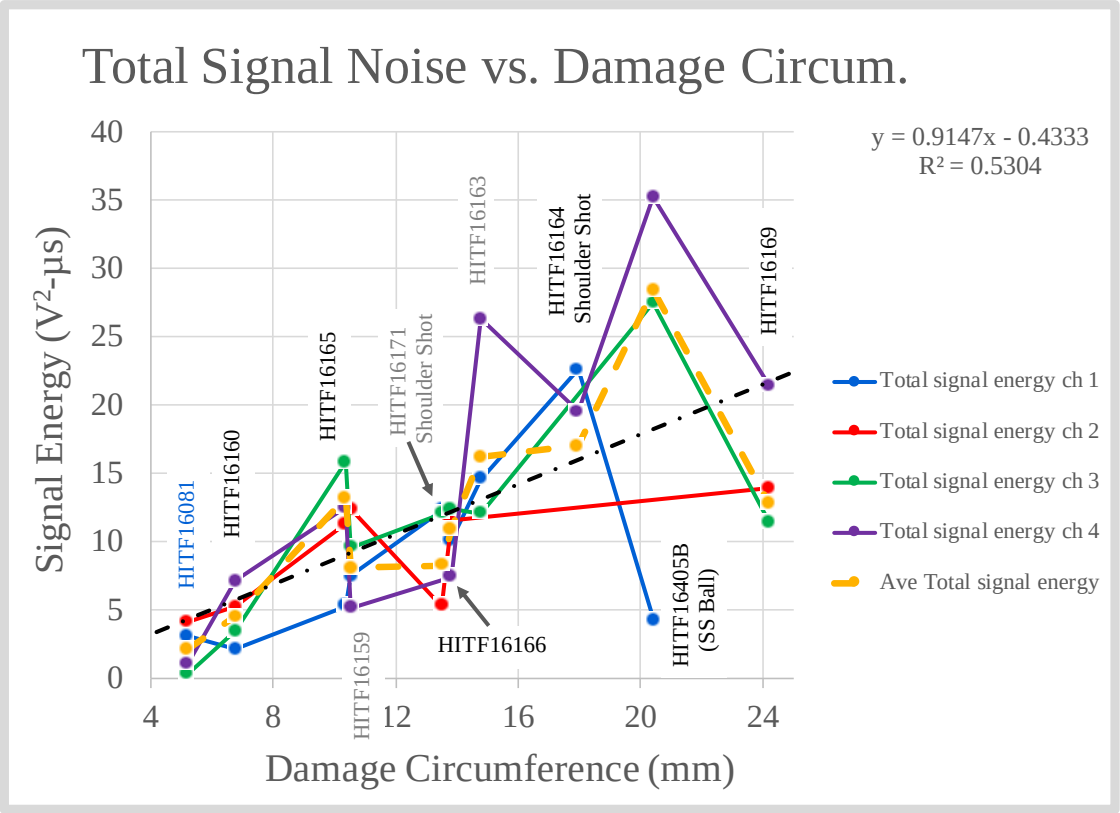

Figure 47. The total signal energy plotted against the estimated damage circumference. The vertical scale is the signal energy and scales from 0 to 40 V^2 µs. The horizontal is the damage circumference and ranges from 0 to 0.024 m. The graphs also displayed the linear fit to the average total signal energy data and its correlation coefficient.

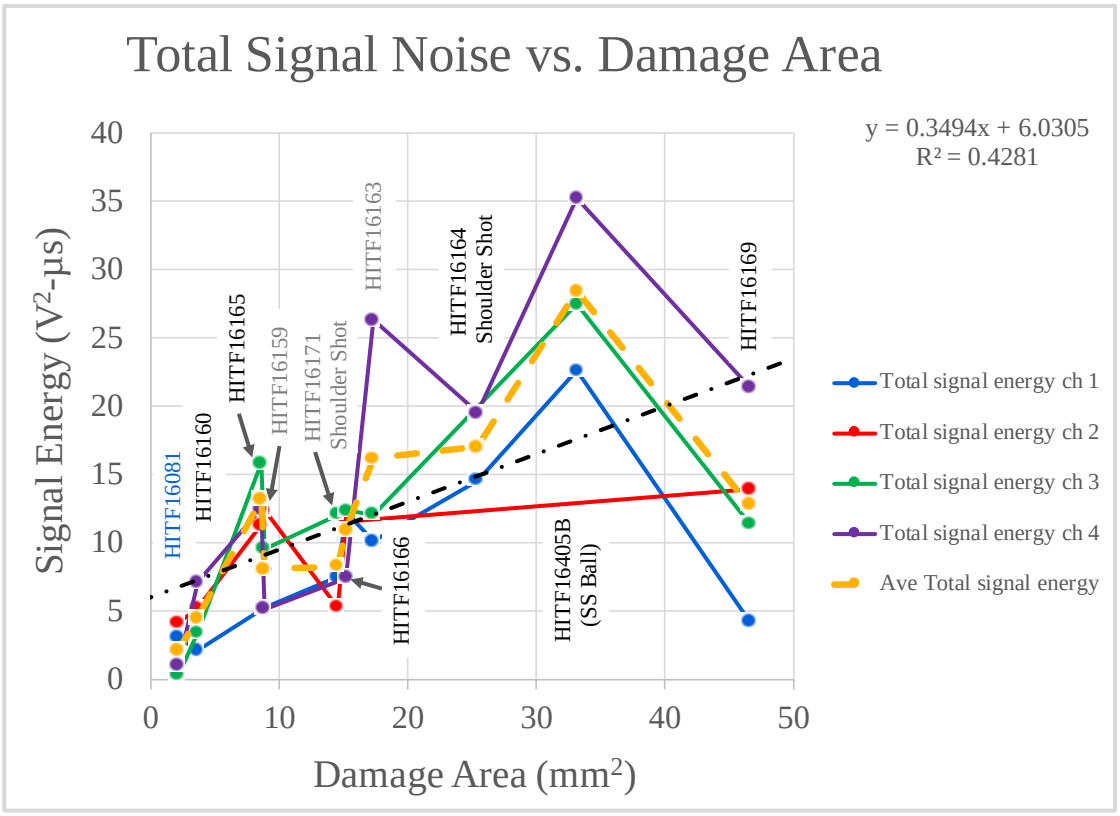

Figure 48. The total signal energy plotted against the estimated damage area. The vertical scale is the signal energy and scales from 0 to 40 V^2 µs. The horizontal is the damage area and ranges from 0 to 50 m^2. Also displayed is the linear fit to the average data and its correlation coefficient.

To further explore the signal source's components, plots of the background noise levels were generated and plotted first against the impact's circumference in Fig. 49, and then plotted against the damage area in Fig. 50. The labels in both figures follow the format used in Fig. 47 and 48. Venting noise sources should depend on the amount of free edge that is presented to the air flow as that is where the source of the turbulence is generated, hence there could be a stronger dependence on the circumference of the penetration than the area of the penetration. In addition, the circumference represents a free edge where there is less structural support and damage growth is possibly more likely to occur there than in a supported wall region, which would lead to more acoustic emission signal noise energy. Hence, the background noise sources might be more related to the circumference of the penetration than the damage area of the impact site. Inspection of Figs. 49 and 50 show that the noise generated vs. Signal Energy is variable and neither Fig. 49 or 50 show a good relationship between the background signal energy and the damage circumference or damage area. While both graphs show weak linear correlation, the correlation of the Signal Energy vs. the Damage Circumference is only slightly better than with Damage Area.

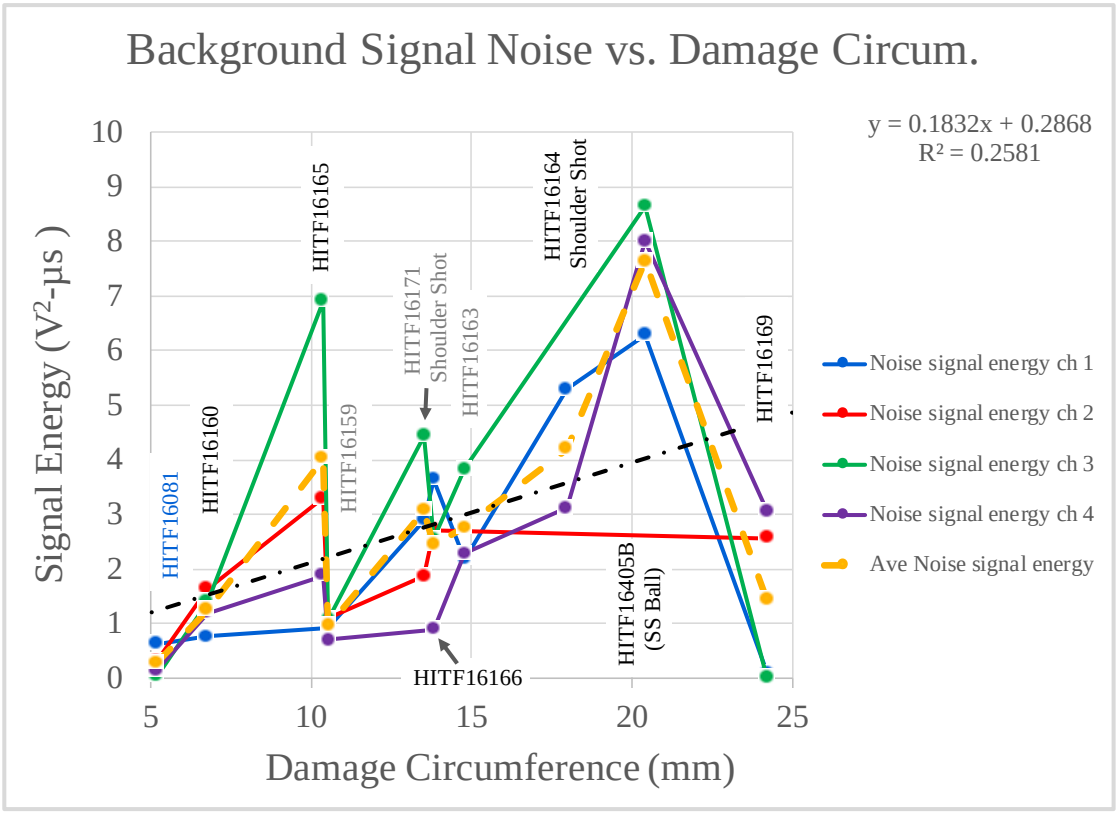

Figure 49. Background noise signal energy plotted against the estimated damage circumference. The vertical scale is the signal energy and scales from 0 to 10 V^2-µs. The horizontal is the damage circumference and has the same range as Figure 47. Also displayed is the linear fit to the average data and its correlation coefficient.

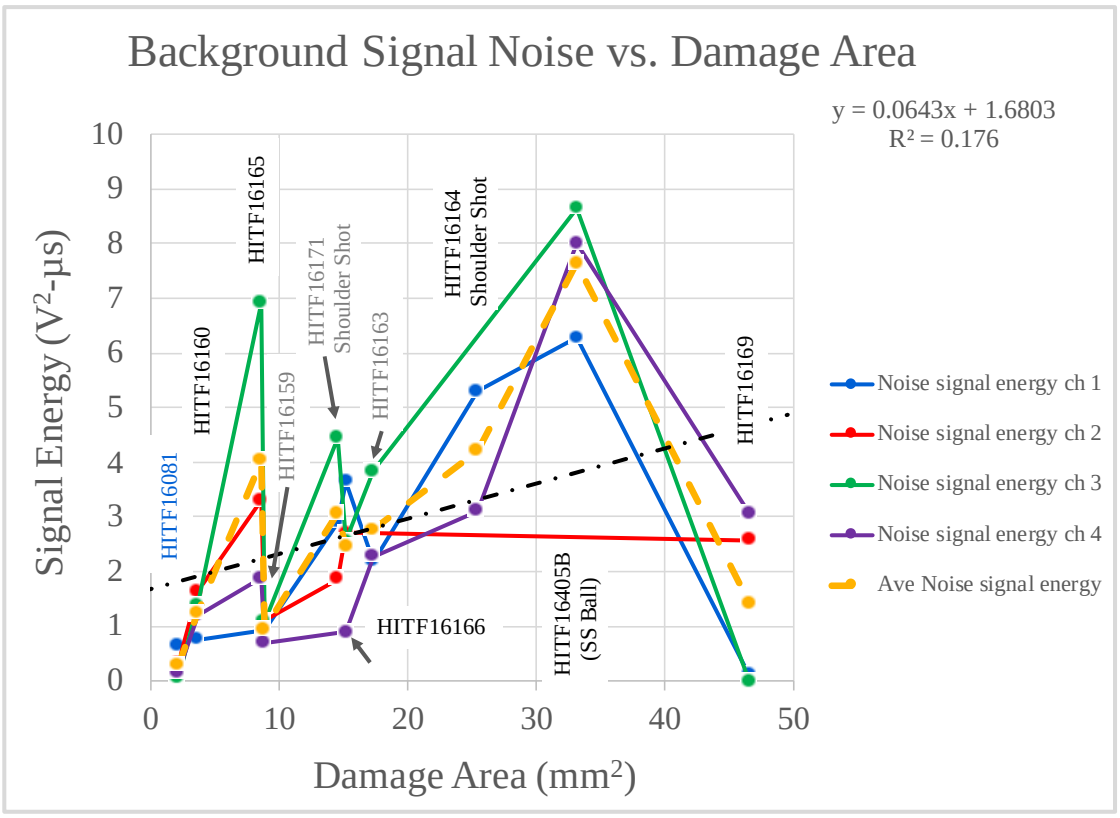

Figure 50. Background noise signal energy vs. damage area. The vertical scale is the signal energy and scales from 0 to 10 V^2-µs. The horizontal is the damage area of the impact site and has a range of 0 to 50 mm^2. Also displayed is the linear fit to the average data and its correlation coefficient.

Fig. 51 shows data that represents the impact signal energy, which we define as the difference between the total signal energy minus the background noise signal energies, i.e. Fig. 47 data minus Fig. 49 data plotted against the circumference of the damages. Similarly, Fig. 52 represents the impact signal energy, which is Fig. 48 data minus Fig. 50 data, vs the damage area. The labels in both figures follow the format used in Fig. 47 and 48. Viewing the data in both graphs shows that the noise levels for the impact signals are still highly variable. Neither correlation coefficient for the linear relationship of impact noise vs damage circumference levels nor the correlation coefficient of the linear relationship for impact noise levels vs. damage area are strong correlations. The correlation of the impact signal noise is a little better with the damage circumference than with the damage area.

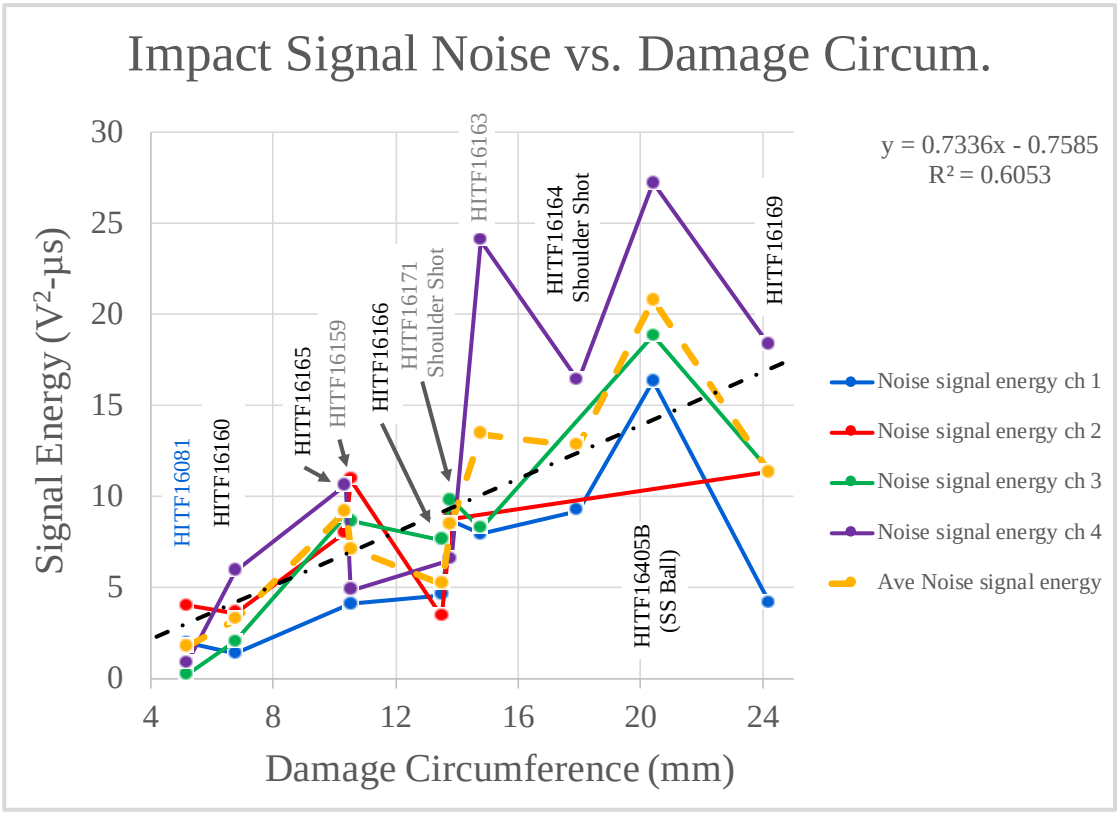

Figure 51. Impact signal noise energy vs. damage circumference. The vertical scale is the signal energy and scales from 0 to 30 V^2 µs. The horizontal is the damage circumference and has the same range as Figure 47. Also displayed is the linear fit to the average impact signal energy data and its correlation coefficient.

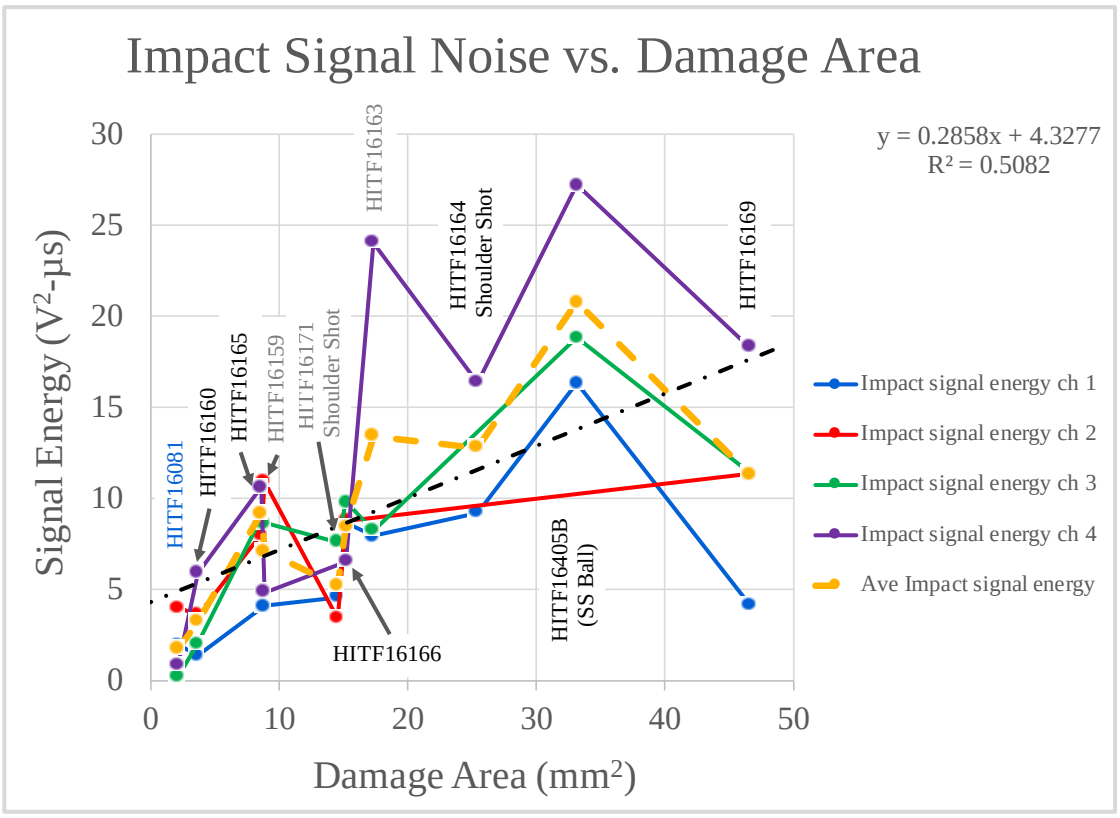

Figure 52. Impact noise signal energy vs. damage hole area. The vertical scale is the signal energy and scales from 0 to 30 V^2 µs. The horizontal is the damage area and has the same range as Figure 48. Also displayed is the linear fit to the average impact signal energy data and its correlation coefficient.

Shots that Penetrated and Detonated COPV

Table 12 is a listing of the hypervelocity shot parameters for the six cases where the projectile penetrated the COPV's wall and resulted in a detonation of the bottle. These puncture shots were in the cylinder region of the COPV, which represents the thinnest region of the COPV liner and overwrap. These HVI shots were made with aluminum projectiles except for HITF16505, which was a small, but denser stainless-steel projectile. The projectile energies ranged from 182 to 495 J. The projectile momenta ranged from 0.0519 to 0.140 Kg-m/s. The column labelled "Perpendicular Momentum" is the momentum component perpendicular to the surface at the impact point.

Table 12. List of HVI shots that penetrated and detonated the COPV.

Test Number / HITF Number/ Tank S/N / Impact Location	Actual tank Pressure (psi)	Projectile Type	Projectile Diameter (m)	Actual Projectile Mass (Kg)	Actual velocity (m/s)	Impact Angle (deg)	Projectile Energy (J)	Projec-tile Momen-tum (kg-m/s)	Normal Projec-tile Momen-tum (kg-m/s)
Part 1									
#5 HITF16161 S/N 189 Cylinder	4014	Al 2017-T4	0.00238	0.00001975	7080	45	495	0.140	0.0989
#6 HITF16162 S/N 188 Cylinder	4226	Al 2017-T4	0.00201	0.00001191	7010	45	293	0.0835	0.0590
Part 2									
#11 HITF16167 S/N 224 Cylinder	4221	Al 2017-T4	0.00172	0.00000741	7010	0	182	0.0519	0.0519
#12 HITF16168 S/N 187 Cylinder	4215	Al 2017-T4	0.00231	0.00001795	7030	60	444	0.126	0.0631
#14 HITF16170 S/N 222 Cylinder	4255	Al 2017-T4	0.0025	0.0000229	4070	45 (est)	190	0.0932	0.0659
#17 HITF16505 S/N 203 Cylinder	4162	SS	0.0013	0.00000882	7120	45	224	0.0628	0.0444

Table 13 describes the resulting damage for the impacts listed in Table 12. In Table 13, there are no dimensions related to the crater surface area size, maximum crater depth, sub-surface damage area, and the liner damage area since these vessels were destroyed by the impact.

Table 13. List of Results of HVI shots penetrated and detonated the COPV

Test Number / HITF Number/ Tank S/N / Impact Location	**Damage Assessments (mm)**
Part 1	
#5 HITF16161 S/N 189 Cylinder	**Rupture occurred. Overall impact damage** = complete rupture of tank occurred during impact; there was minor secondary debris and was deemed non-influencing to the test. The COPV tank remnants were all along the target tank floor and the large remnants secured/imaged.
#6 HITF16162 S/N 188 Cylinder	**Rupture occurred. Overall impact damage** = complete rupture of tank occurred during impact; there was minor secondary debris and was deemed non-influencing to the test. The COPV tank remnants were all along the target tank floor and the large remnants secured/imaged.
Part 2	
#11 HITF16167 S/N 224 Cylinder	**Rupture occurred. Overall impact damage** = complete rupture of tank occurred during impact. The COPV tank remnants were all along the target tank floor and large remnants secured / imaged.
#12 HITF16168 S/N 187 Cylinder	**Rupture occurred. Overall impact damage** = complete rupture of tank occurred during impact. The COPV tank remnants were all along the target tank floor and large remnants secured / imaged.
#14 HITF16170 S/N 222 Cylinder	**Rupture occurred. Overall impact damage** = complete rupture of tank occurred during impact. The COPV tank remnants were all along the target tank floor and large remnants secured / imaged.
#17 HITF16505 S/N 203 Cylinder	**Rupture occurred. Overall impact damage** = complete rupture of tank occurred during impact. The COPV tank remnants were all along the target tank floor and large remnants secured / imaged.

Figs. 53 through 70 show graphs of the AE signals recorded vs. time or frequency for each of the hypervelocity shots that resulted in the COPV's detonation in these tests. The order of these figures directly correlates with the first column of the HITF numbers in Table 12. The figures are ordered with the first view as an “early time close up” view of each AE signal’s channel recordings of an HVI shot over the time range of 120 µs to 240 µs. That graph is followed by a graph of the full amplitude vs. time sequence of the AE results for the shot over the time range of either 0 to 1024 µs or 0 to 2048 µs. HITF16161 and HITF16162 were recorded with 1024 µs of data. The rest of this series were recorded with 2048 µs of data. Those graphs are followed by the frequency vs. magnitude data for each of the sensors for that shot, with the frequency over the range of 0 to 1000 KHz. In each figure, panels (a), (b), (c), and (d) are for sensors 1, 2, 3, and 4, respectively. These impacts recorded 128 µs of pre-trigger data. The system’s gain was at -2 dB per channel. The vertical scale for the figures was ±1.2V for the voltage vs. time graphs. For the voltage vs. frequency graphs, the vertical scale was -70 dB to 0 dB referenced to 1 mv. The graphs of the full voltage vs. time indicate that some sensors are disbonding shortly after the initial impact and all the sensors are failing during the detonation. For a temporal guide on the voltage vs. time graphs, the approximate time indication for the

detonation's initiation is shown as a vertical red band. This data was derived in part from the videos of the hypervelocity shot. In the videos, all the detonations were first detected originating at the impact location and expanding outward from that point. There was no direct timing link between the AE data and the video to allow a better alignment of the detonation time. The video was triggered by the gun flash, which was inside the stripper tank, while the AE data was triggered by the first arrival of the sound wave in the COPV wall at the nearest transducer.

A few general notes on this group of impacts. During these impacts, there was a short latency between the impact time and the bottle's detonation, which is clear between the AE data starting time and the detonation marker. The sensors were being disbonded by the violence of the impact. In fact, none of these sensors or the sensor cables survived the detonation. Once disbonded, the sensors are still attached to the cabling and have not had time to fall away from the bottle. At the moment of detonation, the COPV bottles were disintegrating into shrapnel, with a few pieces of shrapnel accelerating the sensors to high speed away from the COPV. Some preamps and associated remote cabling survived, while some components were hit by shrapnel and damaged.

Fig. 53 displays the time of arrival/temporal results of HITF16161. The sensors' initial responses are similar to previous impacts discussed in earlier sections. The first arrival signal occurred on channel 2, followed by channel 3, then channel 1, and then channel 4.

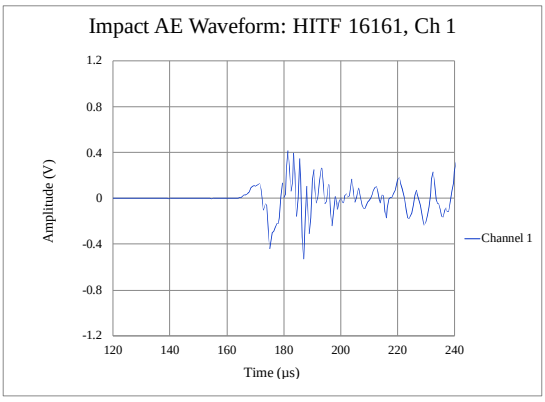

(a) Sensor Channel 1

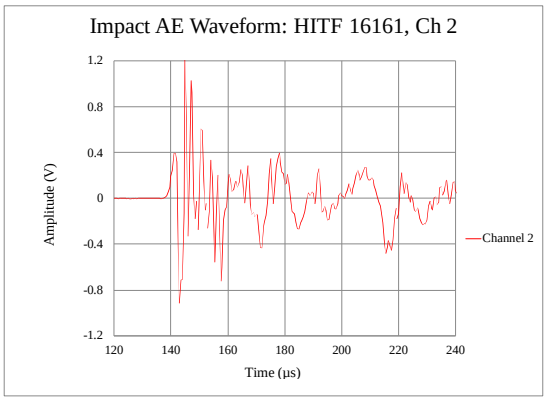

(b) Sensor Channel 2

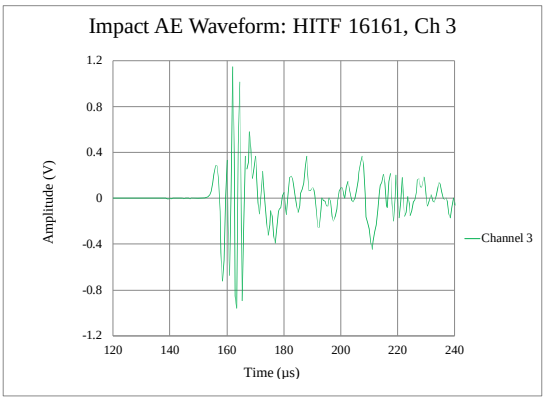

(c) Sensor Channel 3

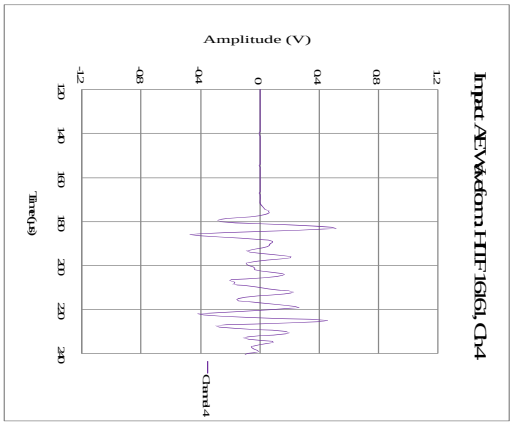

(d) Sensor Channel 4

Figure 53. Time of arrival/temporal results of HITF16161.

Fig. 54 shows the full temporal time recorded for shot HITF16161. It can be seen that signals were abruptly stopping on several channels: channel 2 at about 950 µs and channel 3 at about 430 µs implying that those sensors have disbonded from the COPV as the pressurized bottle continues to disintegrate. Channel 1 also may be disbonding as the signal falls rather abruptly in amplitude at about 650 µs. Channels 1 to 3 show a fairly large signal amplitude until the sensors disbond. This suggests that the fiber matrix composite is continuously breaking. This COPV bottle subsequently detonated at about 1050 µs, shortly after the recorded data ceased, which is highlighted by the vertical red bar at the end of each panel's data. After detonation, all the sensors and some of the preamps were damaged. Hence, it is hard to infer what happened at the bottle's surface because of the bottle's destruction.

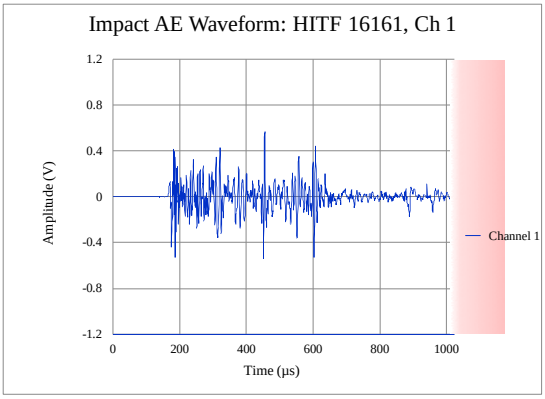

(a) Sensor Channel 1

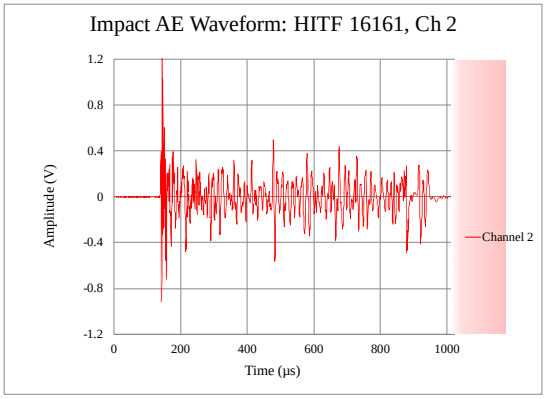

(b) Sensor Channel 2

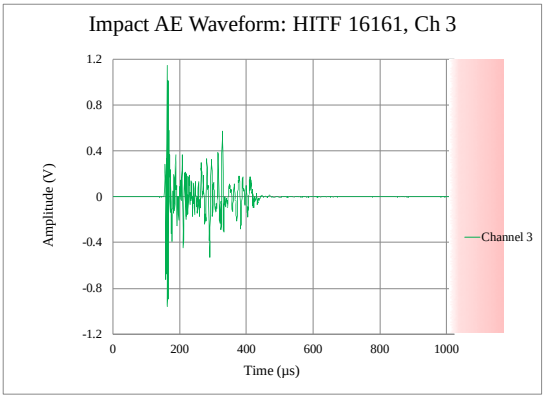

(c) Sensor Channel 3

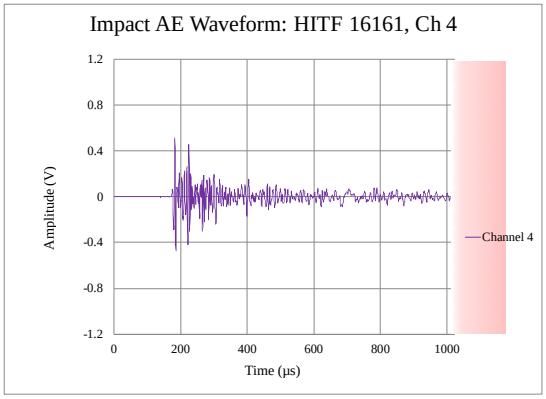

(d) Sensor Channel 4

Figure 54. Full temporal results of HITF16161.

Fig. 55 shows the signal amplitude vs frequency for shot HITF16161. There is the first data peak at about 100 KHz. There is a second peak about 400 to 500 KHz. Sensor 3's lower signal level compared to sensors 1 and 2 shows that the sensor lost contact and quit recording first. Channels 2 shows the most signal overall and reflects that the sensor stayed attached until almost the end of the recorded data. The channel 4, which was on the dome region, had a fairly low signal throughout the recording.

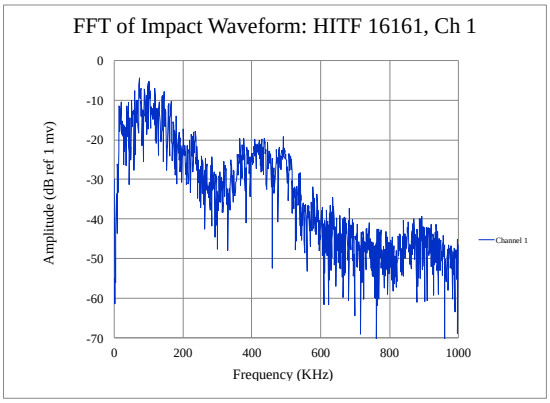

(a) Sensor Channel 1

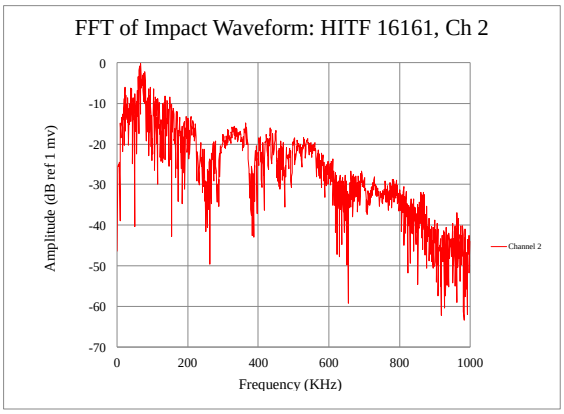

(b) Sensor Channel 2

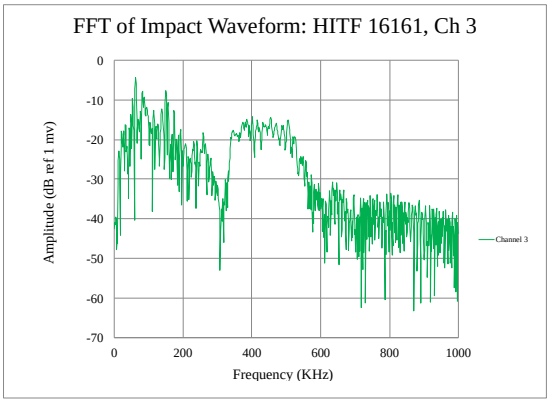

(c) Sensor Channel 3

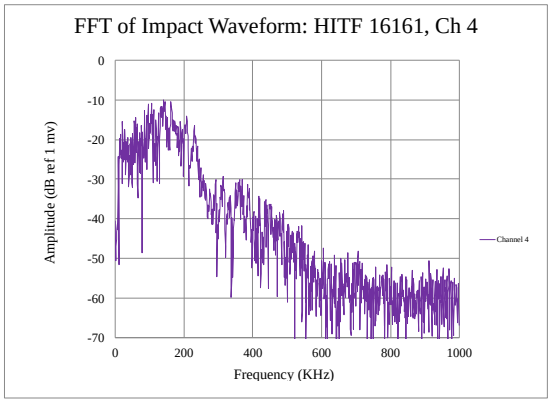

(d) Sensor Channel 4

Figure 55. Frequency results of HITF16161.

Fig. 56 displays the time of arrival/temporal results of HITF16162. In the figure, there is an indication that sensor 2 has disbonded at about 220 µs. The first arrival signal occurred on channel 2, followed by channel 3, then channel 1, and then channel 4.

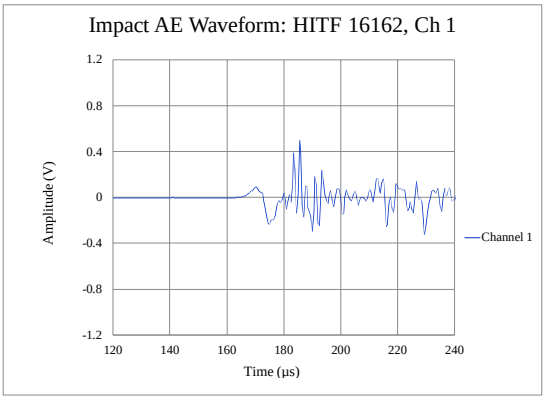

(a) Sensor Channel 1

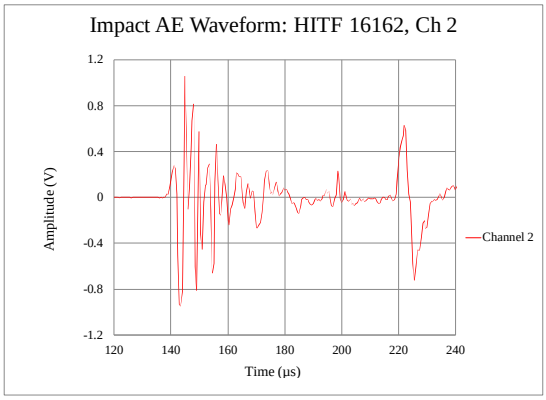

(b) Sensor Channel 2

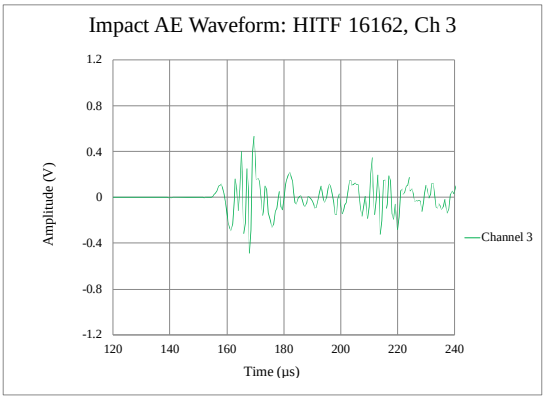

(c) Sensor Channel 3

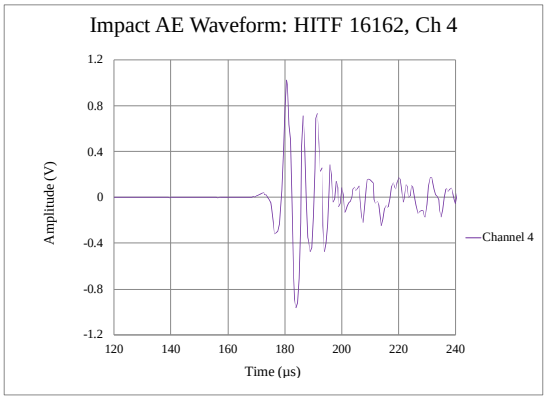

(d) Sensor Channel 4

Figure 56. Time of arrival/temporal results of HITF16162.

Fig. 57 shows the full temporal time recorded for shot HITF16162. It can also be seen that signals were abruptly stopped, especially on channel 2 at about 200 µs, channel 3 at about 450 µs, and channel 4 at about 750 µs, implying that those sensors have disbonded from the COPV as the pressurized bottle continues to experience damage growth. Sensor 1 shows that the venting and the pressure wall's failure progression generates significant noise, since sensor 1 remained attached until the detonation moment. This COPV bottle subsequently detonated at about 900 µs. During that process, the sections of the COPV wall are accelerated outward and collided with the sensors that were disbonded. The times when the signals "restart" reflect when the COPV wall sections are accelerating the sensor outward. Since channel 4 is attached to a dome area, which is anchored, it is the last sensor to record the acceleration outward from the detonation near 1000 µs. It should be noted that the timing of the start of the outward acceleration on individual sensors generally scales with the first arrival times at each sensor. This suggests that the impact location is also the center of the start of the disintegration point. This was also clear from the high-speed video of the impact, where the bottle expands outward from the impact site. Because this bottle detonated near the end of the recording, future recordings after HITF16162 were set to record for 2048 µs to try to ensure the whole failure event is recorded.

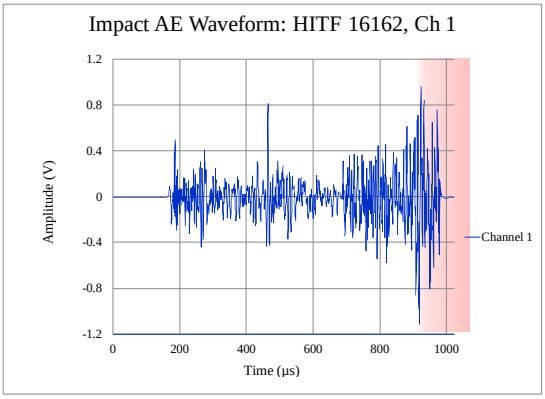

(a) Sensor Channel 1

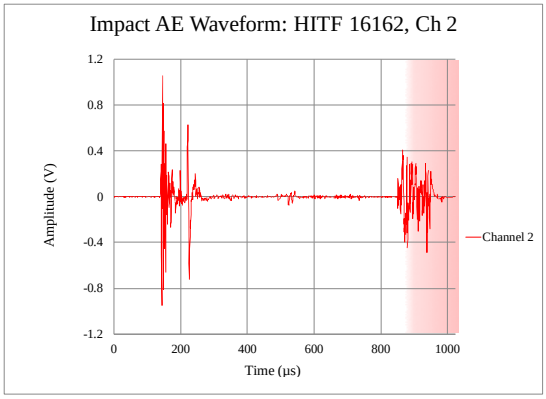

(b) Sensor Channel 2

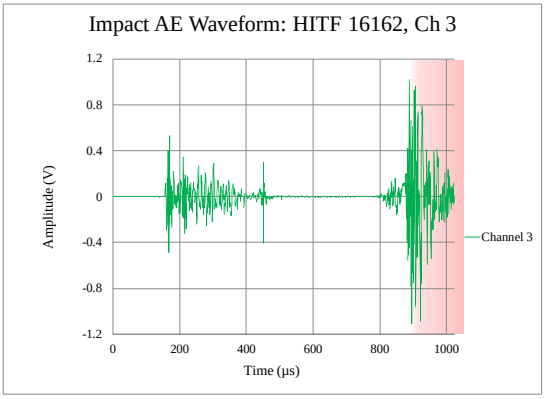

(c) Sensor Channel 3

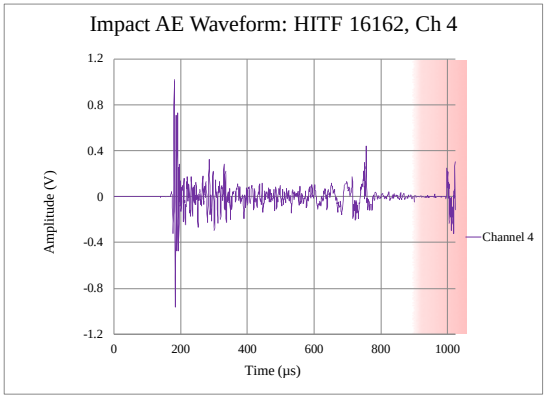

(d) Sensor Channel 4

Figure 57. Full temporal results of HITF16162.

Fig. 58 shows the signal amplitude vs frequency for shot HITF16162. As in the previous shots, there is a peak at about 100 KHz. There is a weak second peak about 400 to 500 KHz. Sensors on channels 2, 3, and 4 show much lower amplitudes. Channel 1 appears the largest in amplitude and also remained bonded for the longest time.

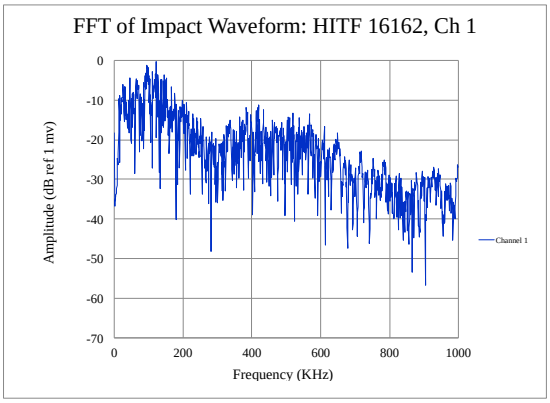

(a) Sensor Channel 1

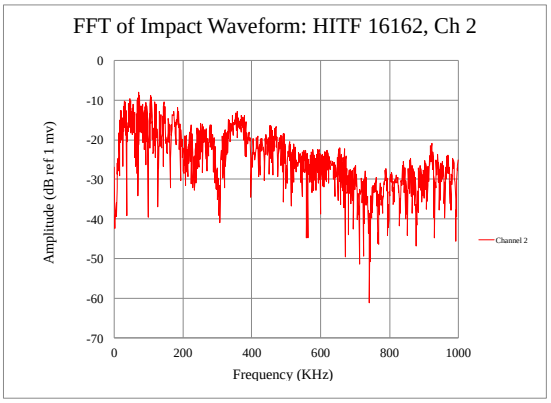

(b) Sensor Channel 2

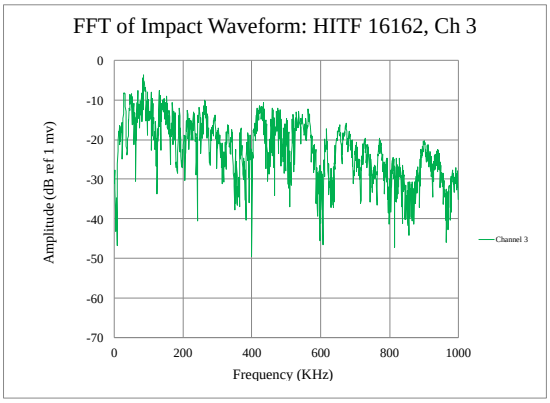

(c) Sensor Channel 3

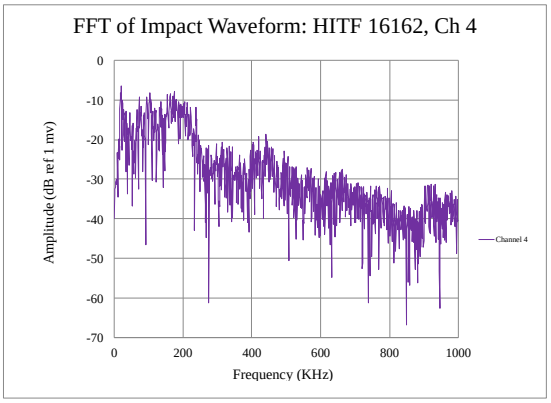

(d) Sensor Channel 4

Figure 58. Frequency results of HITF16162.

Fig. 59 displays the time of arrival/temporal results of HITF16167. The first arrival was on sensor 2 at about 135 µs, followed by sensor 3, then sensor 1, and finally sensor 4.

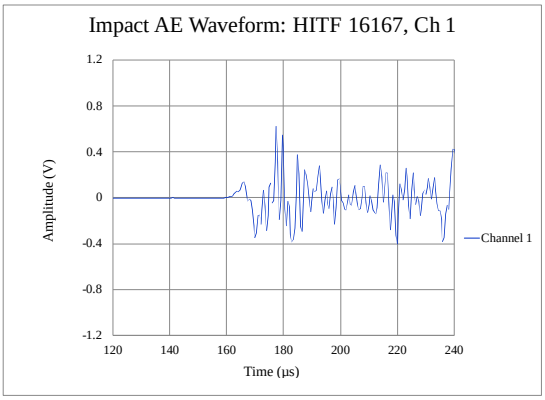

(a) Sensor Channel 1

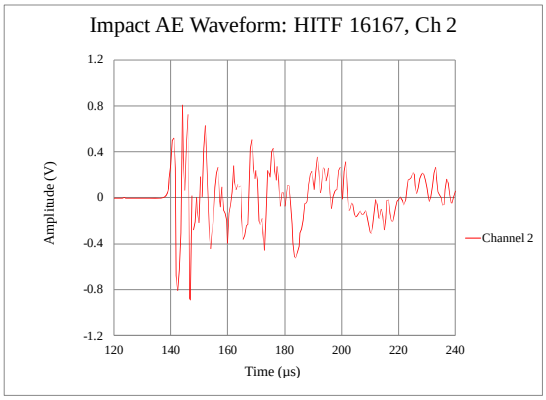

(b) Sensor Channel 2

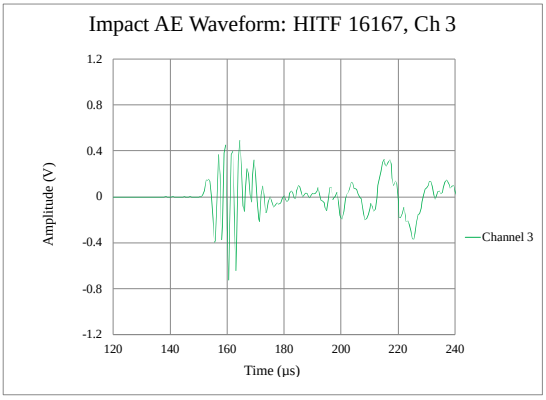

(c) Sensor Channel 3

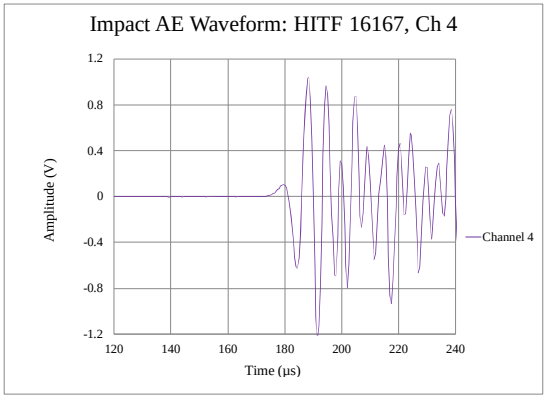

(d) Sensor Channel 4

Figure 59. Time of arrival/temporal results of HITF16167.

Fig. 60 shows the full temporal time recorded for the shot HITF16167. For this impact test and later tests, the data was recorded for 2048 µs. It can be seen in the figure that signals were disappearing, on channel 2, at about 700 µs, while channel 3 may have been partially disbonded around 400–700 µs and channel 4 was disbonding at about 800 µs, implying that those sensors were disbonding from the COPV as the pressurized bottle's damage state continued to grow. This COPV bottle subsequently started detonating at about 750 µs. The times when the signals appear to "restart" with very high amplitudes reflect when the COPV wall sections are accelerating the sensor outward. Since channel 4 is attached to a dome area, which is anchored, it is the last sensor to record the acceleration outward from the detonation starting at about 850 µs.

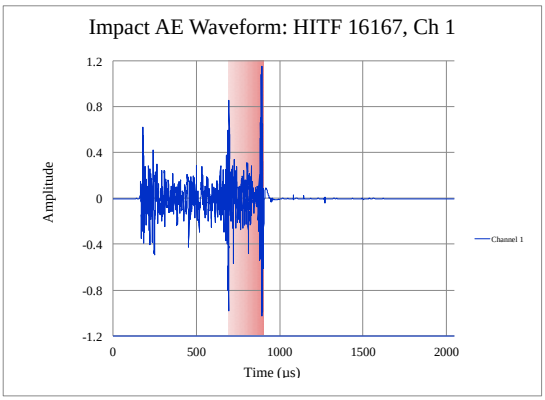

(a) Sensor Channel 1

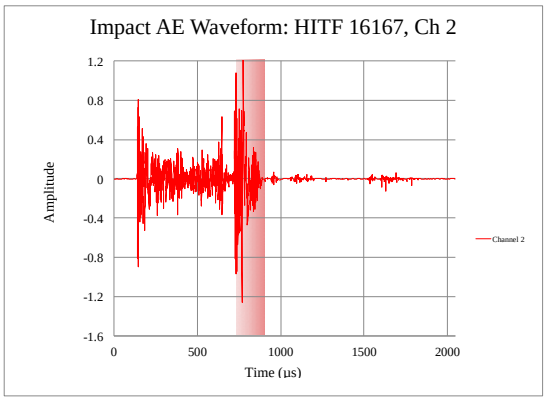

(b) Sensor Channel 2

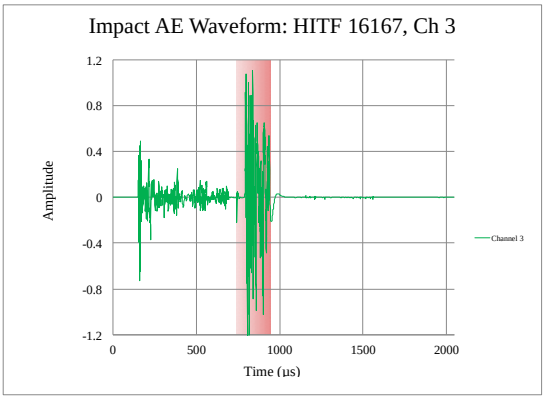

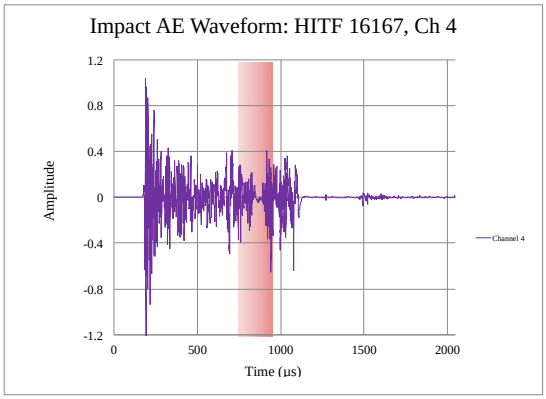

(c) Sensor Channel 3 (d) Sensor Channel 4

Figure 60. Full temporal results of HITF16167.

Fig. 61 shows the signal amplitude vs frequency for shot HITF16167. As in the previous shots, there is a peak at about 100 KHz. There is a weak second peak about 400 to 500 KHz in sensors 1 and 3. All the channels show strong amplitudes which reflects that the sensors were recording very large signals, even if for only over a limited time.

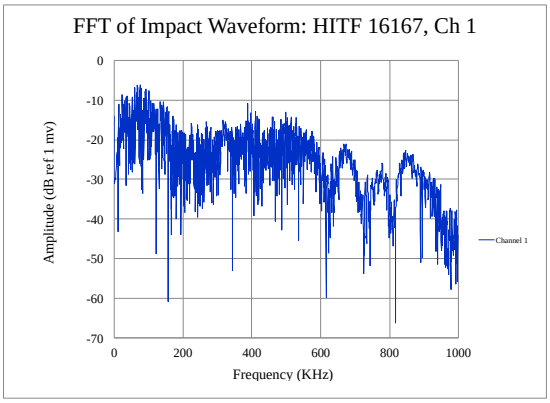

(a) Sensor Channel 1

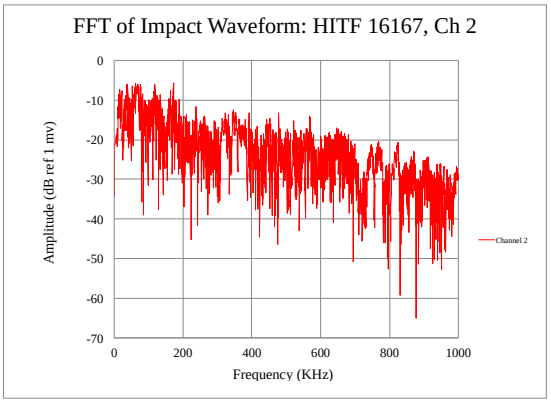

(b) Sensor Channel 2

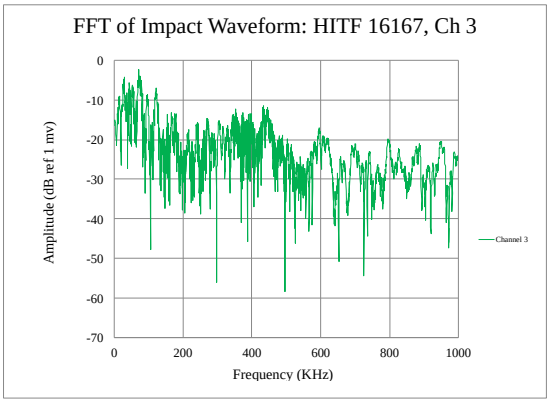

(c) Sensor Channel 3

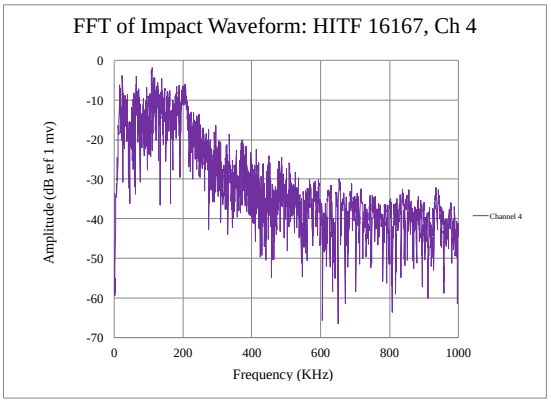

(d) Sensor Channel 4

Figure 61. Frequency results of HITF16167.

In Fig. 62, for shot HITF16168, the first arrival signal occurred on sensor 2, followed by sensor 3, and then sensor 1 and finally on sensor 4.

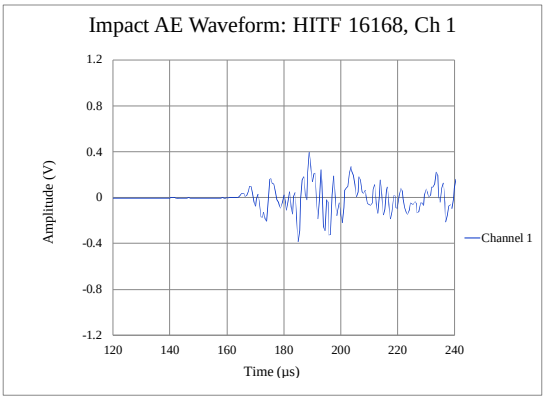

(a) Sensor Channel 1

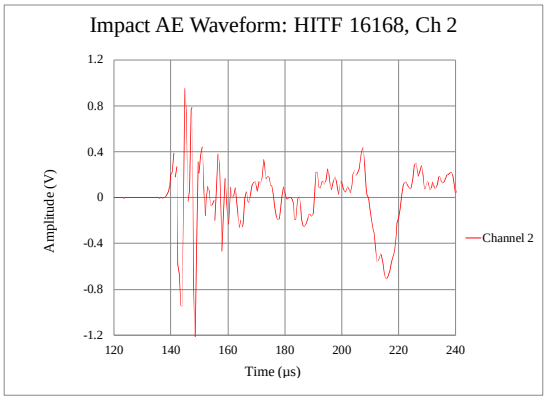

(b) Sensor Channel 2

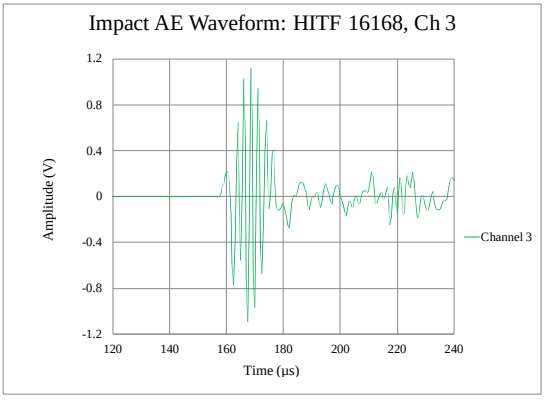

(c) Sensor Channel 3

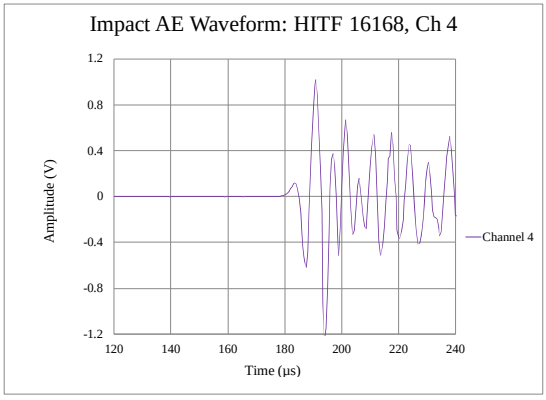

(d) Sensor Channel 4

Figure 62. Time of arrival/temporal results of HITF16168.

Fig. 63 shows the full temporal time recorded for the shot HITF16168. On channels 2 and 3, there is evidence that those sensors disbonded prior to detonation. The sensors on channels 1 and 4 appear to have remained bonded until the bottle detonated. This COPV bottle appears to show the initial time of detonated at about 750 µs on sensors 1 and 3. Sensor 4 shows the signal disappears at about 1100 µs. Since channel 4 is attached to a dome area, which is anchored, it is the last sensor to record the acceleration outward from the detonation. The times when the signals "restart" reflect when the COPV wall sections are accelerating the sensor outward.

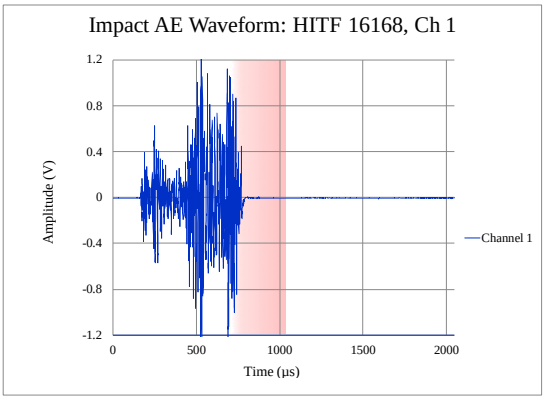

(a) Sensor Channel 1

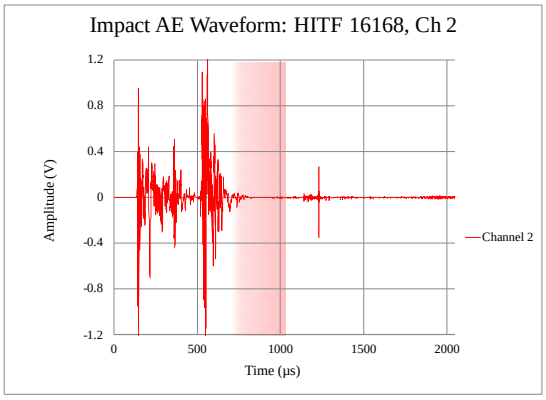

(b) Sensor Channel 2

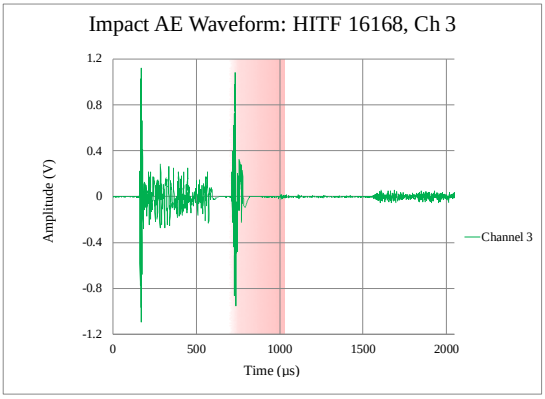

(c) Sensor Channel 3

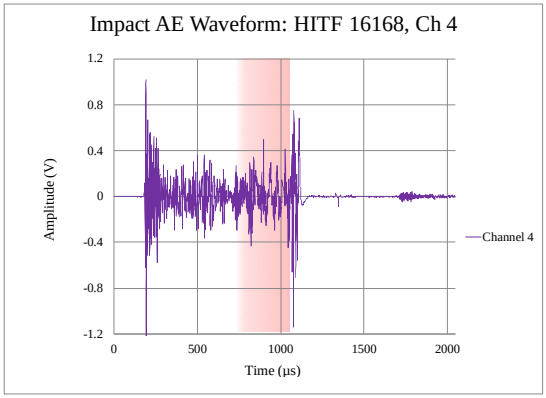

(d) Sensor Channel 4

Figure 63. Full temporal results of HITF16168.

Fig. 64 shows the signal amplitude vs frequency for shot HITF16168. As in the previous shots, there is a peak at about 100 KHz. There is a second peak about 400 to 500 KHz that can be seen in sensor 1 and 3, but not for on sensor 2 and 4. Sensors 1, 2 and 4 show signal amplitudes that are relatively high. Sensor 3 had the overall smallest amplitudes as it experienced early disbonding and a weak acceleration term at the detonation point.

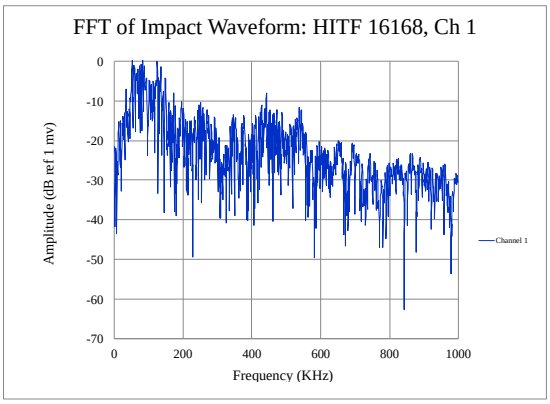

(a) Sensor Channel 1

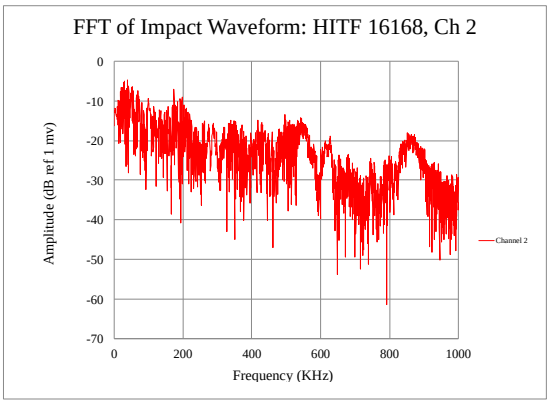

(b) Sensor Channel 2

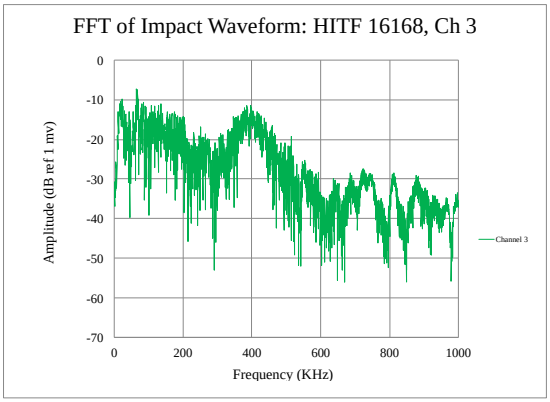

(c) Sensor Channel 3

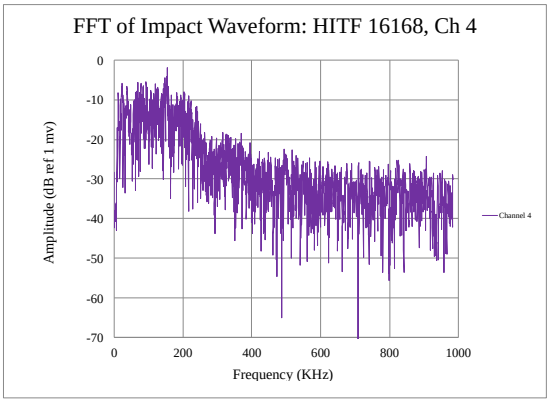

(d) Sensor Channel 4

Figure 64. Frequency results of HITF16168.

In Fig. 65, for shot HITF16170 the first arrival signal occurred on sensor 2, followed by sensor 3, and then sensor 1, and finally on sensor 4.

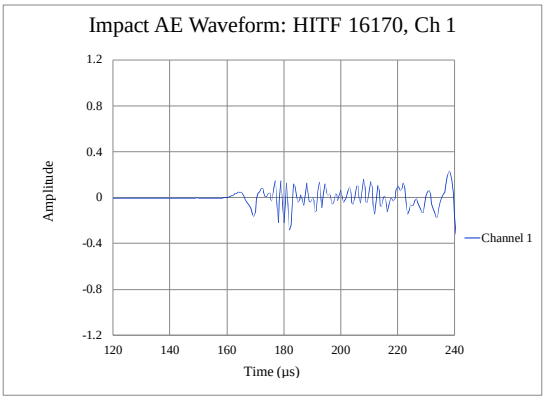

(a) Sensor Channel 1

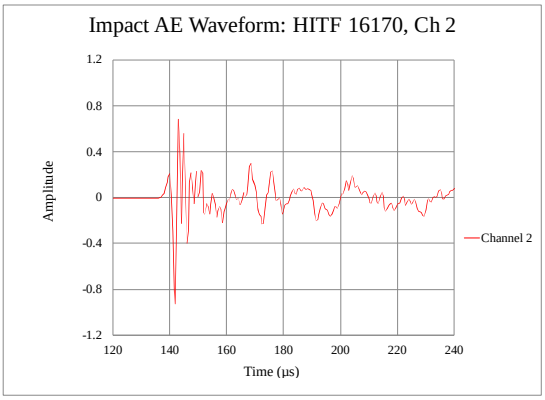

(b) Sensor Channel 2

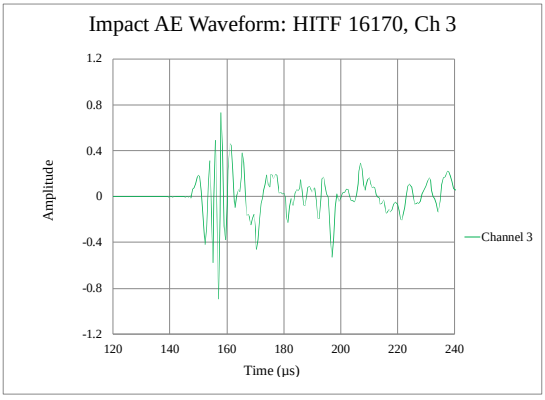

(c) Sensor Channel 3

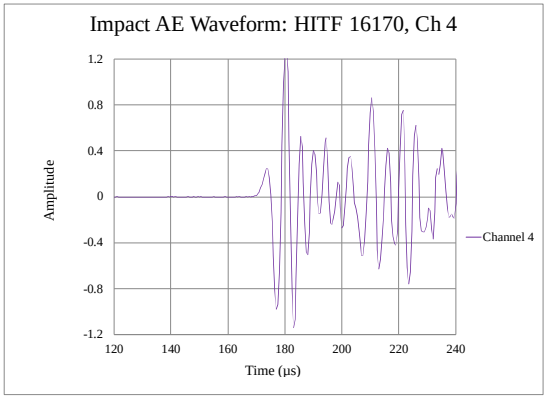

(d) Sensor Channel 4

Figure 65. Time of arrival/temporal results of HITF16170.

Fig. 66 shows the full temporal time recorded for shot HITF16170. This COPV bottle subsequently detonated near 2000 µs. The times when the signals "restart" reflect when the COPV wall sections are accelerating the sensor outward. Since the data recorded in this shot stopped at 2048 µs, the full view of the detonation signal was lost.

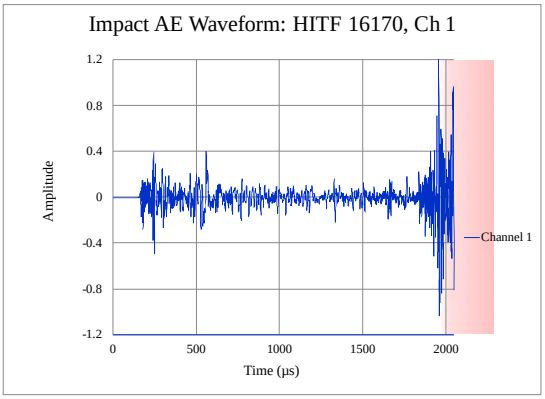

(a) Sensor Channel 1

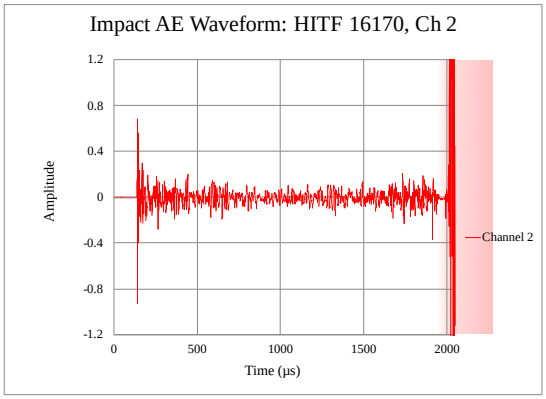

(b) Sensor Channel 2

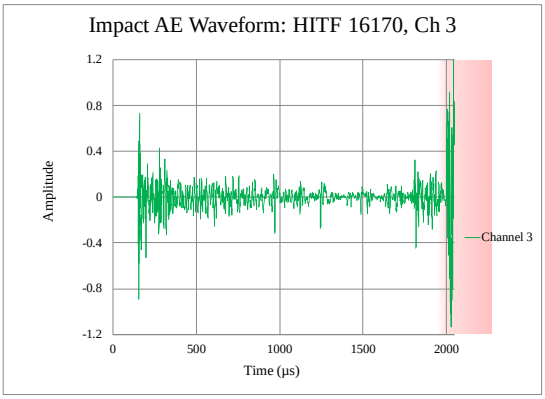

(c) Sensor Channel 3

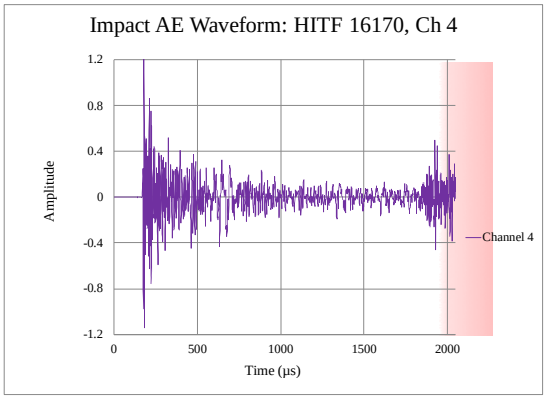

(d) Sensor Channel 4

Figure 66. Full temporal results of HITF16170.

Fig. 67 shows the signal amplitude vs frequency for shot HITF16170. As in the previous shots, there was a peak at about 100 KHz. Only channel 1 seems to show much of a second peak at about 400 to 500 KHz.

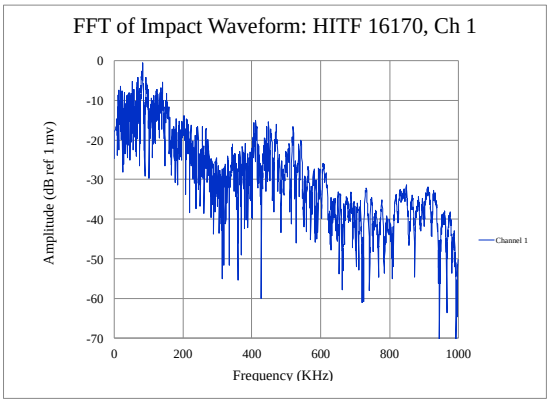

(a) Sensor Channel 1

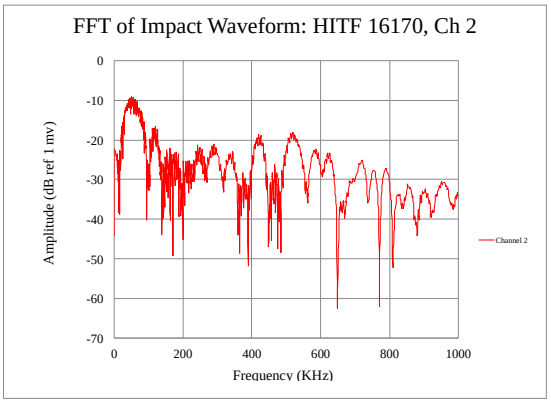

(b) Sensor Channel 2

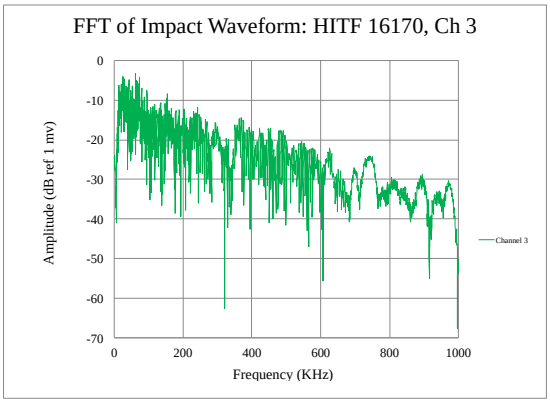

(c) Sensor Channel 3

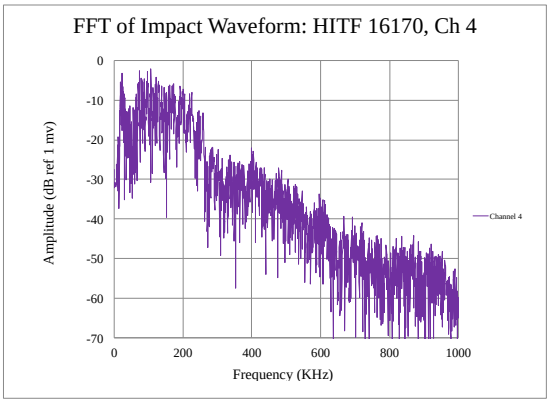

(d) Sensor Channel 4

Figure 67. Frequency results of HITF16170.

In Fig. 68, the early data from HITF16505 is shown. The first arrival signal occurred on sensor 2, followed by sensor 1, and then sensor 3, and finally on sensor 4.

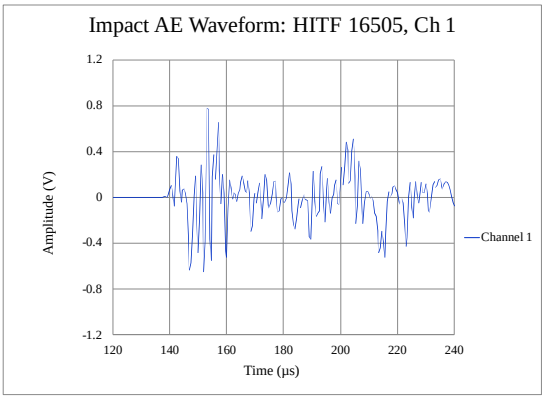

(a) Sensor Channel 1

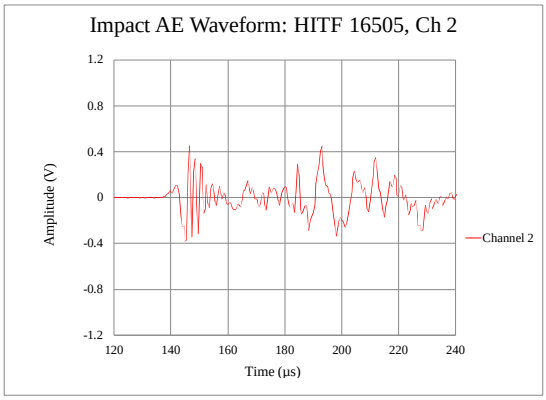

(b) Sensor Channel 2

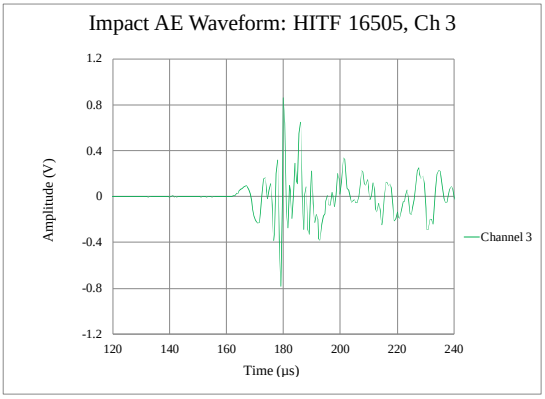

(c) Sensor Channel 3

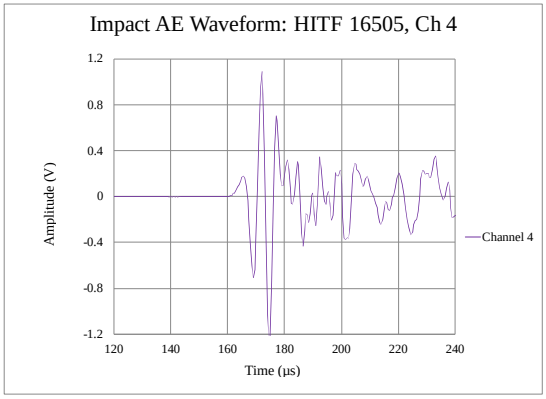

(d) Sensor Channel 4

Figure 68. Time of arrival/temporal results of HITF16505.

Fig. 69 shows the full temporal time recorded for the shot HITF16505. Channels 1 and 2 appear to have disbonded or lost electrical connection as the signals on those channels appear to be lost after about 300 µs. In addition, sensor 2 appears to be weaker than the other sensors attached to the cylinder section, which suggests that the channel may have partially disbonded at the time of impact. This COPV bottle subsequently detonated at about 400 µs. Only channel three shows good evidence of the sensor being accelerated as the COPV wall segments fly outward. Sensor 1 and 2 appear to be dead at that point. It is possible that these sensors' piezo elements and faceplate structures may have been broken off by the violence of this impact. This suggestion of sensor failure can't be confirmed as all the sensors were destroyed by the detonation. Since channel 4 is attached to a dome area, which is anchored in the test fixture, it does not appear to accelerate outward from the detonation during the time recording.

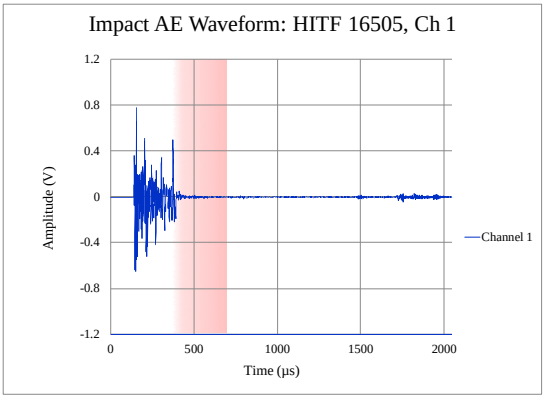

(a) Sensor Channel 1

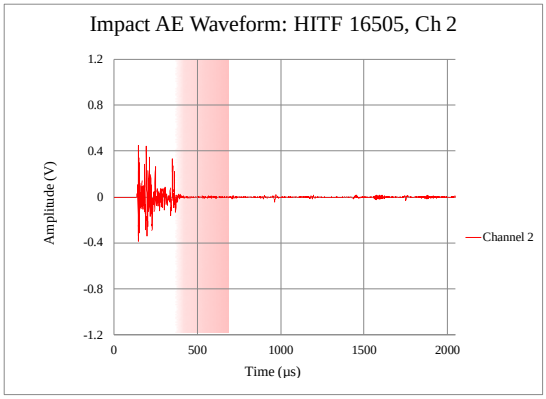

(b) Sensor Channel 2

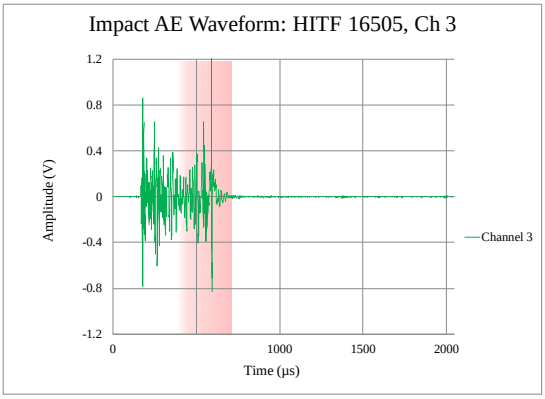

(c) Sensor Channel 3

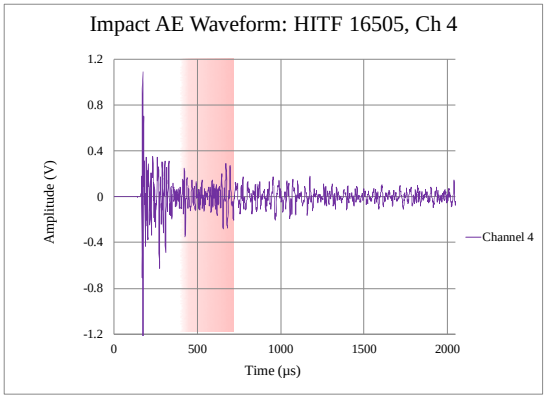

(d) Sensor Channel 4

Figure 69. Full temporal results of HITF16505.

Fig. 70 shows the signal amplitude vs frequency for shot HITF16505, which was the last shot in this series of testing. As in earlier shots, there was a peak at about 100 KHz. All the channels show a second peak at about 400 to 500 KHz. Channel 2 shows a lower amplitude, which reflects the fact that its signal was weaker overall in Fig. 69.

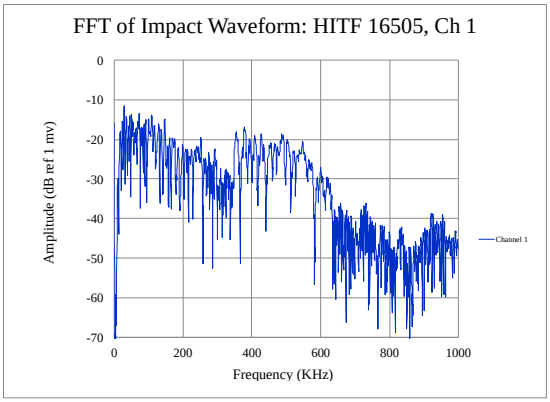

(a) Sensor Channel 1

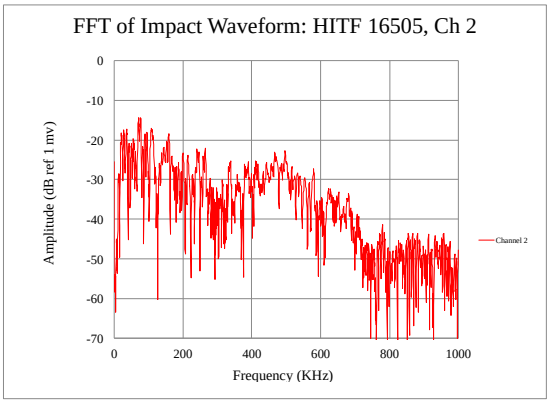

(b) Sensor Channel 2

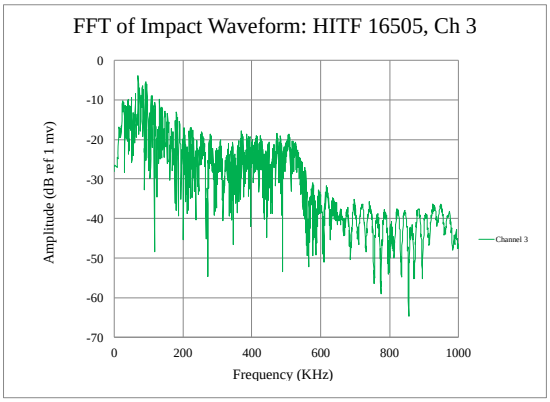

(c) Sensor Channel 3

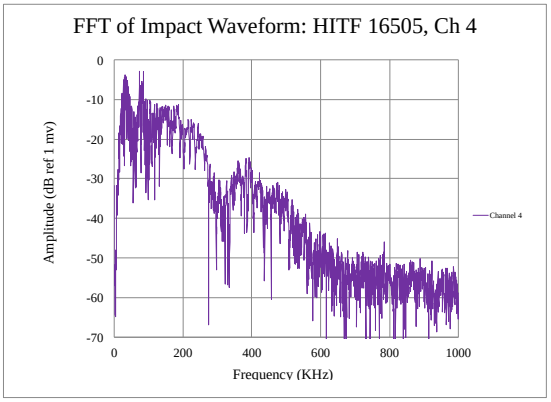

(d) Sensor Channel 4

Figure 70. Frequency results of HITF16505.

Table 14 shows the HTIF numbers, their targeted locations, and the relative time shifts from each of the four sensors regarding the earliest sensor's signal's arrival.

Table 14. List of Target Locations and Temporal Results of HVI shots that penetrated and detonated the COPV

Test Number / HITF Number/ Tank S/N / Impact Location	Target position axial (m)	Target position circum. (deg)	Target angle (deg)	Delta time sensor 1 (in µs)	Delta time sensor 2 (in µs)	Delta time sensor 3 (in µs)	Delta time sensor 4 (in µs)
Part 1							
#5 HITF16161 S/N 189 Cylinder	0.254	180	-45	27.5	0	15	35.5
#6 HITF16162 S/N 188 Cylinder	0.254	180	-45	27.5	0	17	32
Part 2							
#11 HITF16167 S/N 224 Cylinder	0.254	180	0	23	0	13	36.5
#12 HITF16168 S/N 187 Cylinder	0.254	180	-60	26	0	19.5	41.5
#14 HITF16170 S/N 222 Cylinder	0.254	180	-45	23.5	0	9.5	32.5
#17 HITF16505 S/N 203 Cylinder	0.298	90	-45	3.5	0	25.5	25.5

Table 15 shows the estimated impact locations based on the delta time data from Table 14. As before, adjustments in the velocity were made for this group of shots on pressurized COPVs. It was set at 20% above the velocities used for the unpressurized bottles to help account for the effect of the high pressure and temperature of the bottles on the velocity of ultrasound in the bottle's walls. Since the bottles in Table 15 detonated, there was no way to verify the actual impact locations to certify the data in the last column in Table 15. In this set of data, the location estimates were referenced to their target locations. The errors of location were on the same order of magnitude as the errors for the impacts that did not penetrate and the impacts that penetrated and vented.

Table 15. Impact location table for penetrating impacts with detonations showing the AE impact location calculation. Similar to the cases of the non-penetrating impacts and impacts with venting, the velocity values, for this group of shots were set at 20% above the velocities used for the unpressurized bottles because of the effect of the high pressure and temperature in the bottles' wave velocity.

Shot No.	Target of Axial Location of Impact (m)	Target of Circum. Location of Impact (m)	Estimated Axial Location of Impact (m)	Estimated Circum. Location of Impact (m)	Estimated Temporal Offset (μs)	Velocity Adjustment for Pressure*	Estimated Location Error (m)
Part 1							
#5 HITF16161 S/N 189 Cylinder	0.254	0.260	0.255	0.225	2.98	additional 20%	0.0356
#6 HITF16162 S/N 188 Cylinder	0.254	0.260	0.315	0.254	1.47	additional 20%	0.0612
Part 2							
#11 HITF16167 S/N 224 Cylinder	0.254	0.260	0.264	0.254	4.20	additional 20%	0.0117
#12 HITF16168 S/N 187 Cylinder	0.254	0.260	0.276	0.254	3.23	additional 20%	0.0234
#14 HITF16170 S/N 222 Cylinder	0.254	0.260	0.242	0.254	6.25	additional 20%	0.0135
#17 HITF16505 S/N 203 Cylinder	0.298	0.130	0.173	0.135	8.495	additional 20%	0.125

* See ref. (1, 2)

Efforts to extract significant information from the signal energies in these instances where the COPV's detonated are much more problematic than for the previous cases of impact with no penetration or impact with penetrations and venting. Here, the signals have become much more complex with the added features of disbonding and detonation effects. In particular, we do not have consistently long time records to work with. The lack of consistency in the impact's time record length made use of the signal energy problematic for comparison.

Summary

Acoustic emission measurements were performed on COPVs undergoing hypervelocity impacts while under high pressure as a component of an NESC sponsored study to understand how COPVs might respond to hypervelocity MMOD impacts. The test objectives of the AE part of this testing were to see if Acoustic Emission could be used to predict post impact failure of a pressurized COPV. This represented a challenging effort as the complexity of the damage from HVI events to COPVs led to AE signals that were very complex in form and required non-standard processing sometimes.

In these tests, the hypervelocity impact resulted in one of three states of damage that had different outcomes for a COPV. In the first case, the HVI event did not fully penetrate a pressurized COPV, and the COPV held its pressure. In a second case, the HVI event penetrated the pressurized COPV resulting in the bottle venting, which quickly relieved the pressure on the COPV's walls. In that case, damage growth in the COPV's pressure wall at later times was avoided. In the third and final case, the HVI event penetrated the pressurized COPV allowing venting to start, but within two milliseconds or less, the damage growth in the pressurized wall was growing quickly enough and became extensive enough to overcome the pressure wall's structural integrity, at which time, the remaining bottle pressure caused the COPV to rupture explosively.

Where the hypervelocity impact did not penetrate the COPV pressure wall, the post impact acoustic emissions were much smaller than the original impact signal and there weren't very many singular events recorded after the initial event. This showed that the COPV quickly reached a new stable stress equilibrium with the internal pressure, and a few indications of new damage growth in the COPV were clear. These tests did not address latent damage growth that might arise at the damage site because of issues such as pressure cycling or other variable loading effects. For the first arrival signals, the impact signal had a good phase-referenceable signal usable for event triangulation. The non-pressurized wave velocities generated reasonable location estimates. When pressurized to MEOP, wave speeds in the pressure wall increased and required a change to the unpressurized velocities of ~20%. The non-penetrated COPV bottles showed a general increasing AE signal energy behavior with respect to the increasing impactor energy, and an increasing visible damage region. In the frequency domain, the AE signals showed a few strong frequencies near ~100 KHz and ~400-500 KHz.

Where the hypervelocity impact penetrated the COPV pressure wall, and the bottle vented the gas, the AE signals in the time domain demonstrated a more complex ultrasonic wave structure than the non-penetrating case. Besides the initial impact signal, there was sound from the escaping gas and noise arising from damage growth. These impacts all had clear first arrival signals. After the initial impact signal, none of the later signals recorded showed much of any phase relationship between the different sensors, so they were treated as uncorrelated.

Some effort was made to see if the signal energy from different impact types, non-penetrating vs. penetrating, could be segregated into components from impact damage, gas venting noise and contributions from damage growth in the COPV. A comparison of the damage region vs. various

signal energy components, i.e. leak noise or damage growth noise, showed relatively weak correlation with estimates of either the damage region's circumference or its area.

Once the impactor penetrated the COPV, the signal energy vs. impactor energy was variable. Besides the impactors' energy not being fully deposited into the pressure wall upon a penetrating impact, the damage growth sounds and the sounds from the gas escaping also distorted the relationship between signal energy and impact energy. In the frequency domain, the AE signals continued to show a few strong frequency regions near ~100 KHz and ~400-500 KHz as was seen in the case of the impactor not penetrating the pressure wall.

Where the hypervelocity impact penetrated the COPV pressure wall, and the bottle detonated, the AE signals in the time domain showed the same types of signals recorded by the case where the projectile penetrated and vented the COPV, plus, they also showed additional signal structure related to damage growth in the bottle. For the first arrival signal, the impact signals continued to show good phase referenced signals. Besides the impact signal, there was noise from the escaping gas and noise that involved damage growth, none of which could show much of any phase relationship between the different sensors. Some sensors were dislodged by the impact while other sensors disbonded or were damaged because of the extensive damage growth occurring in the COPV as the pressure wall continued to fail. The detonation of the COPV usually happened between hundreds of microseconds to a few milliseconds after impact. At that point, the transducers, including those that had become disbonded would become impacted by the COPV pieces and would show a strong acceleration signal with the COPV wall pieces accelerating outward. Beyond that point in time, the transducer signal was lost. In the frequency domain, the AE signals showed a decreasing signal with increasing frequency. The evidence of the 100 and 500 KHz "peaks" were still evident, but not always as strong as in the other COPV impacted groups, in part because of the more limited data record lengths as the sensors did not stay attached over the full-time record.

Conclusion

Regarding the initial goal for this work, for COPV bottles that were impacted, but did not suffer penetration, the AE signals ceased after a short period of time after impact. This indicated that subsequent damage growth in the COPV bottle's ceased and the bottles stabilized structurally. Hence, trying to detect post impact damage growth from an impact did not appear fruitful, at least for the case of static pressurization.

The measurement of other damage states such as penetration and venting or penetration and detonation, while measurable, happened quickly. In particular, it was difficult to see a process that might predict the explosive failure of the bottles in a timely manner so that the AE data could be used to reasonably respond in a fashion that might safe the system.

References

1. Gandhi, N., Michaels, J. E., and Lee, S. J., "Acoustoelastic Lamb Wave Propagation in Biaxially Stressed Plates", ARFL, Report no. AFRL-RX-WP-TP-2012-0279, March. 2012,
2. Qu, J., and Liu, G., "Effects of Residual Stress on Guided Waves in Layered Media," Review of Progress in Quantitative Nondestructive Evaluation, Edited by D.O. Thompson and D.E. Chimenti, Vol. 17, no. 1, pp1635-1642, 1998, P1enwn Press, New York,
3. Volarovich, M. P., and Balashov, D. B., (Application of Ultrasound to Test Materials), v23, p63, 1961, (In Russian).

4. Kortbeek, P. J., Trappeniers, N. J., and Biswas, S. N., “Compressibility and Sound Velocity Measurements on N_2 up to 1 GPa”, Int, J. of Thermophysics, v9, n1, p103, 1988
5. Madaras, E. I, “On-Orbit Leak Detection and Location System Status”, ISS Leak Detection and Repair Subcommittee Technical Interchange Meeting Feb. 2-6, 2009, Moscow, Russia.

REPORT DOCUMENTATION PAGE

Form Approved
OMB No. 0704-0188

1. REPORT DATE *(DD-MM-YYYY)*
1-11-2019

2. REPORT TYPE
Technical Memorandum

3. DATES COVERED *(From - To)*

4. TITLE AND SUBTITLE

NESC Composite Overwrapped Pressure Vessel Hypervelocity Impact Study: Phase A–Acoustic Emission Review

5a. CONTRACT NUMBER

5b. GRANT NUMBER

5c. PROGRAM ELEMENT NUMBER

6. AUTHOR(S)

Madaras, Eric I.; Nichols, Charles T.

5d. PROJECT NUMBER

5e. TASK NUMBER

5f. WORK UNIT NUMBER
869021.03.07.01.08

7. PERFORMING ORGANIZATION NAME(S) AND ADDRESS(ES)

NASA Langley Research Center
Hampton, VA 23681-2199

8. PERFORMING ORGANIZATION REPORT NUMBER
L-21074

9. SPONSORING/MONITORING AGENCY NAME(S) AND ADDRESS(ES)

National Aeronautics and Space Administration
Washington, DC 20546-0001

10. SPONSOR/MONITOR'S ACRONYM(S)
NASA

11. SPONSOR/MONITOR'S REPORT NUMBER(S)
NASA-TM-2019-220423

12. DISTRIBUTION/AVAILABILITY STATEMENT

Unclassified-
Subject Category 16
Availability: NASA STI Program (757) 864-9658

13. SUPPLEMENTARY NOTES

14. ABSTRACT Acoustic emission (AE) measurements were performed as a component of a NASA Engineering and Safety Center (NESC) sponsored study to understand how Composite Overwrapped Pressure Vessels (COPV) respond to hypervelocity impacts (HVI) while pressurized. Of general interest to the NESC was whether there were any obvious indications in AE data that could foretell pending failure after an impact. It was of particular interest, where an HVI event did not fully penetrate a pressurized COPV, to detect post-impact AE events that could indicate damage growth under continued pressure loading that might allow experts to anticipate future failure. Where an HVI event penetrated the COPV, it was of some interest to know if AE events supported an assessment of the initial degree of damage and correlated with whether the bottle vented or detonated.

15. SUBJECT TERMS

16. SECURITY CLASSIFICATION OF:			**17. LIMITATION OF ABSTRACT**	**18. NUMBER OF PAGES**	**19a. NAME OF RESPONSIBLE PERSON**
a. REPORT	**b. ABSTRACT**	**c. THIS PAGE**			STI Help Desk (email: help@sti.nasa.gov)
U	U	U	UU	101	**19b. TELEPHONE NUMBER** *(Include area code)* (757) 864-9658